ANALYSIS OF CERTAIN ASPECTS OF CANAL SUBIRRIGATION

BY

R CALEB BRUHN

THESIS

Submitted in partial fulfillment of the requirements
for the degree of Master of Science in Agricultural and Biological Engineering
in the Graduate College of the
University of Illinois Urbana-Champaign, 2021

Urbana, Illinois

Master's Committee:

Professor Richard Cooke, Chair and Adviser
Professor Prasanta K. Kalita
Research Assistant Professor Jorge Alberto Guzman Jaimes

ABSTRACT

Canal irrigation provides water to crop roots by controlling the level of the water table. Parallel earthen canals spaced throughout the field are filled with water which seeps out into the soil. Under the right environmental conditions, such as fields underlain by a low permeability layer, a properly designed system will maintain saturated conditions just below the root zone of the crop which will result in the correct proportions of water and air in the root zone. A finite element numerical model was used to analyze multiple variations in canal design and impermeable layer depth. An analytical equation was developed from the results for the purpose of providing a relatively simple yet accurate method for the design of such irrigation systems. A site for installation of a pilot scale project was selected in collaboration with colleagues from Njala University, Sierra Leone. Soil samples were collected from the site and instruments were installed to monitor the operating performance of the system. Measured soil properties were entered into the numerical model along with other inputs assuming a worst-case scenario to predict the associated performance. It was concluded that canal irrigation would provide adequate water to crops at the project site. The design equation can be written in the form of $q = \frac{8KD_e(n-h_e)+4K(n^2-h_e^2)}{L_e}$ where $D_e = 0.77983D$, $L_e = 0.97185L$, $h_e = h + 0.00452S + 0.01301$, and q is the seepage rate from the canal (m/day), K is the saturated hydraulic conductivity of the soil (m/day), n is the depth of water in the canal (m), D is the depth from the bed of the canal to the impermeable layer (m), L is the canal spacing (m), h is measured midway between canals as the height of the water table above the bed of the canals (m), and S is the slope of the canal bank (m/m). The dependence of the water table profile upon the shape of the canal has previously been neglected by some authors and studied for cases other than canal irrigation by others.

ACKNOWLEDGMENTS

This project would not have been possible without the excellent professional and personal support of my advisor, Dr. Richard Cooke.

I extend grateful acknowledgement to the College of ACES International Graduate Research Grant which funded my trip to Sierra Leone. I also gratefully acknowledge Dr. Martin Thalheimer for providing the code from his original work cited in Chapter 6 and the References.

The invaluable contributions of Dr. Paul Fischer, Dr. Patrick Sawyer, Richard Williams, Austen Motily, Navo Yambaso, Emmanuel Kangoma, James Lusiene, and many others also furthered the quality of the finished product.

For my Savior, Jesus Christ, the One in Whom I live and move and have my being

TABLE OF CONTENTS

CHAPTER 1: INTRODUCTION

Continuous evaluation, adaptation, and improvement of agricultural water management is as important in Sierra Leone as it is everywhere else. It is crucial to note that many smallholder farmers lack the means to obtain all of the technologies used in developed countries; in addition, any given one is not necessarily a good fit to the environmental context of West Africa. Accordingly, much research into accessible, contextually appropriate, improved agricultural practices– including dry season water management– is being conducted at Njala University in Sierra Leone. The university has been working with national and international partners like the University of Illinois Urbana-Champaign both to research such practices and to disseminate the information to farmers throughout the country (Amadu et al., 2017).

Sierra Leone has agronomically-favorable environmental factors which include a humid climate with 3,000 – 5,000 mm of rainfall per year in coastal areas and 2,000 – 2,500 mm inland. Despite favorable conditions for rice production, the country imports over 80% of the amount it consumes. Rice is the primary food staple of Sierra Leone; imports are valued at more than one hundred million US dollars every year (Amadu et al., 2017). Most of the rice grown in Sierra Leone is rainfed: production occurs during the rainy season, which lasts from May until November, with harvest in August or September. The stored grain often runs out before the following year's harvest as virtually no crops are grown during the dry months (December to April). Hunger peaks just before harvest, when as much as forty five percent of households suffer food insecurity (Amadu et al., 2017). Dry season irrigation is one solution to this problem being investigated by Njala University and its partners.

Irrigation is concerned with various means of controlling water movement throughout a geographic region in order to achieve a desired (usually uniform) distribution available to crops.

Several irrigation technologies are available. They can be broadly categorized into surface systems and pressurized systems (Clemmens et al., 2007). Surface irrigation systems include basin, border strip, and furrow. The first of these involves enclosing the whole or part of a field and completely leveling the area. Once the surface is entirely level it may be shaped into ridges or beds, but the height of these features is minor relative to the basin edges and are kept uniform throughout the basin. Irrigation is applied such that it floods the entirety of the basin before it is shut off and the ponded water infiltrates. Border strip and furrow irrigation are more similar to one another than to basin irrigation. In the former system, land is graded into strips having a constant slope. Ridges or borders enclose either side of each strip, forcing irrigation water applied at one end to travel to the other. The latter system also forces water to travel a certain length, but it travels within evenly spaced furrows which are graded to a constant slope.

Pressurized irrigation systems include various kinds of sprinklers as well as microirrigation methods (Solomon et al., 2007). In these systems water is conveyed through pipes to discrete outlet points. The pipes may be permanently fixed in one place, as in the case of solid set systems, or they may move. Hand move or portable sprinkler systems involve significant labor, while those moved by mechanical means do not (side roll sprinklers, gun-type sprinklers, center pivots, lateral move, and low energy precision application systems). The preceding systems distribute water into the air before it reaches the crop, as do microspray systems. On the other hand, bubbler and drip (trickle) irrigation systems apply water directly to the soil surface, while what Solomon et al. (2007) refer to as subsurface drip irrigation applies the water below the soil surface. The major determinant for a pressurized system to be categorized as micro or not, is the discharge rate.

In general, surface irrigation systems require significantly more labor than pressurized systems, which generally require significantly more capital investment than surface systems. However, the more land leveling that is required for surface irrigation to succeed on a farm, the more cost is involved.

Although they vary inversely to one another, an irrigation system which minimizes both labor and capital investment is desirable. The specific optimum when balancing tradeoffs between the two costs depends upon the context in which the irrigation system is to be installed. For smallholder farms in Sierra Leone, there was ample motivation to select a system which does not require capital investment in mechanized land leveling equipment, nor in pipe and nozzles. A system which would not demand too much time and labor from farmers in the form of timing surface water flows was also required (Clemmens et al., 2007). Thus, there was reason to explore options beyond conventional forms of irrigation.

Inspiration came from a recent development in agricultural drainage which is the concept of water table management. The topic is discussed at length by Fouss et al. (2007) and Skaggs (1999b), among others. The part of this management system most relevant to the present work is the secondary use of drainage systems for irrigation. All drainage systems work by gravity whether the means of water conveyance is perforated pipe or earthen canals. They are designed to lower the water table of a field, and thus exist below the level of the crop roots. Accordingly, when they are modified so that water flows in reverse, this configuration is termed subsurface irrigation, or subirrigation.

In the United States, subsurface irrigation is typically accomplished via buried perforated pipe. However, it can also be accomplished via steady-state infiltration from open, earthen canals where a consistent water level is maintained, as in the Netherlands (Skaggs, 1999b). There would be no need for investment to develop perforated pipe production and installation technology or infrastructure in Sierra Leone before this form could be adopted. Further, it could be installed by manual labor, without the need for mechanized trenchers or other specialized equipment for the laying of pipe or the levelling of land. Once installed it would require lower labor to operate than any of the surface irrigation systems. Thus, economically and operationally speaking, the potential of canal subirrigation for use in Sierra Leone was worth investigating.

The research broadly fell into two categories. First, a theoretical understanding of relevant canal subirrigation design parameters was required. In particular, canals are constructed with a variety of cross section geometries including rectangular, trapezoidal, triangular, and parabolic, among others. It was hypothesized that, all else being equal, variation in canal cross section geometry would cause variation of the water table profile. Whether or not to include the variation in canal subirrigation design would depend upon its significance. It was desired that a practical canal subirrigation design methodology would then be developed from the theoretical analysis. Second, it was necessary to examine how well the proposed design would work in the real world. In order to accomplish the two, it was decided that both computational and site-specific analysis were needed.

The investigation documented in this thesis began with a review of the theoretical basis for soil water flow physics described in the scientific literature (Chapter 3). Analytical and computational tools for drainage and irrigation system designs as well as other soil water flow analyses have been built on these principles. One of the computational tools available today is HYDRUS (2D/3D) (Šimůnek and Šejna, 2011). According to the authors, HYDRUS (2D/3D) is a "software package for simulating the two- and three-dimensional movement of water, heat and multiple solutes in variably-saturated media" (Šimůnek et al., 2012). This package includes a numerical solver and a graphic user interface. It will solve flow domains delineated by irregular boundaries and/or which represent nonuniform soil properties and has numerous specialized optional add-ons. Along with the rigorous theoretical basis of the program and extensive validation, the level of complexity it can handle has resulted in wide use for peer-reviewed research (Šimůnek et al., 2012).

Therefore, HYDRUS (2D/3D) (hereafter abbreviated to HYDRUS) was chosen to analyze the physical potential of canal subirrigation in Sierra Leone. In order to facilitate the computational analysis, a project site in Sierra Leone was generalized into a conceptual model representing the soil water physics of canal subirrigation systems (Chapter 4). The conceptual model was implemented in

HYDRUS: i.e., it was translated into program inputs and appropriate program settings. Preprocessing code was developed in python to speed the process along with postprocessing code. The accuracy of the implementation was partially verified through analysis of numerical stability.

While computational tools are more complex and thus better suited to investigational analysis of novel approaches, practitioners who do not have access to these tools need relatively simple, yet sufficiently accurate, analytical equations for system design. Therefore, although HYDRUS was used to analyze the problem, the findings were used to define an analytical design equation. Thus, an analytical solution used in established contexts but modified by correction coefficient(s) was evaluated for suitability to the application (Chapter 5 and Chapter 7). Later, a trial of the irrigation system was installed at a project site on the campus of Njala University. Physical data were collected (Chapter 6) and entered into a HYDRUS model in order to predict the system's performance (Chapter 8). The results of this investigation are discussed in Chapter 9, and conclusions and recommendations are made in Chapter 10.

CHAPTER 2: OBJECTIVES

Specific research objectives were needed to guide the investigation of canal irrigation suitability and provide actionable deliverables from the knowledge gained. These simply consolidated the several components of analysis previously mentioned in the introduction. The objectives were to:

- Using HYDRUS, test the hypothesis that canal cross section geometry affects the location and shape of the water table profile.
- Define an analytical equation suitable for canal subirrigation system design accessible to practitioners without computer access.
- Evaluate the functionality of canal subirrigation in the real-world target setting by empirical measurements and HYDRUS simulation.

CHAPTER 3: LITERATURE REVIEW

Soil is "the layers of generally loose mineral and/or organic material that are affected by physical, chemical, and/or biological processes at or near the planetary surface and usually hold liquids, gases, and biota and support plants" (van Es, 2017). This material forms a matrix full of empty spaces, or pores, which contain varying mixtures of air and water. When the pore space is entirely filled with water it is said to be saturated; otherwise, it is unsaturated. The unsaturated state is critical to plants because their roots must have both oxygen and water. Soil pore space is closely related to the size of the solid particles forming the matrix but is also affected by biological activity and cultural practices such as plowing. Several classification systems for soil particle size exist. For agriculture, three particle size ranges with distinguishably different properties have been identified by the USDA texture classification system (Schoeneberger et al., 2012). Solid particles larger than 2 mm in diameter are classified as gravel and are not counted in the texture classification. Particles that are between 2 mm and 0.05 mm are classified as sand. Particles smaller than this but larger than 2 μm are classified as silt, while anything smaller is considered clay. Soil texture classes are identified on the basis of the percentages of these three components, as shown in Figure 1. It is worth noting that several alternatives to the USDA classification system exist which define somewhat different size ranges for sand, silt, and clay.

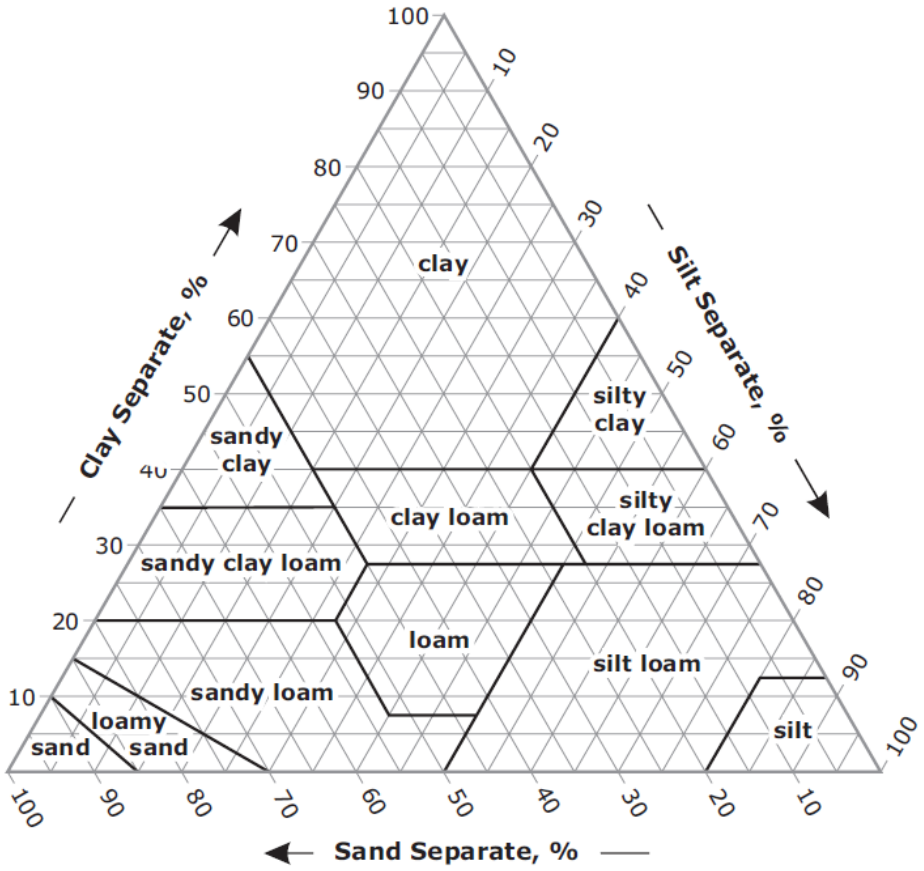

Figure 1. USDA soil texture triangle (Schoeneberger et al., 2012).

The texture of a soil gives a general knowledge of how much water the soil can store. However, knowledge of the way soil responds to a given value of water potential is also necessary in order to determine the amount of water which plants can extract. Total soil water potential is defined by Smith and Warrick (2007) as "the work per unit weight to move an infinitesimal amount of water from some reference state to a given point in the soil" with units of length (here, meters). It is made up of three components:

$$h_T = h_g + h_p + h_a \quad [1]$$

where h_T is the total soil water potential at any point in the soil; h_g is the gravitational potential, which is equal to the given point's elevation compared to the reference point; h_p is the matric or pressure potential; and h_a is the pneumatic potential, which accounts for air pressure. In the majority of cases

variance of pneumatic potential in the soil profile is ignored, and the term neglected, because air pressure is considered to be uniform throughout. "The usual reference state, arbitrarily defined as having zero [matric] potential, is an open air-water interface at some specified elevation and air pressure" (Smith and Warrick, 2007).

The major component of interest in irrigation from Eq. [1] is the matric or pressure potential. Hereafter, the term "(soil) water potential" refers singularly to this component of the total soil water potential. It can be positive or negative at a given location, depending on whether it is greater or less than the gas phase (typically air) pressure at that point. Negative water potential is possible because of adhesion, which is the attraction of water to the soil particles, and because of cohesion, which is the attraction of water molecules to one another. The strength of cohesion is influenced by the curvature of the air-water interface, which is greater in smaller spaces. Thus, water can cohere more strongly in small soil pores than in large ones. As water is removed from soil pores, the influence of these two forces on the remaining water increases and the amount of work required to remove it per unit weight increases. In other words, the soil water potential at that location becomes lower; and so, it becomes more negative since the reference value of zero matric potential is defined at the air-water interface. Saturated soil and subsurface materials have positive water potential, while unsaturated material has negative water potential. Thus, pressure potential can be conceived as a continuous function of water content.

The concept of water potential is of interest in irrigation because it is useful for quantifying soil water movement. Water moves from locations with higher water potential to those with lower potential. As it moves, the water content of the locations increases or decreases respectively. This relationship has been described graphically via the soil water characteristic (retention) curve. Two points on the curve significant for crop water management decisions have traditionally been identified. These are the field capacity and permanent wilting point, illustrated in Figure 2. Although it is now

accepted that these are not precise, unique, or constant soil properties, they are still qualitatively useful (Smith and Warrick, 2007). Field capacity refers to the condition when soil water content is nearly optimal for plant growth. This does not occur at the same value of water potential for every soil, but 1/3 bar (approximately 3.399 meters) is still commonly used as a reasonable estimate. In contrast, the permanent wilting point refers to the condition when soil water content can no longer be extracted quickly enough by plants to maintain turgidity; i.e., they wilt and remain so even when they do not have to transpire. Just like field capacity this does not occur at a fixed value of water potential for every soil, but 15 bar (152.955 meters) is often used.

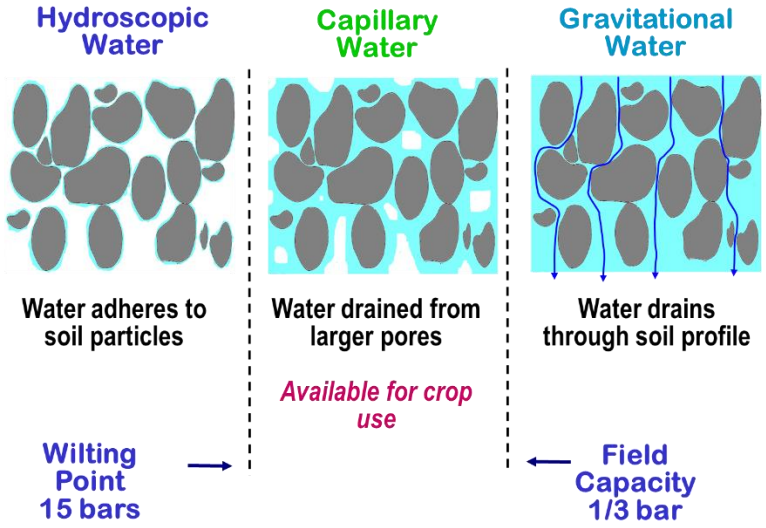

Figure 2. Soil moisture states of significance for crop water management decisions (courtesy of Dr. Richard Cooke).

The unsaturated region extending downward from the soil surface to the groundwater table is also called the vadose zone (Holden and Fierer, 2005). When the upper boundary of groundwater (groundwater table) does not occur within a few meters of the soil surface, soil only forms the top of the vadose zone which then also includes unsaturated subsoil and rock. The vadose zone is a region of constant fluctuations both in the flow of water and the water content and is itself in constant fluctuation with the rise and fall of groundwater depth. Plants need the water table to exist at the right depth below their roots in order to flourish. If it is too close, they do not have enough oxygen; if it is

too deep, they do not have enough water. In Sierra Leone the maximum depth of the groundwater table is typically ten meters (Rhodes et al., 2016). This is not deep enough for the weight of the matrix material above to generate enough pressure to compress the subsoil/rock if the amount of fluid filling the pore space changes.

Soil water is a challenging system to describe with governing equations, but practitioners have spent enough decades of research that they have begun to capture some of the complexity. In brief, a variably saturated flow system is commonly described by the governing equations of Darcy's law and conservation of mass. The expression of Darcy's law for anisotropic porous media when the coordinate axes lie along the principal directions of anisotropy, written in the notation used by Nieber and Feddes (1999), is given by

$$q_x = -K_{xx}\frac{\partial h}{\partial x}$$

$$q_y = -K_{yy}\frac{\partial h}{\partial y} \qquad [2]$$

$$q_z = -K_{zz}\frac{\partial h}{\partial z} + K_{zz}$$

where q_x, q_y, q_z are components of the Darcy flux vector; K is the hydraulic conductivity; x, y, z are Cartesian coordinates; and h is the water pressure head. Nieber and Feddes (1999) also give in-depth derivation of more generalized governing equations.

As previously mentioned, the pressures acting on the vadose zone are not enormous. For this reason, assuming that both fluid water and the solid soil matrix in the vadose zone are incompressible introduces a minimal amount of error so it is a reasonable simplification for analysis of fluid flows there. Further, the air phase which also exists in the vadose zone has been traditionally assumed to play an insignificant role in the fluid flow process, although McWhorter and Marinelli (1999) advocate for the development of governing equations that consider two-phase flow. These assumptions allow the equation for conservation of mass to be written as (Nieber and Feddes, 1999)

$$\Phi \frac{\partial S}{\partial t} = -\left(\frac{\partial q_x}{\partial x} + \frac{\partial q_y}{\partial y} + \frac{\partial q_z}{\partial z}\right) + Q \quad [3]$$

where Φ = porosity of the porous medium; θ = volumetric water content; $S = \left(\frac{\theta}{\Phi}\right)$ = degree of water saturation, which is a function of the water pressure head; Q = source/sink of water; and t = time.

When Eq. [2] is substituted into Eq. [3] Nieber and Feddes (1999) obtain the anisotropic form of the Richards equation as follows

$$\Phi \frac{\partial S}{\partial t} = \frac{\partial}{\partial x}\left(K_{xx}\frac{\partial h}{\partial x}\right) + \frac{\partial}{\partial y}\left(K_{yy}\frac{\partial h}{\partial y}\right) + \frac{\partial}{\partial z}\left(K_{zz}\frac{\partial h}{\partial z}\right) - \frac{\partial K_{zz}}{\partial z} + Q \quad [4]$$

For isotropic conditions $K_{xx} = K_{yy} = K_{zz} = K$. The Richards Equation is used to analyze the saturated and unsaturated flow domains together, typically in numerical simulations. It can also be written in other forms such as the following equation, written in the notation used in HYDRUS (Šimůnek et al., 2012)

$$\frac{\partial \theta}{\partial t} = \frac{\partial}{\partial x_i}\left[K\left(K_{ij}^A \frac{\partial h}{\partial x_j} + K_{iz}^A\right)\right] - S \quad [5]$$

where x_i (i=1,2) are the Cartesian spatial coordinates, K_{ij}^A are components of a dimensionless anisotropy tensor K^A, S is the sink term, and K is the unsaturated hydraulic conductivity function given by

$$K(h, x, y, z) = K_s(x, y, z)\, K_r(h, x, y, z) \quad [6]$$

where K_r is the relative hydraulic conductivity and K_s the saturated hydraulic conductivity. The anisotropy tensor K_{ij}^A is used to account for an anisotropic medium. The diagonal entries of K_{ij}^A equal one, and the off-diagonal entries zero for an isotropic medium. The volumetric water content and hydraulic conductivity of unsaturated soil, given in Eqs. [5] and [6], are in general, highly nonlinear functions of the pressure head. HYDRUS obtains a solution to Eq. [5] which satisfies every imposed Initial Condition (IC) and Boundary Condition (BC) by using the Galerkin finite element method with linear basis functions (Šimůnek et al., 2012).

Analytical calculations before the advent of computer-aided numerical analysis relied on further simplification of the physical-mathematical model for soil-water movement. Drainage system designs were developed which analyzed only the saturated zone flow and are still considered to provide satisfactory accuracy for many applications. Such simplified analytical approaches exist for both steady- and unsteady-state problems. The primary interest in analyzing unsteady flows in the vadose zone is when accounting for a hydrological event which rapidly changes the position of the water table, such as heavy precipitation. When intransient or slowly changing soil water conditions are more significant, a steady-state approach is preferred. This is the situation of interest for dry season irrigation in Sierra Leone because the water table slowly and steadily lowers throughout the season and precipitation events are infrequent.

One steady-state approach used and analyzed by many practitioners is the Dupuit-Forchheimer (D-F) assumptions. The assumptions are as follows.

- The domain is defined as the space between vertical boundaries which extend from the water table to the impermeable base of the aquifer (Figure 3). The impermeable lower boundary is assumed to be horizontal. The water table is the upper boundary.
- Flow in the domain is assumed to be constant with time, horizontal and driven by a hydraulic gradient equal to the tangent of the water table slope (McWhorter & Marinelli, 1999).

Based on these assumptions the following equation can be written for one dimensional flow in the $x\tilde{z}$-plane using the notation of (Bos, 1994a)

$$K\frac{d}{dx}\left(h\frac{dh}{dx}\right)+R=0 \qquad [7]$$

where h is the height of the water table above the impermeable layer and R is a uniform rate of flow across the water table per unit area. R can be either infiltration (positive, or flow into the control volume) or capillary rise driven by evapotranspiration (negative, or flow out of the control volume).

After integration and solving for integration constants by applying appropriate BCs, the following expression is obtained

$$h = \sqrt{h_1^2 - \frac{(h_1^2 - h_2^2)x}{L} + \frac{R}{K}(L - x)x} \quad [8]$$

where h is the height at any intermediate point, h_1 and h_2 are the known elevations of the steady water table at the two vertical boundaries of the domain under consideration, x is the horizontal coordinate of any intermediate point, and L is the horizontal coordinate of point h_2. To determine the flow rate through a vertical section (q_x) several integration and substitution steps are performed to finally arrive at (Bos, 1994a)

$$q_x = \frac{K}{2L}(h_1^2 - h_2^2) - R\left(\frac{L}{2} - x\right) \quad [9]$$

Ritzema (1994) stated that Hooghoudt and Donnan applied the case of positive R and equal water level heights at the vertical boundaries to analyze drainage ditches. Darcy's Equation is also still applicable to this situation such that the right-hand side of Eq. [2] is equal to the right-hand side of Eq. [9] as follows, using the notation of Ritzema (1994)

$$Ky\frac{dy}{dx} = R\left(\frac{L}{2} - x\right) \quad [10]$$

where y is a vertical plane at distance $x \leq \frac{L}{2}$ from the boundaries. The derivative of x can be moved to the right-hand side, the equation integrated, and appropriate limits substituted yielding

$$q = R = \frac{4K(H^2 - D^2)}{L^2} \quad [11]$$

where D is the elevation of the water level above the impermeable layer at the vertical boundaries and H is the elevation of the water table above the impermeable layer midway between them. This form assumes open drainage ditches which reach from the soil surface to the impermeable layer, such that D is equal to the elevation of the water level in the ditch. In order for this equation to be used for drainage canals and tile drains which do not reach all the way to an impermeable layer, it must be modified to

$$q = \frac{8K_b dh + 4K_t h^2}{L^2} \quad [12]$$

for the case of a two-layered profile where K_b is the hydraulic conductivity below the drain, K_t is the hydraulic conductivity above the drain, h is the height of the water table above drain elevation midway between drains, and d is the equivalent depth. (In the case of one layer, $K_b = K_t = K$).

Introduction of the concept of equivalent depth was necessary because the D-F assumptions fail in the immediate vicinity of drainage conveyances which do not reach all the way to an impermeable layer. Also called effective depth, it represents replacement of the vertical boundary which included the drain, located at a distance D above the impermeable layer, with an imaginary vertical boundary "through which the same amount of water would flow per unit time as in the actual situation" (Ritzema, 1994). As illustrated in Figure 3, this replacement boundary changes the domain with converging, non-horizontal flow at the boundary (A) to an equivalent domain that meets the D-F assumptions at the boundary, with equal flow (B). The length of the substituted boundary (the effective depth) is only equal to D if D=0; i.e., if the drain was located at the impermeable layer.

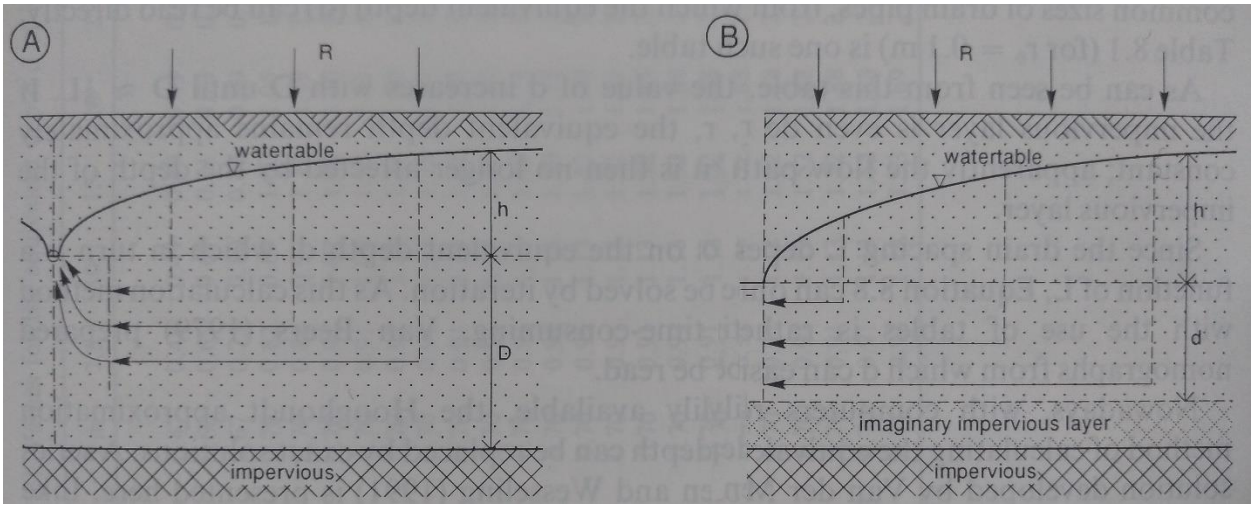

Figure 3. Illustration of the concept of effective depth and Dupuit-Forchheimer boundaries. A combination of horizontal and curvilinear flow (A) is transformed into an equivalent horizontal flow (B) through the use of this concept. After Ritzema (1994), p267.

As previously mentioned, Eq. [12] was developed to analyze the steady-state flow of water between parallel drains. As such, it cannot be directly used in an irrigation analysis. However, Bos and

Wolters (1994) describe what they call the "Inverse Hooghoudt Equation" which Hooghoudt derived from his work on drain tiles. This equation can thus be directly used in the case of subirrigation

$$q = \frac{8K_b d(n-h)+4K_t(n^2-h^2)}{L^2} \quad [13]$$

where *n* is the infiltration head. Infiltration and seepage are used interchangeably in this thesis to discuss the movement of water into the soil through the canal wetted perimeter.

A series of iterative formulae which find an effective depth given drain spacing and hydraulic radius of the drain were developed for tile drains by Hooghoudt and refined by van der Molen and Wesseling (1991) and others (Skaggs, 1999a). Two observations were made about the solution of equivalent depth. First, under the assumption that tile drains flow half full, they have semicircular cross sections and therefore their shape is fully defined by a single measurement, the hydraulic radius. This is not the case for canals which may have triangular, trapezoidal, rectangular, or parabolic cross sections. Eq. [13] calculates the same flow rate for two differently shaped canals having the same hydraulic radius. Second, the hydraulic radius has only a small influence on the solution, reflecting small values of hydraulic radius compared to tile spacing and depth.

A different approach to analyze seepage from open earthen channels was used by Bouwer (1969). He formulated a dimensionless relationship between seepage rate and spatial parameters for three different cases based on a resistance network analog. These included the case where an infinitely permeable layer exists at some distance below the canal and the case in which the canal has a restrictive layer along its wetted perimeter, as well as the case of interest to this investigation which considers an impermeable layer to exist at some depth below the canal. For the latter case, Bouwer briefly discussed the limitations of Dupuit-Forchheimer theory which have motivated the development of concepts such as the aforementioned equivalent depth. Specifically, he found that a relationship derived from D-F assumptions predicts a linear increase in seepage even as the depth to the impermeable layer increases to infinity. Further, the relationship for rectangular canals is exact while for trapezoidal canals

it is inexact, although at impermeable layer depths less than three times the canal bed width, "reasonably accurate solutions can be obtained" (Bouwer, 1969).

Dupuit-Forchheimer assumptions fail in the region near a canal because of curvature and convergence in the flow. To overcome this, other investigators have considered the system in two or more domains. Far away from the canal where D-F assumptions of horizontal flow are valid the flow is calculated according to D-F theory, while in its vicinity other analytical equations have been developed. The regions are then combined to solve the total system flow. According to Bouwer (1969), Dachler developed an equation which requires the use of charts defining the relationship of spatial parameters to a curve factor which is used for calculation of the flow immediately adjacent to the canal. A trial-and-error procedure must generally be used until the flow calculated for the two regions is equal. Such a procedure was undesirable for irrigation design in Sierra Leone considering that better alternatives were available.

Bouwer (1969) further mentioned that Ernst divided the flow system into three component systems. One of these, the vertical component, is only significant when the flow passes through a layer of localized low hydraulic conductivity. The horizontal component is based on D-F assumptions, while the radial component accounts for converging flow near the canal. As described by Bouwer in his Eq. 7, the combined formula developed by Ernst includes eight parameters. Bouwer noted that for this equation, "excellent agreement is obtained with the analog results" for "relatively small values" of depth to impermeable layer and water table depth (Bouwer 1969).

In contrast, Bouwer obtained solutions for a complete range of values of these two parameters, including infinity, using a resistance network analog. He expressed the results in dimensionless graphs in his Figure 7. The figure presents solutions for a single cross-sectional geometry, but directions were given for how to apply the solution to other shapes. Bouwer argued that the geometry of the canal does in fact influence the rate of seepage, with the magnitude of the change dependent on soil and

water table conditions. He stated that the water depth in the center of the canal and the width of the water surface were the two most important factors influencing seepage rate. Further, for any given value of these two parameters he found that the seepage decreases from rectangular cross section to trapezoidal cross section with a minimum at triangular cross-section.

Bouwer (1969) also discussed inclusion of the influence of unsaturated flow in calculations of seepage rate. He presented an equation he had derived which simplifies the unsaturated hydraulic conductivity curve to a step function. Then a layer of flow at the top of the water table with an effective depth and saturated hydraulic conductivity may be used in the calculation of the total flow system instead of the actual height of the capillary fringe. The capillary fringe is a zone of saturated material with negative water potential that exists at the top of the water table. This was yet another example of the use of an effective or equivalent depth boundary substitution.

CHAPTER 4: CONCEPTUAL MODEL

Figure 4 documents a specific canal subirrigation system. As this figure elucidates, the canal examined in this work was distinct from the existing concept of an irrigation canal. An irrigation canal is a water conveyance structure which directs flow from some source, such as a river, to one or more crop fields. The structure discussed in the present work operates as a water application structure. It would operate as the final link in the chain between a water conveyance structure and the crops, or more specifically the soil, in a field. Thus, it may occur as shown in the figure – a structure connected to a water source through pump and pipe – but it may just as easily exist at the end of an irrigation canal. For this reason, no unique name for the structure has been decided upon, other than to emphasize that its purpose is for subirrigation.

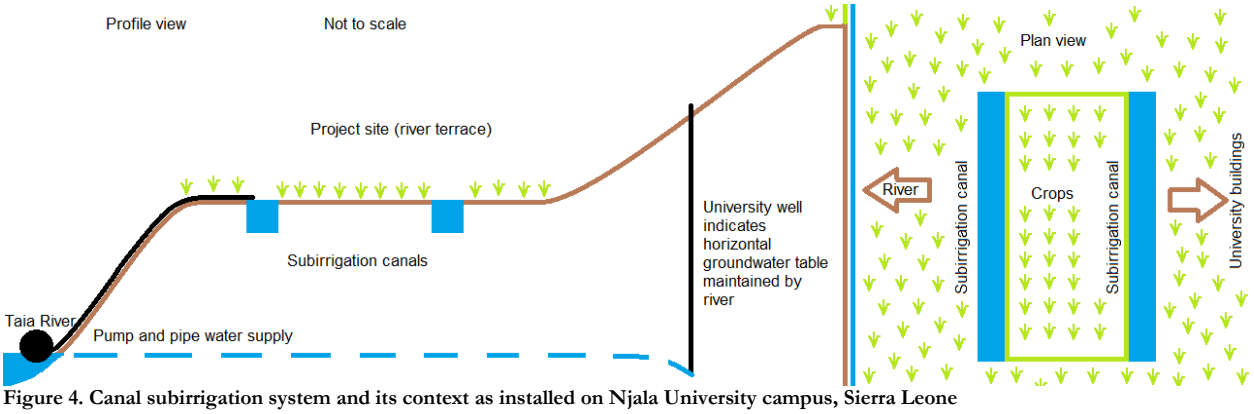

Figure 4. Canal subirrigation system and its context as installed on Njala University campus, Sierra Leone

In the particular system shown in Figure 4, the canals were constructed with rectangular cross section. Yet, in practice, canals cannot or should not always be constructed with a rectangular cross section. The hypothesis that canal geometry affects the water table profile was tested in order to provide practitioners with an analytical equation which remains usefully accurate for various geometries. Bouwer made a strong case for issues with any analytical equation derived from Dupuit-Forchheimer theory. However, the solution he provided seemed too cumbersome for the intended audience. The validity of D-F assumptions for steady-state flow in regions away from the canals has

been well-established. It was hypothesized that Eq. [13] would work well as a base model for which correction factor(s) could be empirically deduced from the parameter ranges of interest using HYDRUS. The equation attributed by Bouwer to Ernst could have been another viable option. However, it was slightly more complex than Eq. [13] and was not explored. Further, although many waterways constructed by humans have a parabolic cross section, this geometry was not considered in the analysis.

Figure 4 can be reduced to only those features relevant for analysis of the generalized canal subirrigation system. A field may have multiple parallel subirrigation canals, but it was only necessary to consider two. Since there is not significant flow within these structures, analysis may be confined to the plane perpendicular to the long dimension of the canals. The resultant conceptual model is shown in Figure 5. The notation used throughout the entire remainder of this thesis is defined according to this figure.

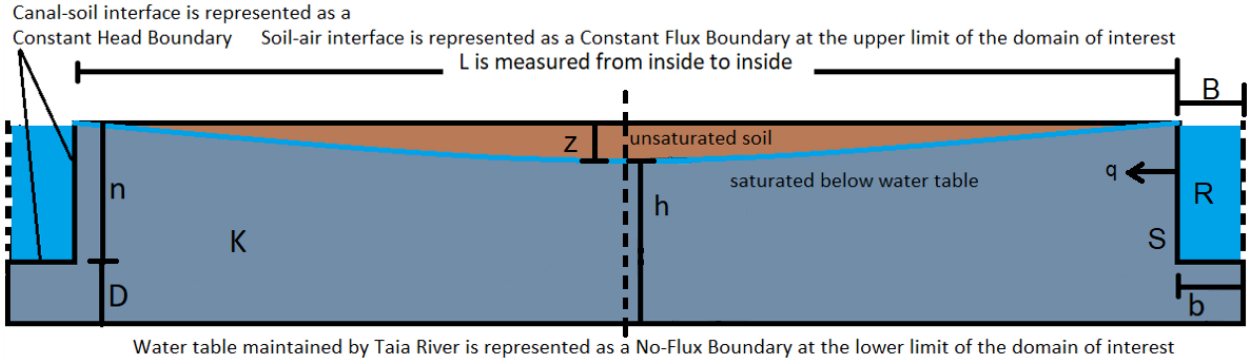

Figure 5. Conceptual model.

In the case of canals, infiltration head (n) is the same as the depth of water in the canal and Hooghoudt's theory relates it to canal spacing (L) and the depth from the bed of the canal to the impermeable layer (D) as given by what will be referred to as the Hooghoudt Equation, modified from Eq. [13] to

$$h = -D + \sqrt{D^2 + 2Dn + n^2 - \frac{qL^2}{4K}} \qquad [14]$$

The irrigating water table profile is always hyperbolic according to Dupuit-Forchheimer theory. The entire curve of a hyperbola can be reconstructed from just three points, and two of these were always fixed by the water level in the canals. So, the depth midway between drains (z) was the third point to be determined, and thereby it was used to represent the entire water table profile in the analyses. Alternatively, when comparing HYDRUS results to values calculated by the Hooghoudt Equation, the elevation from canal bed to the midpoint of the water table (h) was used. These two variables can easily be interchanged using the relationship $n + z = h$ (z is given as a negative number in this work).

Only half of each canal was considered in the analyses which, assuming symmetry, focused on a model centered halfway between canals. Accordingly, b is defined as the half-width of the canal bed, while B is the half-width of the canal at the ground surface. The hydraulic radius of the canal cross-section (R) is the same for half a canal as it is for the full canal. Finally, the slope of the canal bank perpendicular to flow (S) is defined as the ratio of horizontal length per unit of vertical length. All other model parameter units are in length, except saturated hydraulic conductivity (K) which has units of length per time. The meter was selected as the measure of length, while days were selected as the measure of time. As shown in the figure, a single layer system with one value for K was modeled for the sake of simplicity.

CHAPTER 5: CONCEPTUAL METHODS

Analysis of how satisfactorily relatively simple analytic equations compare to a more computationally complex numerical solution of the conceptual model of interest shown in Figure 5 consisted of five parts. Before the question could be examined, the conceptual model had to be implemented in python and HYDRUS using procedures common to all numerical simulation scenarios. Later, the stability and appositeness of the implementation was checked. Once implemented, analyses for the purpose of identifying a single control variable which would adequately represent variation of canal cross-section geometry was performed first. Next, the influence of the variation of this geometry control variable on the water table profile was simulated, along with how it interacted with the model parameters used in the Hooghoudt Equation. Lastly, multiple regression was used to fit analytic equations to the HYDRUS data and identify the best one.

5.1 HYDRUS AND PYTHON SETTINGS

Several simplifications were embodied in the conceptual model given by which were thus also included in the HYDRUS model setup along with the model parameterization, spatio-temporal discretization, and boundary conditions. Layered, heterogeneous, anisotropic alluvial soils were represented as a single, uniform medium. The bottom was represented as a horizontal, totally impermeable layer, the top was represented as a horizontal surface with a single constant demand for water, and symmetry was assumed for the sides. It was assumed that the water table slowly and steadily lowers throughout the dry season and precipitation events are infrequent, thus a steady-state analysis would be appropriate. The other conditions of the model are described next.

Within HYDRUS a 2D–General, Vertical Plane XZ model was selected, with units in meters. All options in the Main Processes and Add-on Modules window were unchecked to obtain a steady state simulation. All other windows up through the Iteration Criteria window were left in their default

settings. In the following window the single-porosity van Genuchten – Mualem model with air entry value of -2 cm was selected (van Genuchten, 2021). Default Sandy Clay Loam properties were selected from the drop-down menu of the built-in soil catalogue. These properties are listed in Table 1. A different set of model spatial parameters was imported for each simulation run using "Import Geometry from Text File." No time discretization was used since the program solved for a steady-state condition, and variation of the spatial discretization was examined as discussed in Section 2 of this chapter.

Table 1. HYDRUS material properties for the van Genuchten – Mualem soil water model.

Name	Qr (-)	Qs (-)	Alpha (1/m)	n (-)	Ks (m/day)	I (-)
Sandy Clay Loam	0.1	0.39	5.9	1.48	0.3144	0.5

In all these HYDRUS simulations the pressure head initial condition (IC) was set to equilibrium from lowest located nodal point. It was assumed that irrigation would begin at the end of the rainy season, as soon as the river flood waters have receded from the soil surface, but before the soil is no longer at field capacity. Further, the IC pressure head of the lowest point was set to a value equal to the elevation of water free surface in the canal above that point. This was critical to achieving convergence for steady state solutions.

Implementation of boundary conditions (BCs) in HYDRUS are shown in Figure 6. No-flux BCs were selected for the lower boundaries of the model. This included every boundary, horizontal and vertical, below the canal beds. A no-flux BC on the bottom horizontal boundary reflects the assumption that in the real world the bottom of the field will either be an impermeable layer, or a water table imposed by the nearby river. In the latter case another assumption is that the vertical boundaries of the river's water table restrict flow, so all water added by irrigation in the project site will "sit" on top of the river's water table. The no-flux BC occurs on the vertical boundaries below the canal beds as a result of the model symmetry apparent in Figure 5. The canal beds and banks were

input as constant head BCs with equilibrium from the lowest located nodal point. The pressure head was set to the value that matched the depth of water in the canal for a given run. The simulated water free surface elevation was set equal to the soil surface elevation for simplicity. The soil surface BC was implemented as a constant flux BC of -0.00315 m/day.

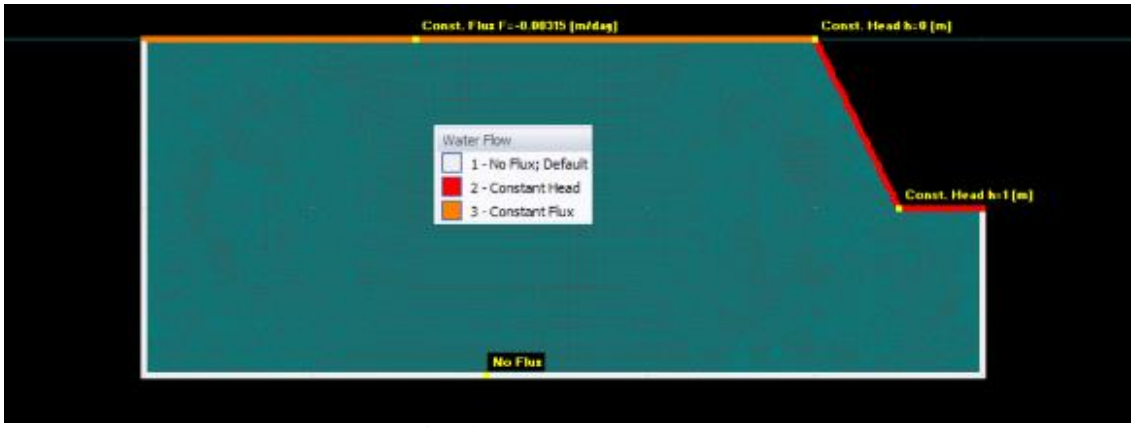

Figure 6. Boundary condition implementation in HYDRUS.

Neither the water table profile nor the elevation midway between drains is a direct output of the HYDRUS program. Outputs do include the final pressure head of each node as well as its coordinates. For this reason, a postprocessing python script was written to read the output files and calculate the water table profile of each HYDRUS simulation run, then plot that data as well as save it to another text file.

Further, in order to facilitate rapid analysis of multiple model representations in HYDRUS, a python-based preprocessing script was developed. A user would enter six lists of desired values: one list for each model parameter D, L, n, b, and S; and, optionally, one list of soil layer boundaries (variable name p). The optional list p was not used in the present chapter. It was used in the site-specific methods documented in Chapter 6, where its use is also discussed.

A flow chart of the preprocessing code is shown in Figure 7. Each of the first five parameter lists must contain either a single entry or the same number of entries as every other list containing more than one entry. The code calculates cartesian coordinate pairs for points which define the

dimensions of the model for each set of entries common to all five lists of parameters, generating a number of output text files equal to the number of entries in the parameter lists. This was accomplished in two steps. First, a for loop iterates through sets of list entries and for each iteration appends the calculated coordinates into a new row in separate x– and z–coordinate arrays which have a number of rows equal to the number of domains. Second, a single data frame is created from each row.

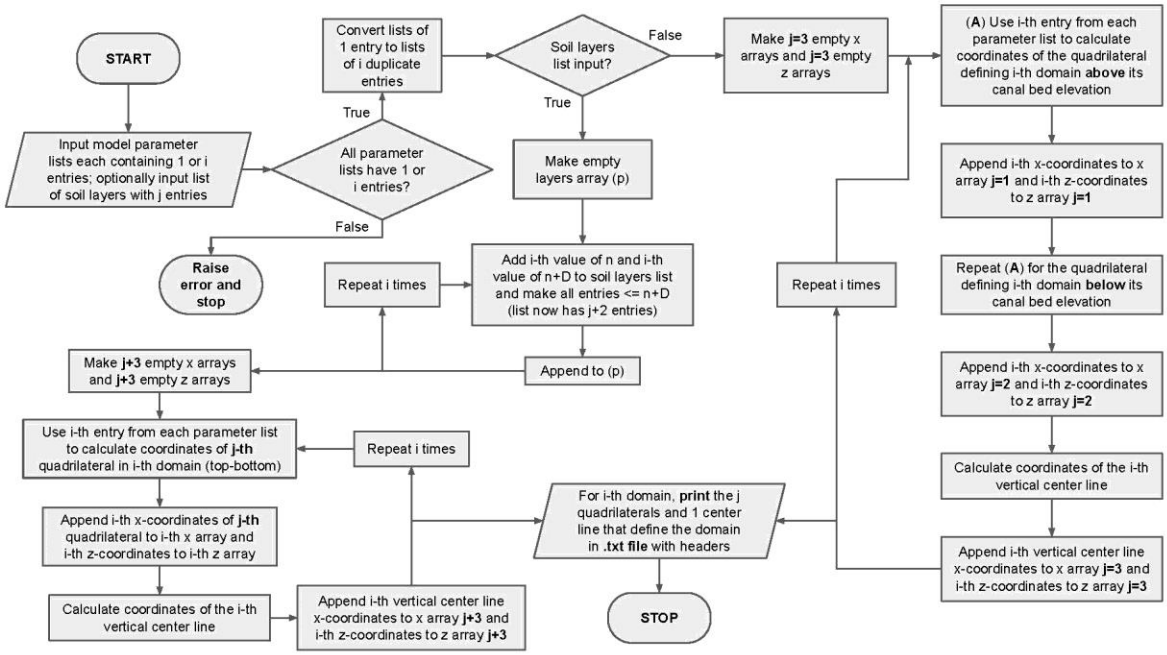

Figure 7. Flow chart describing python preprocessing code.

Each data frame is output to a text file formatted such that HYDRUS correctly interprets it when the option to "Import Geometry from Text File" is selected. Before each set of coordinates the keywords "OBJECT=SURFACE_LINES" are written. This script minimized coordinate calculation errors, defines multiple related models in a single execution, and enabled model definition within HYDRUS to consist of a four-step dropdown menu selection rather than multiple coordinate edits. It also defines a centerline for the program to treat as a surface boundary. This line is populated with

nodes by the program during mesh generation, and the output from these nodes was used in postprocessing the solution.

After a HYDRUS simulation, node coordinates are output in a file which also contains information about edges and other objects which were not relevant to this analysis. Therefore, once the file was read into a data frame in a python postprocessing program, the other information was removed. The pressure head values of the nodes are output in a separate file of ten columns and as many rows as necessary. The python data frame read in from this file had to be rearranged into a single column. Once this was done, that column was connected to the coordinate information, which likewise listed the x–coordinate of each node in a single column and the z–coordinate of each node in a single column. The three columns were used as the three separate dimensional arguments of a python function called ***tricontour*** (Caswell et al., 2021) to interpolate from the data the x– and z–coordinates of the line with a pressure head value selectable by the user. To plot the contour which described the water table profile, zero meters was the value entered.

In order to plot the rest of the model around the water table profile the coordinate data were further manipulated. The HYDRUS output file lists the model definition nodes (i.e., those nodes defined by the user) before it lists the rest of the nodes which make up the spatial discretization of the model. The python code takes advantage of this by requiring the user to enter the number of points defining the HYDRUS domain, then creating a data frame from that many first entries of the file. Coordinates are sorted first by ascending x-values, then divided in half. The first half is sorted by ascending z-values, and the second half by descending z-values. As a result, the plot of the sorted coordinates coherently delineates the model boundary. Model parameters L, n, D, and S are calculated and reported in the title of the plot. The Spyder integrated development environment was used to run the code, which made it easy to save the figures using that program's built-in features. An example is illustrated by Figure 8.

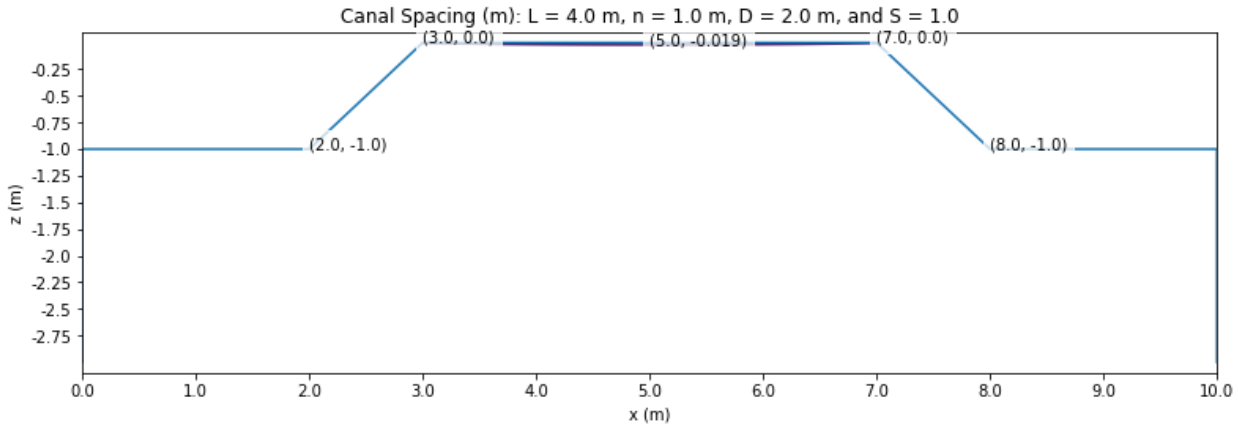

Figure 8. Example of graphical output generated by python post-processing code.

A separate calculation was performed to locate the depth of the water table at the midpoint between canals. This made use of the Lagrange interpolation polynomial function available from the python scipy library (Virtanen et al., 2021). A subset of the node data, the nodes located along the centerline that was input to HYDRUS from the preprocessing code, were used in this calculation. The function conducts nonlinear interpolation between the nodes and is thus more accurate than the ***tricontour*** function, which only performs linear interpolation. A flow chart of the postprocessing code is shown in Figure 9.

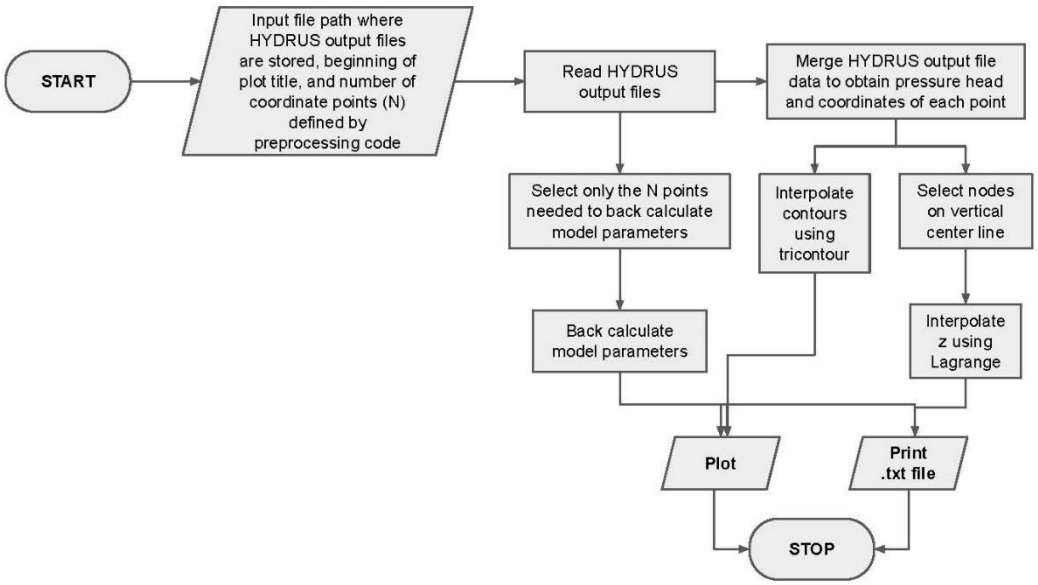

Figure 9. Flowchart of python postprocessing code.

5.2 NUMERICAL STABILITY

Convergence did not occur in the largest simulated models without a larger mean finite element size than used for the smallest models, so the influence on convergence and on solution precision in HYDRUS of user-selected values for the two discretization parameters of target FE size and stretch factor was investigated. At first attempts were made to improve solution precision via FE-Mesh Refinement window options for the centerline and two additional vertical lines a short distance away on either side as shown in Figure 10.

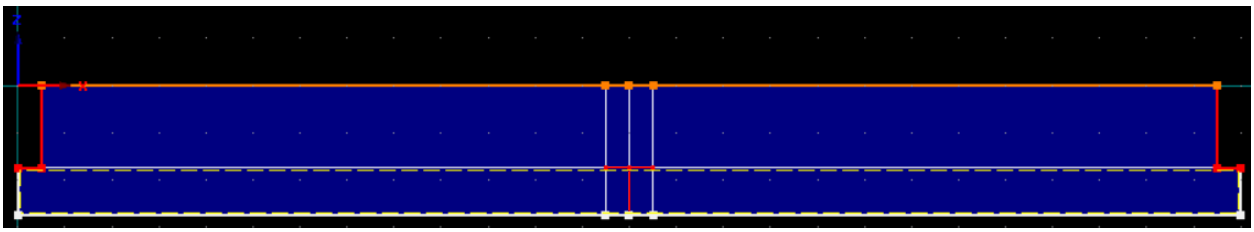

Figure 10. Model geometry created for nonuniform mesh refinement. Lines highlighted in red in center were deleted in some simulations.

This did not have the desired effect: as the spacing between nodes on these lines decreased, the solution value oscillated. Dr. Paul Fischer suggested a uniform spacing rather than refinement on the lines only (cite personal communication, March 2021). Six models were tested with target FE sizes ranging from 0.200 to 0.016 meters and horizontal stretch factors ranging from 4 to 0.251 using this approach (Šimůnek and Šejna, 2009). Uniform mesh refinement achieved the desired effect on solution precision. Table 2 defines the model parameters of these six trials.

Table 2. Six HYDRUS finite element discretization trials with b = 0.5 meters.

Trial Name	Canal Spacing, L (m)	Canal depth, n (m)	Bed to impermeable layer, D (m)	Bank slope, S (m/m)	Area (m²)
A	5	0.75	0.50	0	6.75
B	5	0.50	0.75	0	7
C	5	0.25	0.75	0	5.75
D	5	0.25	0.75	1	6.1875
E	15	1	1	0	31
F	11	1	1	0	23

The results of the convergence trials were used to optimize values for the two discretization parameters in the FE-Mesh Parameters window during the following investigations of canal cross-

section and comparison with analytical flow equations. For each of these investigations a single model length and height was used several times with a series of canal cross-section geometries. The largest mesh area for each model occurred with a triangular canal geometry. A suitably small element size was determined for the trapezoidal model area this created, and then all other canal cross sections for that model length and height were analyzed under the same discretization parameters. The discretization parameters determined for all trials are given in Table 3.

Table 3. Discretization parameters for HYDRUS domain trials.

Trial Name[a]	L = 4	L = 9	L = 11	L = 14	L = 19	n = 0.25	n = 0.5	n = 0.75	n = 1.25	n = 1.5	n = 1.75	D = 0	D = 1	D = 3	D = 4
Area[b] (m^2)	27	42	48	57	72	27	36	40	56	66	75	14	31	65	82
Target FE size (m)	0.035	0.035	0.038	0.042	0.067	0.038	0.038	0.038	0.038	0.038	0.038	0.038	0.038	0.038	0.046
Stretch factor	1	2	2	2	2	2	2	2	2.2	2.2	2.2	2	2	2.4	2.7

[a]Name reflects the value of the domain parameter of interest for that trial (m). [b]Area of the domain, rounded to the nearest m^2, when $S = 3$.

5.3 GEOMETRY

Consider triangular, trapezoidal, and rectangular canals. The hydraulic radius (R) of every one of these geometries may be defined as

$$R = \frac{B^2 - b^2}{2S\left(b + \sqrt{\left(\frac{B-b}{S}\right)^2 + (B-b)^2}\right)} \quad [15]$$

where S, b, and B are defined in Figure 5 (Chapter 4) and Figure 11 (below).

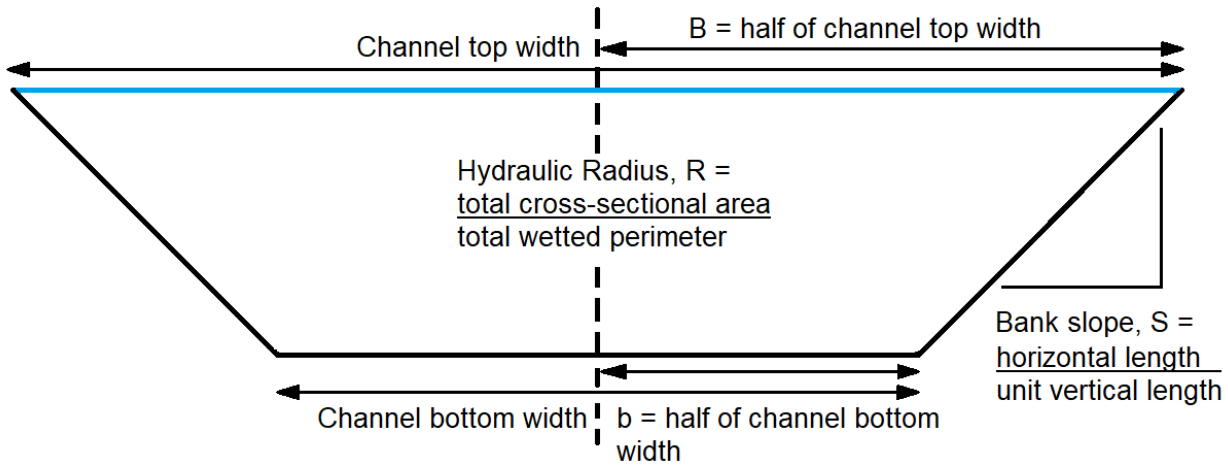

Figure 11. Canal cross-section geometric parameter definition.

Equation $R = \frac{B^2 - b^2}{2S\left(b + \sqrt{\left(\frac{B-b}{S}\right)^2 + (B-b)^2}\right)}$ [15] defines the three parameters which, along with *n,* completely describe the canal cross-section geometries under consideration. These four parameters are collectively referred to as "geometry parameters." The canal spacing (*n*) is accounted for in the Hooghoudt Equation. For this reason, it is not included here, but rather with the other "domain parameters" of canal spacing (*L*) and depth to impermeable layer (*D*) which are analyzed separately. For the geometric analysis only one value for each domain parameter was considered: L = 11 m, D = 1 m, and n = 1 m. However, analysis of other canal depths demonstrated the same results (see Chapter 7 for details).

Physical canals cannot be constructed with negative dimensions, and so the geometric parameters are constrained to be positive. Accordingly, for a given value of *n,* the geometry parameters in fact over-define the canal cross-section. That is, the values of only two of the parameters may be freely selected; upon this, the value of the other two are required to satisfy

$$B = b + S \times n \qquad [16]$$

as well as Eq. [15] and the positivity constraint.

Thus, to change the geometry of a canal of a given depth, only one geometric parameter may be kept constant. The other three parameters will always vary proportionally to one another according to Eq. [15] and as shown in Figure 11. So, it was difficult to *a priori* designate only one of the geometric parameters as the primary independent variable. However, a single, primary independent variable – a control variable – was desired for simplicity of analysis. A single control variable would enable irrigation designers and practitioners in developing countries to apply the results of this study quickly and easily in their specific context. If one of the geometric parameters could be identified as having a greater influence on the location of the midpoint water table depth than the others, that would serve as the most logical candidate for a control variable.

Each geometric parameter was compared to the others with regard to its effect on the location of the midpoint water table depth (z). The comparison was not straightforward because of the interdependence of the parameters. Early on the decision was made to leave one parameter constant in these simulations. The other three parameters were then treated as the control variable one by one, and the resulting variation of z was analyzed. As a result, all four parameters served as the control variable three times; each time with a different one of the other three parameters held constant.

Akkuzu et al. (2007) recorded water depth (n in this work), water surface width (B), and wetted perimeter (P) for trapezoidal tertiary irrigation canals in Turkey in their Table 3. From these values it has been calculated that all canals had bed widths (b) which ranged from approximately 0-1 m. Further, all canal bank slopes (S) but one were calculated to range from $S = 1$ to 1.7. Canal bank slopes should range from no steeper than $S = 0.5$ in alluvial soil and hard compact earth to no steeper than $S = 2$ in sandy loam, according to Table 34 of FAO (Coche et al., 1992). Slightly stricter minimum slopes are recommended by (Bos, 1994b) in his Table 19.3 where slope groupings are based on the Unified Soil Classification System.

In consideration of these recommended canal bank slopes, the maximum S analyzed was 3 (three horizontal length units to one vertical). At that slope, the top width of a one-meter-deep triangular canal ($b = 0$m) would be six meters. Given the goal to be relevant for field work, and the belief that practitioners would not be likely to dig a canal wider than six meters, the maximum value of b and B used in the analysis were both three meters. The minimum values used for these three parameters were a ratio of zero for S and zero meters for b and B. These values gave a minimum R of zero meters and a maximum of 0.750 m.

5.4 DOMAIN

Upon determination of the most significant geometric parameter, the interactions of the domain parameters with it were analyzed with regard to the resulting variation of the water table

profile. A range of domain parameters were selected which attempted to approximate average environmental conditions in the regions of Sierra Leone thought relevant. Table 4. Values for domain parameters. lists the values of the parameters of this domain. For each simulation, the values referred to as the "default" domain were assigned to the two parameters which were not the parameter of interest. In other words, domain parameters were varied one at a time while keeping the others constant. For each combination of domain parameters, seven canal cross-section geometries were simulated by varying S from 0-3 in increments of 0.5 m/m.

Table 4. Values for domain parameters.

Domain parameter	Canal spacing, L	Canal depth, n	Depth from canal bed to impermeable layer, D
Minimum (m)	4	0.25	0
Default (m)	11	1.00	2
Maximum (m)	19	1.75	4
Count	5	7	5

In the last row of the table, the number of different values tested for each domain parameter is listed. For each of five different canal spacings, seven different canal depths, and five different impermeable layer depths, the same seven canal cross sections were simulated. However, the default domain was not triple counted: $L = 11$, $n = 1$, $D = 2$ m was only numerically solved once for each S, not three times. Thus, a total of 105 domains were evaluated. Only three simulations could not be made to converge, resulting in 102 numerical solutions to analyze.

5.5 REGRESSION

The final conceptual analysis conducted was a comparison of data calculated by analytical equations to those calculated numerically by HYDRUS. Several linear and nonlinear regression models, listed in Table 1, were tested. The goal was to find a model that would calculate values within one centimeter of the numerical solutions. If several such models could be found, the simplest model would be preferred. A simple model with only a few parameters would allow quick and easy calculations to be performed by practitioners in the field.

Table 5. Regression models.

Model Name[a]	Equation[b]
L1	$\beta_0 \mathrm{H}$
L2	$\beta_0 + \beta_1 \mathrm{H}$
L3	$\beta_0 + \beta_1 S + \beta_2 \mathrm{H}$
L4	$\beta_0 + \beta_1 S + \beta_2 S^2 + \beta_3 \mathrm{H}$
N10	H, where $\hat{D} = \beta_0 D$
N20	H, where $\hat{D} = \beta_0 D$ and $\hat{L} = \beta_1 L$
N21	$\beta_2 S + \mathrm{H}$ where $\hat{D} = \beta_0 D$ and $\hat{L} = \beta_1 L$
N30	H, where $\hat{D} = \beta_0 D$, $\hat{n} = \beta_1 n$, and $\hat{L} = \beta_2 L$
N31	$\beta_3 S + \mathrm{H}$, where $\hat{D} = \beta_0 D$, $\hat{n} = \beta_1 n$ and $\hat{L} = \beta_2 L$
N22	$\beta_2 S + \beta_3 + \mathrm{H}$, where $\hat{D} = \beta_0 D$ and $\hat{L} = \beta_1 L$
N32a	$\beta_3 S + \beta_4 + \mathrm{H}$, where $\hat{D} = \beta_0 D$, $\hat{n} = \beta_1 n$ and $\hat{L} = \beta_2 L$
N32b	$\beta_3 S + \beta_4 S^2 + \mathrm{H}$, where $\hat{D} = \beta_0 D$, $\hat{n} = \beta_1 n$ and $\hat{L} = \beta_2 L$
N33	$\beta_3 S + \beta_4 S^2 + \beta_5 + \mathrm{H}$, where $\hat{D} = \beta_0 D$, $\hat{n} = \beta_1 n$ and $\hat{L} = \beta_2 L$
N90	$\hat{D} = (\beta_0 + \beta_1 S + \beta_2 S^2) D$, $\hat{n} = (\beta_3 + \beta_4 S + \beta_5 S^2) n$, *and* $\hat{L} = (\beta_6 + \beta_7 S + \beta_8 S^2) L$

[a]L = linear, number = number of coefficients to be fitted, linear multiple regression. N = nonlinear, first digit = number of coefficients within Hooghoudt Equation to be fitted, second digit = number of external coefficients to be fitted, by nonlinear multiple regression. The sum of the two digits is the total number of estimated coefficients in the nonlinear regression. [b]Where H is the Hooghoudt Equation given by Eq. [14], $\boldsymbol{h = -D + \sqrt{D^2 + 2Dn + n^2 - \frac{qL^2}{4K}}}$.

Building regression models one coefficient at a time creates nested models; that is, each model is exactly the previous model with one new term added. This allows formal comparison of the models using the F-test. This test determines whether the additional term had a significant influence on lowering the variance between the model and the data. Models L1 through L4 are nested, as are models N10 through N90. Not every nonlinear model in the latter list exists in the same nest, however. Four distinct pathways emerge in the middle of the list. One nested set option is N10, N20, N21, N22, N32a, N33, and N90. The second major set of nested models is N10, N20, N30, N31, N32a, N33, and N90. The third and fourth options are identical to the first and second, respectively, except for the replacement of N32a by N32b. F-tests are included in Appendix A.

CHAPTER 6: SITE-SPECIFIC METHODS

Analysis of how the proposed irrigation system would work in the real world consisted of two parts. First, a trip was taken to Njala University, Mokonde, in Sierra Leone, in order to collect physical data. A site located near the Taia River on university-managed farmland had been selected for analysis, and a pilot-scale irrigation system installed. Upon returning to the United States, the physical data was analyzed and incorporated into a HYDRUS model. A worst-case scenario was then simulated, and the predicted performance of the irrigation system examined.

6.1 DATA COLLECTION

The trip to the project site began in May 2021, at the end of the dry season in Sierra Leone. It lasted for 29 days during which rains occurred approximately every other day. During this time the river was farther than three meters below the ground surface of the field although it has historically flooded the location at the height of the rainy season. Figure 12 illustrates at the site two vertical-walled trenches had been dug, approximately parallel to the river, and parallel to one another with $L = 5.76$ m. The canal which was farther from the river is referred to as F, while the canal which was closer to the river is referred to as N. Both canals were approximately one meter wide and one meter deep. Appendix B illustrates soil profiles encountered at the project site.

Figure 12. Irrigation canals at project site.

Values of saturated hydraulic conductivity were determined via the inverse auger hole method (van Hoorn, 1979), using the hand auger described in a following paragraph. The tests were conducted at two depths within and near each canal, F and N, and three depths midway between the canals, referred to as C. A hole which had been bored as deep as the auger could reach indicated three soil layers, not including topsoil. As shown in Figure 13, the hole was located approximately 70 cm away from the midpoint, toward the far canal. Thus, saturated hydraulic conductivity was tested at depths that aligned with these layers (approximately 30, 100, and 130 cm), also shown in Figure 13.

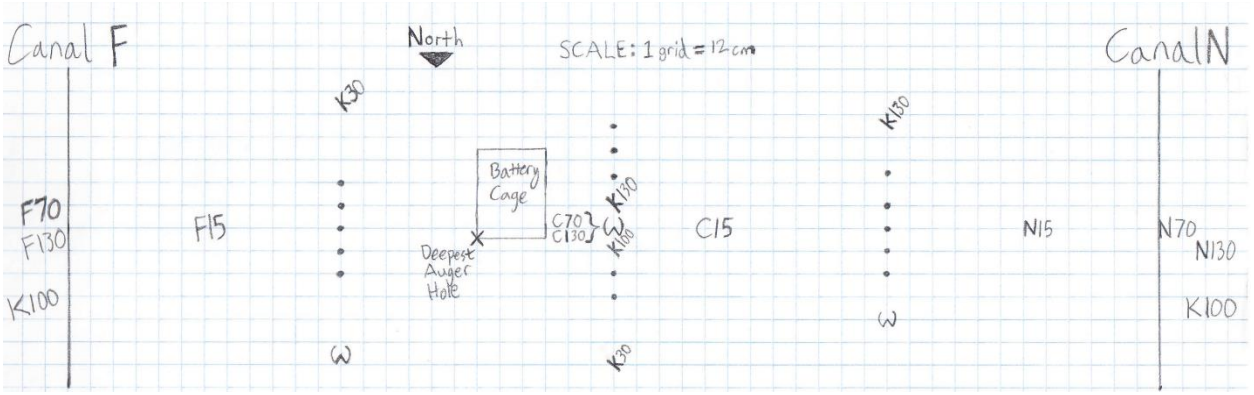

Figure 13. Map of the locations of field instruments. X = deepest auger hole, • = tensiometer location, W = observation well, K = hydraulic conductivity test location, N, C, and F = soil core sample location, |= canal bank.

In addition, soil samples were collected via Eijkelkamp core rings taken from three depths at each canal and midway between them (C, F, and N; locations noted in Figure 13). In Chapter 8, each sample is identified by its location letter followed by the depth at which it was collected (15, 70, and 100 cm). These three sample depths were selected to capture site conditions in the crop root zone, approximate center of the canal walls, and in the canal beds. Cores taken from midway between the canals were formed of disturbed soil excavated at the desired depth using the hand auger. Soil was then repacked into a sample ring, with care taken to both represent only the layer found at the depth of interest and to try to recreate the bulk density of the undisturbed soil. Samples were analyzed for particle size distribution, bulk density, and moisture retention, and the values were input to a HYDRUS simulation of the irrigation experiment.

Particle size analysis was conducted by the hydrometer method in the Quality Assurance laboratory of Njala University, located in Mokonde, Sierra Leone. Arrangements with the lab were not made until the end of the trip, and the trip ended before the analysis was performed. In addition, due to a lack of experience with the hydrometer method and not realizing there are several variations in use, the specific method was not verified while in-country. Through communication with the lab after the fact, to the best of our knowledge the procedure created and subsequently improved by Bouyoucos (1962) was used to obtain the hydrometer readings. The only known modification was that the

dispersive agent used was composed of 40g sodium hexametaphosphate and 10g of sodium carbonate dissolved in 1L water.

According to (Ashworth et al., 2001), several updates to the hydrometer method have taken place since Bouyoucos' 1962 publication. Since then, researchers have shown that the measurement originally prescribed to occur at two hours overestimates the amount of clay in the sample, and that the best time for this second measurement is after six hours. Others have shown that temperature correction is unnecessary when a control sample at the same temperature is measured with the rest. In this case, the hydrometer reading of the control is simply subtracted from each sample reading before the conversion calculation. The control is a volume of water with the same concentration of dispersing agent as the samples, but which contains no soil. The lab in Sierra Leone took second measurements at two hours.

A sand suction table was constructed based on the design found in (Rashid-Noah, 1981) to measure moisture retention curves of the soil samples. Theory and design of the apparatus elucidated in that dissertation were followed, with the following modifications. One standard Sierra Leonian sink (34 x 40 x 14 cm) was installed on a frame approximately 1.2 m tall. A three-foot length of clear, flexible PVC tubing (1¼" outer diameter, 1" inner diameter Tygon) was attached to the end of the pipe that came with the sink using tile tape. The bowl of the sink was filled with three layers of sand. The bottom layer (approximately 6 cm) was coarse sand that passed through a 1 mm sieve. The ~5 cm deep middle layer was sand that passed through a medium sieve. The top layer was fine sand which passed through a 150-micrometer sieve; this layer was 0.4 cm thick. The tubing was fastened to the frame at the same level as the surface of the sand. Water was poured in until all of the sand was saturated, and the entire apparatus was full. A picture of the setup is shown in Figure 14.

Figure 14. Sand suction table constructed from a standard sink. Soil samples shown on left.

Nine soil cores collected from the project site for the purpose were placed in a tub with water that reached approximately one-quarter of the core height. There were three sizes of cores, so this was only approximate. After a day the water level was raised to the top of the shortest core and maintained for one more day. The surfaces of all cores appeared saturated at this point, so the cores were removed from the tub, weighed, and placed on the sand suction table as shown in Figure 14. The samples were covered with a plastic bag that was taped around the edges of the bowl of the sink, to minimize evaporation, but was not airtight, to allow the suction of the apparatus to work properly. The samples were weighed periodically to determine the change in moisture content, and then the height of the tube outlet was adjusted downward to increase suction. This analysis took the longest time out of all those mentioned, and time was running out before the trip ended. For this reason, measurement of the oven-dry weights of the soil cores was forgotten.

Prior to the trip, a hand-powered auger was constructed (pictured in Figure 15). This consisted of a commercially-available two-inch earth auger bit with 7/8" pin connection attached to half-inch threaded, galvanized pipe drilled through one end to fit the pin of the auger head. One-foot sections of pipe were connected on either side of a galvanized tee, and this completed the tool. It could be operated at a height of 55", 69", or, if both the two- and four-foot sections were threaded together and pinned to the auger head, it could reach approximately 95" (240 cm).

Figure 15. Hand-powered auger.

Two kinds of instruments for collecting long-term data were brought and/or assembled on the trip. The first of these was a tensiometer. In total, fifteen tensiometers were constructed based on the work discussed in two publications. The design of (Cahn and Chambers, 2019) was followed exactly for four of the tensiometers, while the other eleven were modified in that a hole was bored through each rubber stopper and clear, flexible tubing installed (1/8" ID, 1/4" OD Tygon S3 E-3603). These tubes were connected to MXP5100DP pressure transducers and circuitry in a slight modification to Thalheimer's (2013) design. Only eleven tensiometers were electronically monitored because at the time of purchase only eleven pressure transducers were available.

Motorcycle batteries were used to power the tensiometer electronics. These were housed in a five-gallon Jerry can for protection from the elements. One deviation from Thalheimer's (2013) design was lack of solar powered recharge. No means was available to secure the small solar panels intended for this task. The ready availability of motorcycle batteries and off-site charging capacity were thought likely to provide more reliability.

The other significant deviation from Thalheimer's (2013) design was that sensors were connected to circuit boards in sets of three and one set of two, with each set sharing one power supply and one ground, to reduce the number of wires running from the Arduino Uno microcontrollers to the sensors. Tubing and wiring were completed before the trip to Sierra Leone, which left inflexibility in the location of the sensor circuits. These could not be contained in the Jerry can with the batteries for protection because then they would not reach to the tensiometers, which were installed in a layout inspired by (Bosch et al., 1994), reported in Figure 13. Instead, these circuits were placed in plastic water bottles and fastened to stakes a short height above the ground.

The second type of data logger brought onsite was Onset Computer Corporation's HOBO U20L-04. These loggers measure pressure and temperature and are intended for use in water depths up to 13 feet. Observation wells were installed on the project site as shown in Figure 13. Twenty-foot

lengths of two-inch PVC were purchased in Sierra Leone for this purpose. The pipe was cut into two three-meter-long sections and one 2.7 m length, based on the material available. Holes were drilled the length of the pipe to provide connection to the groundwater at every depth. The location of each observation well was bored using the two-inch auger and working the tool as far down as it would go, approximately 95 inches. The pipe was inserted into the hole as far as it would go by hand, then pounded down farther using a hammer. Twenty to thirty centimeters of pipe was left above the soil surface. Holes were drilled in 2" end caps and fitted with wire from which a Hobo logger was hung. Then the end caps were placed on the well openings. Some pictures of the instrument setup are included in Appendix B.

6.2 MODEL IMPLEMENTATION

The optional list of soil layers included in the python preprocessing code was implemented for the simulation of the project site. The list of soil layer boundaries (p) is independent of the other lists and is used for every domain generated. Each entry in this list represents the lowest z-coordinate of its respective soil layer. It was used to represent the free water surfaces of the canals as lower than the ground surface as well as to represent multiple soil layers.

A HYDRUS simulation was conducted with the goal of estimating a worst-case cropping scenario using the sampled data. Again, a 2D–General, Vertical Plane XZ geometry was selected, with units in meters. This time, however, the default selection of Water Flow in the following window was unchanged so an unsteady-state simulation was performed, which was necessary since the complexity of multiple material properties prohibited a steady-state solution. In the Time Information window, Final Time was set to 180 days, the Initial Time Step was set to 1×10^{-6}, Minimum Time Step = 1×10^{-10}, Maximum Time Step = 1 day, Time-Variable Boundary Conditions was selected, and the Number of Time-Variable Boundary Records = 10. Importantly, the default single Print Time (Count = 1) remained unadjusted in the Output Information window. This was critical for the python post-

processing code to work properly. In the Iteration Criteria window, Maximum Number of Iterations was set to 100. Again, the single-porosity van Genuchten – Mualem model with air entry value of -2 cm was selected. All other parameters in the windows prior to the Water Flow Parameters window were left in their default settings and values.

Table 6 lists properties of the ten materials added to the domain. Nine of them were simulations of the soil samples whose properties had been measured at the project site (see Chapter 8 for all the values). The predictions of the van Genuchten – Mualem soil hydraulic model parameters for each sample were calculated by the Neural Network Prediction subroutine built into HYDRUS, selectable in the Water Flow Parameters window, based on the measured texture percentages and bulk density for each sample. Values of saturated hydraulic conductivity calculated by the subroutine were different than those measured, so the measured values replaced the neural network predicted values. The mean of measured K values was larger than of predicted K values, so the substitution gave a more conservative simulation. The tenth material was the HYDRUS default Sand, which has the highest K value of the program's defaults. It was used in a layer from two to ten meters deep in the simulation, where soil properties had not been measured. In addition, the HYDRUS default Sandy Clay Loam properties listed in Table 1 are reprinted here for ease of comparison. Two thirds of the samples exhibited lower K than the Sandy Clay Loam used in initial theoretical analysis with HYDRUS.

Table 6. Properties of the ten materials composing a numerical simulation of the project site.

Name	Qr (-)	Qs (-)	Alpha (1/m)	n (-)	Ks (m/day)	I (-)
C15	0.0513	0.5181	4.16	1.5893	0.143	0.5
C70	0.0576	0.446	2.35	1.4552	0.119	0.5
C130	0.0676	0.4485	1.48	1.4585	0.423	0.5
F15	0.0545	0.4289	3.11	1.6286	0.143	0.5
F70	0.0722	0.422	1.94	1.363	14.54[a]	0.5
F130	0.0781	0.4131	1.59	1.3433	0.313[b]	0.5
N15	0.0674	0.4496	1.73	1.4401	0.143[c]	0.5
N70	0.0742	0.5	1.88	1.4185	0.111	0.5
N130	0.0495	0.428	3.68	2.0519	0.203	0.5
Sand	0.045	0.43	14.5	2.68	7.128	0.5
Sandy Clay Loam	0.1	0.39	5.9	1.48	0.3144	0.5

[a]Average of the two K values measured for K100 in Table 22. [b]Average of K values for C130 and N130. [c]Average of K values for C15 and F15.

Nine values for K were used instead of fewer average values because of the variability of soil properties throughout the project site. This is discussed in more depth in Chapter 9, Section 3. It was desirable to use each measurement in association with its location in the site. To model this, the HYDRUS domain above 2 m deep was divided vertically into three sections and horizontally into three sections as shown in Figure 16. Each of the nine regions thus created encompassed one of the nine points where a soil sample was collected, and the entire region was assigned the texture, bulk density, and K of its respective sample. Two soil sample locations did not have an associated K measurement, so each of these was assigned an average of the K measured in association with the other two samples collected at the respective depth as indicated in Table 6. A horizontal average was used because soils are more homogenous in this direction than vertically. The abrupt transitions between regions in the HYDRUS model contributed to a conservative analysis because sharp soil property boundaries restrict flow.

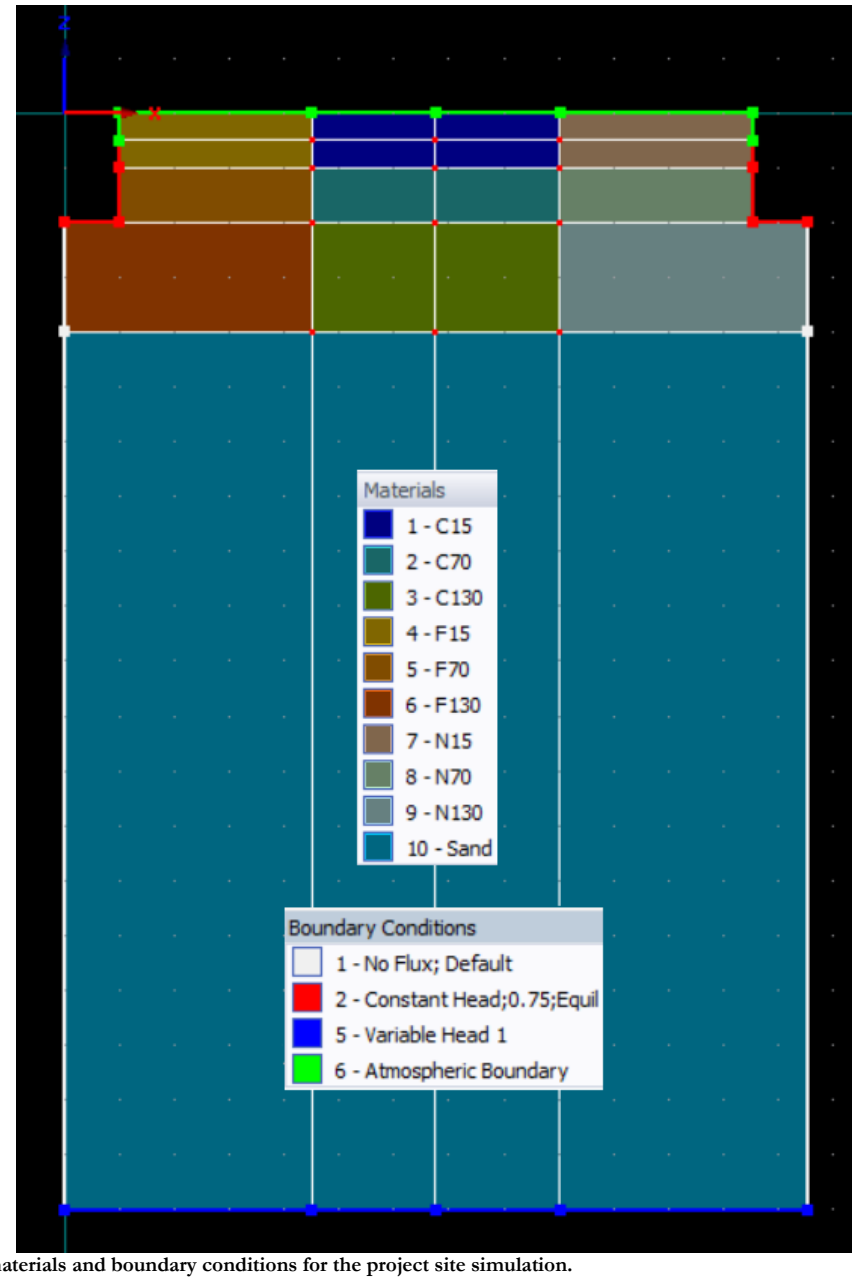

Figure 16. Domain materials and boundary conditions for the project site simulation.

During the course of an irrigation season, it is likely there will be occasions when the pump will not work or for some other reason the water level in the canals will drop. With this in mind, the canals were simulated at three quarters capacity with a constant head Boundary Condition (BC) of Equilibrium from Lowest Node, which had a value of 0.75 m. The quarter of a meter above the free water surface had the same atmospheric BC as the upper, horizontal surface of the domain. The properties of the atmospheric BC are edited in the Time Variable Boundary Conditions window that

appears after the Water Flow Parameters window if Time-Variable Boundary Conditions is selected in the Time Information window. In this window, the value of hCritA for each row was set to 300 m per (Rassam et al., 2003). This constrains the simulation so that it does not create an unrealistically large water tension on the boundary in order to maintain the constant flux value of -0.008 m/day which was entered in the column called Evap. in each row as well. All rows of the Transp. column were set to zero, as the value entered in Evap. was obtained from literature which presented values of evapotranspiration and thus accounted for both evaporation and transpiration.

The value of –0.008 m/day was, in fact, an overestimation of worst-case evapotranspiration. (Kling et al., 2017) provided a map of annual values at the regional scale, which included 14 countries in West Africa. When the total annual evapotranspiration was divided by 180 days, representing the dry season, this estimate was obtained. Clearly this is an overly conservative number because evapotranspiration also occurs during the rainy season. However, given the variability of weather patterns and the influence of climate change, the value does not seem too unreasonable of a margin over the value of -0.006 m/day measured in one study during the dry season in the same region (Mbagwu, 1985).

The major difference between the worst-case scenario and the previous theoretical simulations was that the bottom of the domain had a variable head BC instead of a no-flow BC (Figure 16). This represented the decrease in water table maintained by the Taia River as the dry season progresses. For the first row of column Var.H-1 in the Time Variable Boundary Conditions window, a value of 9.75 m was entered so that this BC matched the initial condition of Equilibrium from Lowest Node = 9.75 m. Subsequent rows were each decreased by 1 m such that the value entered in the tenth row was 0.75 m, representing the river at its lowest stage at the end of the dry season. Target FE size was set to 0.050 m with a Stretch Factor of two.

CHAPTER 7: CONCEPTUAL RESULTS

Results of the conceptual analyses are reported in the same order as the discussion of conceptual methods for ease of comparison. Python and HYDRUS implementation procedures generated large data sets. Uniform mesh refinement provided acceptably convergent solutions, while nonuniform refinement did not. Geometric analysis indicated that canal bank slope should be selected as the control variable representative of cross-section geometry. Although the domain parameters interacted with the influence of S on z, this effect was relatively small. Statistical analysis of various multiple regression models indicated satisfactory fit was achieved by a constant S-coefficient included with other model terms mirroring Hooghoudt's equivalent depth. This correction appeared to be different for canals than that developed for tile drains.

7.1 HYDRUS AND PYTHON SETTINGS

Python and HYDRUS outputs were too large to place within the main text of this work, so they are provided in the appendices. The full python preprocessing code is included in Appendix C. The value of L, n, D, S, b, B, R, and z for each HYDRUS simulation are reported in Appendix D. Key data are discussed at length throughout the remainder of this section. The full python postprocessing code is available in Appendix E.

7.2 NUMERICAL STABILITY

Table 7 reports the results of nonuniform mesh refinement in the model. The oscillatory variation of the solutions which were calculated at decreasing FE sizes was considered unacceptable. The values would vary by several millimeters and sometimes even by more than a centimeter. Instruments are readily available to practitioners which are capable of measurement to millimeter precision, so this was the precision demanded of HYDRUS solutions.

Table 7. Nonconvergence of nonuniform mesh refinements in a domain where $L = 25$, $n = 1.75$, $D = 1$, $S = 0$, $b = B = 0.5$ (m).

FE Refinement (m)	z (m) [a]	z (m) [b]	z (m) [c]	z (m) [d]	z (m) [e]
0.220	0.3268	0.3273	0.3203	0.3203	0.3273
0.100	0.3268	0.3274	0.3204	0.3210	0.3210
0.050	0.3267	0.3270	0.3205	0.3209	0.3209
0.030	0.3261	0.3274	0.3209	0.3200	0.3200
0.010	0.3264	0.3271	error[g]	0.3212	0.3208
0.008	0.3258	0.3271	-	0.3212	0.3202
0.005	error[f]	error[f]	-	0.3209	0.3203

[a]FE Refinement, as indicated, occurs on centerline for all five tests, while in the rest of the domain the program's default target FE size of 0. m was used. [a]has no additional refinement lines. All other tests have two additional vertical "sidelines" 0.5 m left and right of centerline. [b]No refinement on sidelines. [c]Same refinement on all three lines. [d]All three lines began with refinement = 0.220 m. On following steps, sideline refinement was one step behind centerline refinement until sideline refinement = 0.050 m – i.e., when centerline refinement = 0.050 m, sideline refinement = 0.100 m. [e]Sideline refinement was one step behind centerline refinement until sideline refinement = 0.030 m. [f] "Error No. 12 during the generation of 2D FE-mesh. Fundamental triangulation failed…" [g]Solver error.

Uniform mesh refinement returned acceptably precise solutions documented in Table 8-Table 13. In these tables the number of elements is reported as number of nodes. Each table illustrates the results of refinement trials in a single model. The tables are abridged as reported below. For the full dataset see Appendix F. Several interesting results emerged.

Table 8. Uniform mesh refinement in Domain A ($L = 5$ m, $n = 0.75$ m, $D = 0.5$ m, $b = 0.5$ m).

Target FE size (m)	Stretch Factor	Nodes	z (m)
0.200	1	334	-0.0306
0.100	1	1111	-0.0302
0.050	1	4444	-0.0301
0.040	1	7630	-0.0301
0.030	1	11876	-0.0301
0.021	1	22448	-0.0300
0.020	1	-	no solution
0.020	1.1	21909	-0.0300
0.020	1.5	16232	-0.0301
0.020	1.9	13054	-0.0300
0.020	4	6558	-0.0300

First, as had already been experienced, at large target FE sizes the numerical solution tended to be up to several centimeters different than that calculated for small FE. FE smaller than a certain maximum size would all return the same value to sub-millimeter significance (±0.0001 m), no matter how much smaller they became, until the program failed to converge. This value was taken to be the true numerical solution for the given domain. References to "accuracy" within this discussion refer to how close to this value the numerical solution was under given conditions.

Table 9. Uniform mesh refinement in Domain B (L = 5 m, n = 0.5 m, D = 0.75 m, S = 0, b = 0.5 m).

Target FE size (m)	Stretch Factor	Nodes	z (m)
0.200	1	370	-0.0324
0.100	1	1116	-0.0320
0.050	1	4640	-0.0318
0.040	1	7254	-0.0318
0.040	1.5	4632	-0.0318
0.040	2	3512	-0.0318
0.040	2.5	2858	-0.0317
0.040	3	2310	-0.0317
0.020	1	26367	-0.0318
0.020	1.5	20463	-0.0318
0.020	2	14907	-0.0318
0.020	2.5	11087	-0.0318
0.020	3	9231	-0.0318
0.016	3	13591	-0.0318

A second interesting result was the magnitude of the range in the number of elements of a given model discretization which would return the true value, once the FE size threshold was satisfied. The difference between maximum and minimum number of elements was anywhere from 24057 reported in Table 9 to 5770 reported in Table 12. There was also variation between these trials in the actual values of the maximum and minimum number of elements. Table 9 had the largest maximum at 26367, while Table 12 had the smallest maximum of 11979. Table 10 reports the smallest minimum (1248), and Table 13 reports the largest minimum (9198). The magnitude of the range and maximum number of elements in each model before convergence failed strongly correlate with the area of the model (Table 2 in Chapter 5).

Table 10. Uniform mesh refinement in Domain C (L = 5 m, n = 0.25 m, D = 0.75 m, S = 0, b = 0.5 m).

Target FE size (m)	Stretch Factor	Nodes	z (m)
0.050	1	3901	-0.0394
0.050	3	1248	-0.0392
0.040	1	5394	-0.0394
0.040	3	1807	-0.0392
0.030	1	7882	-0.0394
0.030	3	3324	-0.0393
0.020	1	24071	-0.0394
0.020	3	7705	-0.0393
0.019	1	-	no solution
0.019	2	13689	-0.0394
0.019	3	8338	-0.0393
0.019	4	6419	-0.0393
0.018	2	-	no solution
0.018	3	9347	-0.0393
0.018	4	-	no solution

Third, convergence was shown not to be only affected by the size of the elements. Table 12 and Table 13 show this the most clearly, but Table 10 does as well. What is interesting about Table 12 is that for certain target FE sizes and stretch factors, convergence was achieved through deletion of certain interior boundary lines. The last two rows of Table 12 are identical in the discretization parameters listed. However, for the penultimate row the model's middle horizontal line was deleted, while for the last row the lower vertical centerline was deleted instead (see Figure 10 in Chapter 5 for definition of these two lines). Table 13 shows that nonconvergence does not merely occur at endpoints of a range of values for the stretch factor. Rather oddly, the model lacks convergence in patches throughout the otherwise suitable range.

Table 11. Uniform mesh refinement in Domain D (L = 5 m, n = 0.25 m, D = 0.75 m, S = 1, b = 0.5 m).

Target FE size (m)	Stretch Factor	Nodes	z (m)
0.050	3	1356	-0.0427
0.050	2.5	1633	-0.0427
0.050	2	2158	-0.0426
0.050	1.5	2873	-0.0426
0.050	1	4239	-0.0425
0.050	0.5	8506	-0.0423
0.050	0.3	15083	-0.0421
0.050	0.251	18081	-0.0421
0.020	3.475	7419	-0.0422
0.020	3.476	7424	-0.0422
0.020	3.477	7430	-0.0421
0.019	2	15158	-0.0422
0.019	4	6954	-0.0421
0.017	4	8393	-0.0421

Last and most interestingly, an important conclusion can be made from these results. That is, since it is possible for HYDRUS to calculate the true numerical solution at a range of FE sizes, minimizing the number of elements to some standard value across all models is not necessary. The most important thing to do is run a few simulations with each model until the same solution has been calculated several times. This will be the true numerical solution for that model. Any further reduction in element size (increase in number of elements) will not change the value – even if the element size for the model in question is two or three times larger than the element size in the smallest model simulated.

Table 12. Uniform mesh refinement in Domain E (L = 15 m, n = 1 m, D = 1 m, S = 0, b = 0.5 m).

Target FE size (m)	Stretch Factor	Nodes	z (m)
0.050	3	6209	-0.1556
0.050	2	9401	-0.1558
0.050	1.5	11979	-0.1558
0.044	2.9	8061	-0.1556
0.044	3	7932	-0.1557
0.040	3	-	no solution
0.038[a]	3	10915	-0.1558
0.038[b]	3	10985	-0.1558

[a]Middle horizontal line deleted. [b]Lower vertical centerline deleted.

This conclusion allowed for the optimization of a single target FE size and stretch factor for use with a series of models sharing the same domain parameter values but having different canal cross-

section geometries. The largest mesh area for each series of models occurred in the model with a triangular canal geometry. A suitably small element size was determined for the trapezoidal domain area this created, and then all other canal cross sections for that domain length and height were analyzed under the same discretization parameters. The discretization parameters determined for the trials in this work have already been given in Table 3 in Chapter 5.

Table 13. Uniform mesh refinement in Domain F (L = 11 m, n = 1 m, D = 1 m, S = 0, b = 0.5).

Target FE size (m)	Stretch Factor	Solution?	z (m)
0.035	1.0	Yes	-0.0871
0.035	1.1 - 1.3	No	-
0.035	1.4 - 1.9	Yes	-0.0870
0.035	2	No	-
0.035	2.1 - 2.5	Yes	-0.0870
0.035	2.6	No	-
0.035	2.7	Yes	-0.0869
0.035	2.8	No	-
0.035	2.9	Yes	-0.0869
0.030	1.0 - 2.0	No	-
0.030	2.1 - 2.2	Yes	-0.0869
0.030	2.3 - 2.5	No	-
0.030	2.6	Yes	-0.0869
0.030	2.7	Yes	-0.0870
0.030	2.8 - 2.9	No	-

7.3 GEOMETRY

The results of the geometric analysis are reported in Figure 17-Figure 20. These figures highlight the sensibility of the comparison; that apples are being compared to apples, not to oranges. Each dataset in a plot shares the same two axes and covers the same range of values on the independent variable axis as at least one other dataset to which it can be compared. Figure 20 is the one figure where all three datasets do not overlap. What is not quite as clear from every one of these figures is the magnitude in the range of values for each dataset. These magnitudes are reported in Table 14 for easier comparison.

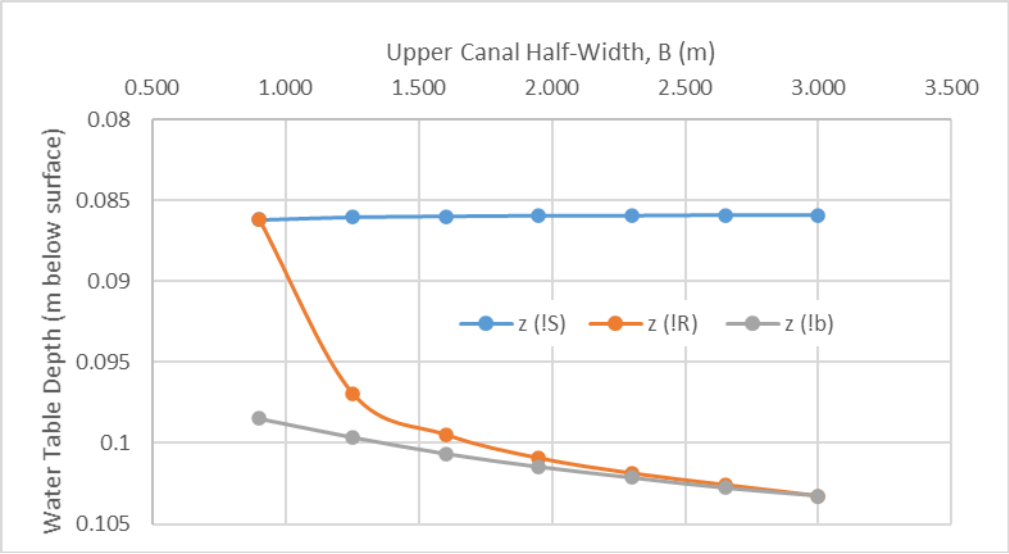

Figure 17. Midpoint water table depth, *z* (m), as a function of upper canal half-width, *B* (m) for three geometry constraint cases: 1. Constant canal bank slope, *S* (_H:1V); 2. Constant hydraulic radius, *R* (m); 3. Constant lower canal half-width, *b* (m).

Figure 17-Figure 20 and Table 14 most strongly support that the most significant geometry parameter is the bank slope. When *S* is held constant the variation in the midpoint water table depth ($\tilde{z}$) is smaller than when other parameters are held constant. The figure legends use a notation where the logical value "not" is represented by "!". For example, $\tilde{z}(!R)$ designates those datasets where *R* is held constant; thus, "$\tilde{z}$ is not a function of *R*." Some conflicting results are apparent.

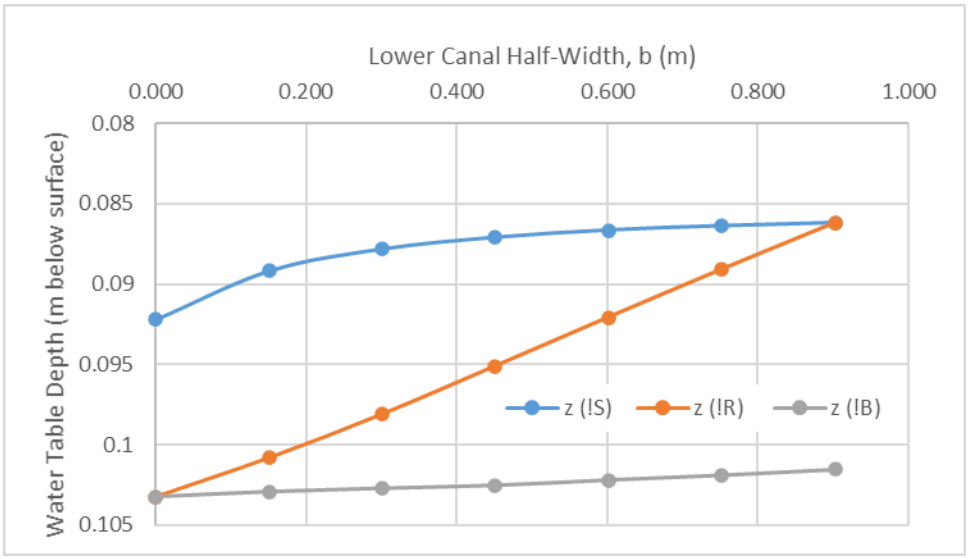

Figure 18. Midpoint water table depth, *z* (m), as a function of lower canal half-width, *b* (m) for three geometry constraint cases: 1. Constant canal bank slope, *S* (_H:1V); 2. Constant hydraulic radius, *R* (m); 3. Constant upper canal half-width, *B* (m).

The first of these is that, in Figure 17 and row 4 of Table 14, *S* appears more significant than *b* and in Figure 18, *B* appears more significant than *S*; but in Figure 19, *b* appears more significant than *B*. This generates the inconclusive and illogical arrangement $b > B > S > b$. Once *R* is treated as the independent variable in Figure 20, *S* appears to be more significant than both *b* and *B*. Clearly, Figure 20 contradicts Figure 18 in the comparison of *S* with *B*. However, both comparisons of *S* with *b* show that the former is more significant. In addition, both comparisons of *B* with *b* show that the latter is more significant. Thus, it was concluded that $S > b > B$.

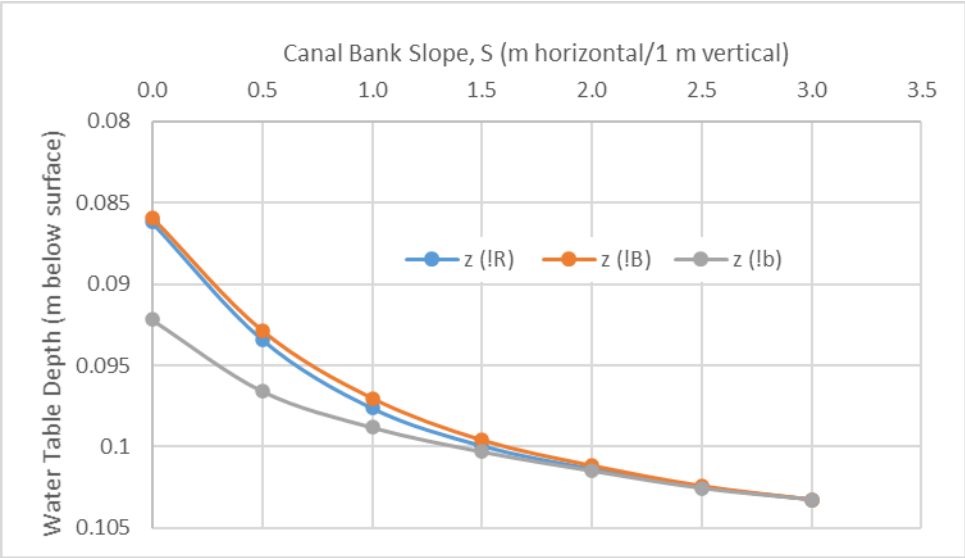

Figure 19. Midpoint water table depth, *z* (m), as a function of canal bank slope, *S* (_H:1V) for three geometry constraint cases: 1. Constant hydraulic radius, *R* (m); 2. Constant upper canal half-width, *B* (m); 3. Constant lower canal half-width, *b* (m).

The second contradictory result is that it is clear from all comparisons except one than *R* is the least significant geometric parameter. Figure 19 and row 1 of Table 14 report this contradictory comparison between *z(!R)* and *z(!B)*. Significantly, the variation of each dataset is not only the same order of magnitude, but the difference between the two is only in the last digit. In other words, as functions of *S,* the two datasets are almost indistinguishable. In contrast, when these two parameters are compared in Figure 18 and row 2 of Table 14, the magnitude of the variation of *z(!R)* is one order of magnitude larger than *z(!B)*. Thus, the most logical arrangement of parameter significance, despite the two contradictions, is $S > b > B > R$.

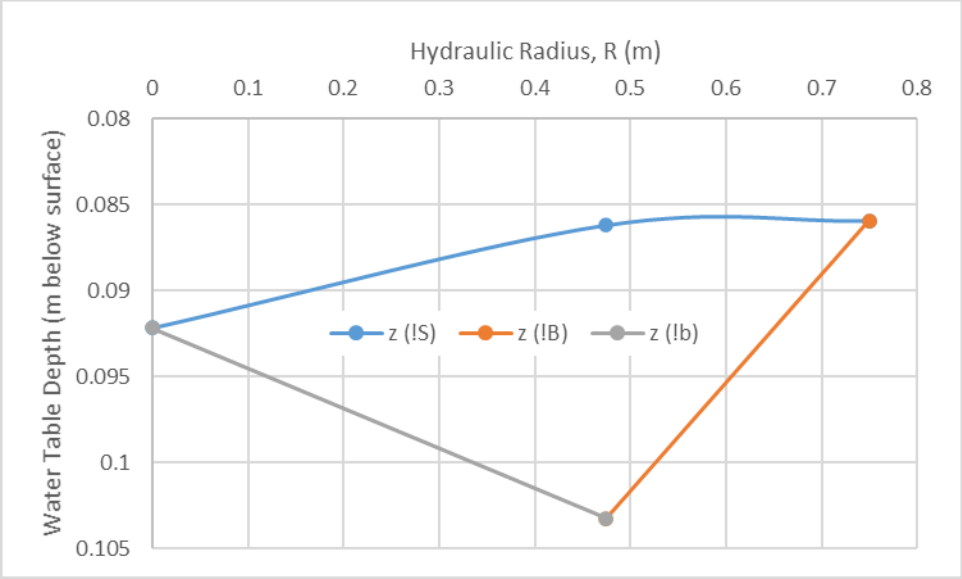

Figure 20. Midpoint water table depth, *z* (m), as a function of hydraulic radius, *R* (m) for three geometry constraint cases: 1. Constant canal bank slope, *S* (_H:1V); 2. Constant upper canal half-width, *B* (m); 3. Constant lower canal half-width, *b* (m).

Bank slope (*S*) was selected as the singular control variable with which to analyze the effect of variation in canal cross-section geometry on the water table profile. Since a change in *S* would produce the greatest change in z, an analytic equation which would take it into account would produce the most conservative correction. As the geometric analysis showed, an increase in *S* resulted in decreasing z. This change in z occurred at a decreasing rate, resulting in a relationship between *S* and z which looks like a quadratic curve.

Table 14. Magnitude in the range of values for each geometry dataset.

	z (!S)	z (!b)	z (!B)	z (!R)
Figure 19	-	1.11E-02	1.73E-02	1.71E-02
Figure 18	6.00E-03	-	1.73E-03	1.71E-02
Figure 17	2.77E-04	4.78E-03	-	1.71E-02
Figure 20[a]	6.00E-03	1.11E-02	-	-
Figure 20[a]	2.65E-04	-	1.73E-02	-

[a]Only part of the range of *S* was compared to z *(!b)* when *R* was the control variable. The other part was compared to z *(!B)*. All units in meters.

7.4 DOMAIN

To compare easily with Bouwer's findings as well as Hooghoudt's, the decision was made to hold *B* constant. This would allow insight as to whether HYDRUS simulated decreasing seepage for a given canal water surface width as the shape changed from rectangle to triangle, as indicated by Bouwer. The results of the domain parameter analyses are reported in Figure 21 – Figure 23. The line

of open circles in each plot represents the default domain, where L = 11 m, n = 1 m, and D = 2 m. It is the same line in all three plots. Figure legends denote the several values of the domain parameter of interest plotted in each respective figure. All units are in meters.

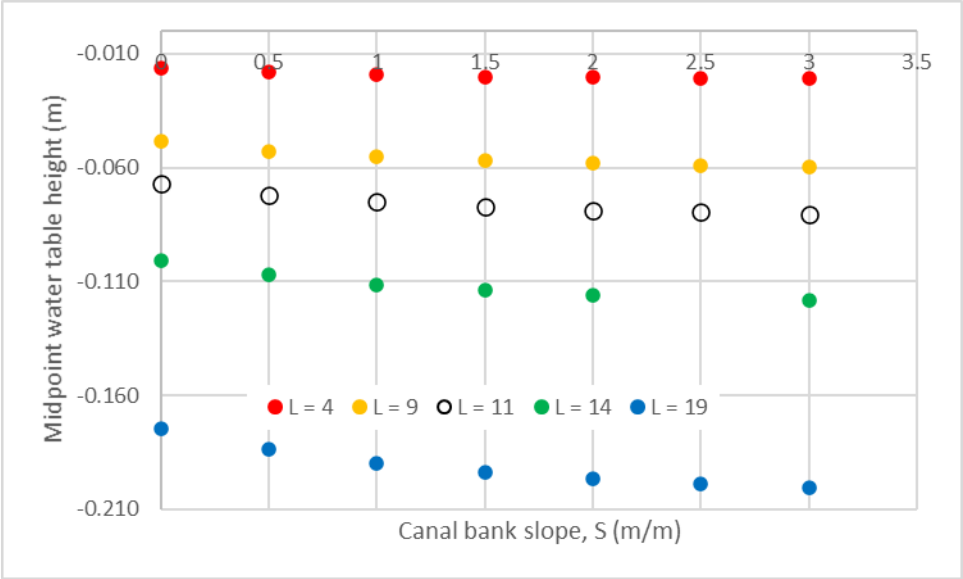

Figure 21. Effect of canal spacing on control variable *S*.

Several observations were made about these figures. Most important and interesting in the analysis of the interactions between domain parameters and geometry parameters was the curvature of the lines. As indicated in the geometric analysis, z varied in response to S as the control variable with what appeared to be a quadratic relationship. However, the quadratic relationship was not the same for every combination of domain parameters. Each figure shows very flattened, almost linear curves at one end of the range of domain parameter values tested, and rounder, more quadratic-looking curves at the other end. Further, the change does not occur in the same way for every domain parameter. Figure 23 shows that the curviness decreased with increasing D, which was the opposite of what occurred with increases in L and n. Within the range of domain parameter values analyzed, the magnitude of this change was greater with D than with the other two, but the ratio of a unit change

in curviness per unit change in *D* was actually less than the ratio for *n,* with both of these ratios greater than that of *L*.

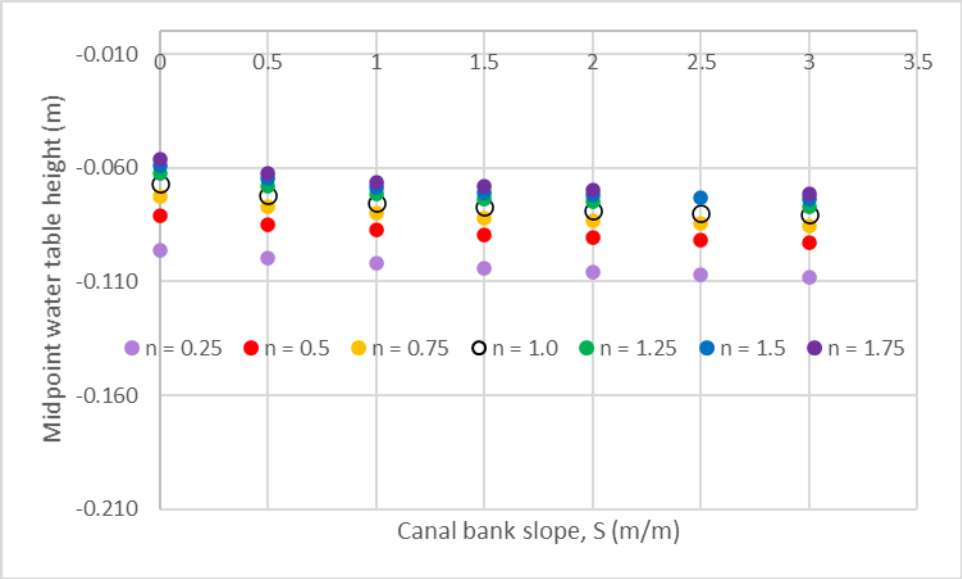

Figure 22. Effect of canal depth on control variable *S*.

The variation in curviness of the datasets meant that there was indeed interaction between the shape of a canal and domain parameters. Not only did an increase in *S* decrease the midpoint water table depth, but the amount of that decrease was dictated by values of the domain parameters in a given scenario. Thus, it was hypothesized that a useful predictive equation would have *S* multiplied by a coefficient which was a function of some combination of *L, n,* and *D*. This is not something which can be determined by linear multiple regression, but it was also possible that a linear regression would provide sufficiently accurate results as to be useful. Therefore, both linear and nonlinear regression models were analyzed.

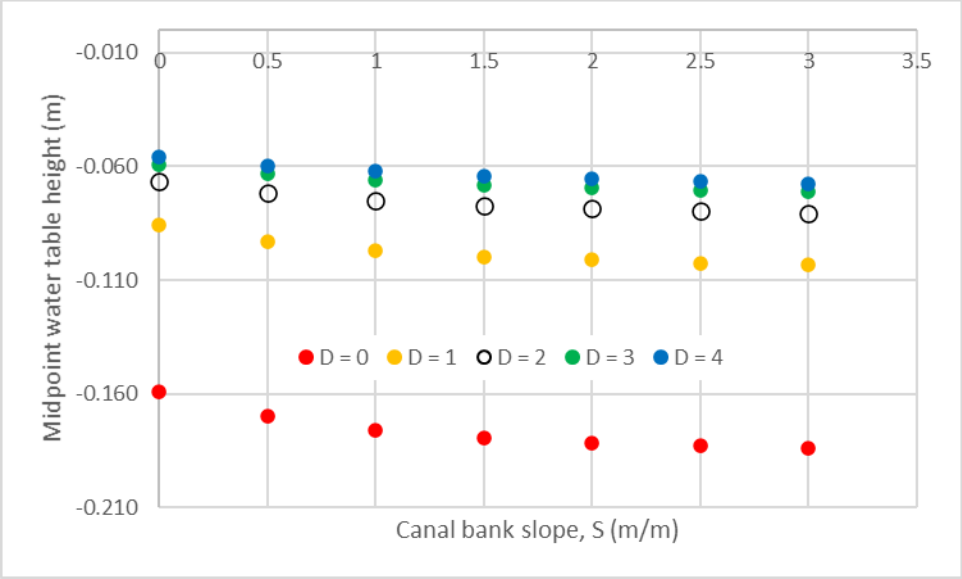

Figure 23. Effect of depth to impermeable layer on control variable *S*.

Two other observations were made regarding the figures. First, an increase in L has the opposite effect on $\bar{z}$ than an increase of either n or D. This aligns with what is expected if the Hooghoudt Equation accurately captures most of the physics of steady groundwater flow. Second, while the magnitude of the change in $\bar{z}$ simulated for varying L is larger than that simulated for the other two domain parameters, the ratio of a unit change in $\bar{z}$ per unit change in L is actually smaller than the change as a function of either D or n. Figure 21 shows that $\bar{z}$ varies from -0.016 m to -0.200 m as L varies from 4 m to 19 m, which is a larger change than shown in the other two figures. But, across the range of values simulated, the ratio of the unit change in $\bar{z}$ per unit change in domain parameter ranged from -1.2% for L, to 3.2% for D, up to 3.5% for n.

What was not so clear from the figures was the influence of the domain parameters on $\bar{z}$. It was observed that the lines cluster closer together at one end of each domain parameter's range than at the other. For example, in Figure 22, there is a visible space between the line of points plotted for n = 0.25 m and the line for n = 0.5 m, while the line of points plotted for n = 1.75 m is almost indistinguishable from the line for n = 1.5 m. This made sense because a change in L, n, or D will nonlinearly change the value of h calculated by the Hooghoudt Equation (Eq. [14]). But it was not

clear from Figure 21 – Figure 23 whether this matched the relationship simulated in HYDRUS. The comparison can be seen better in Figure 24, where the midpoint water table depth (z) is expressed as midpoint water table elevation above canal bed (h). That is, $h = n + z$.

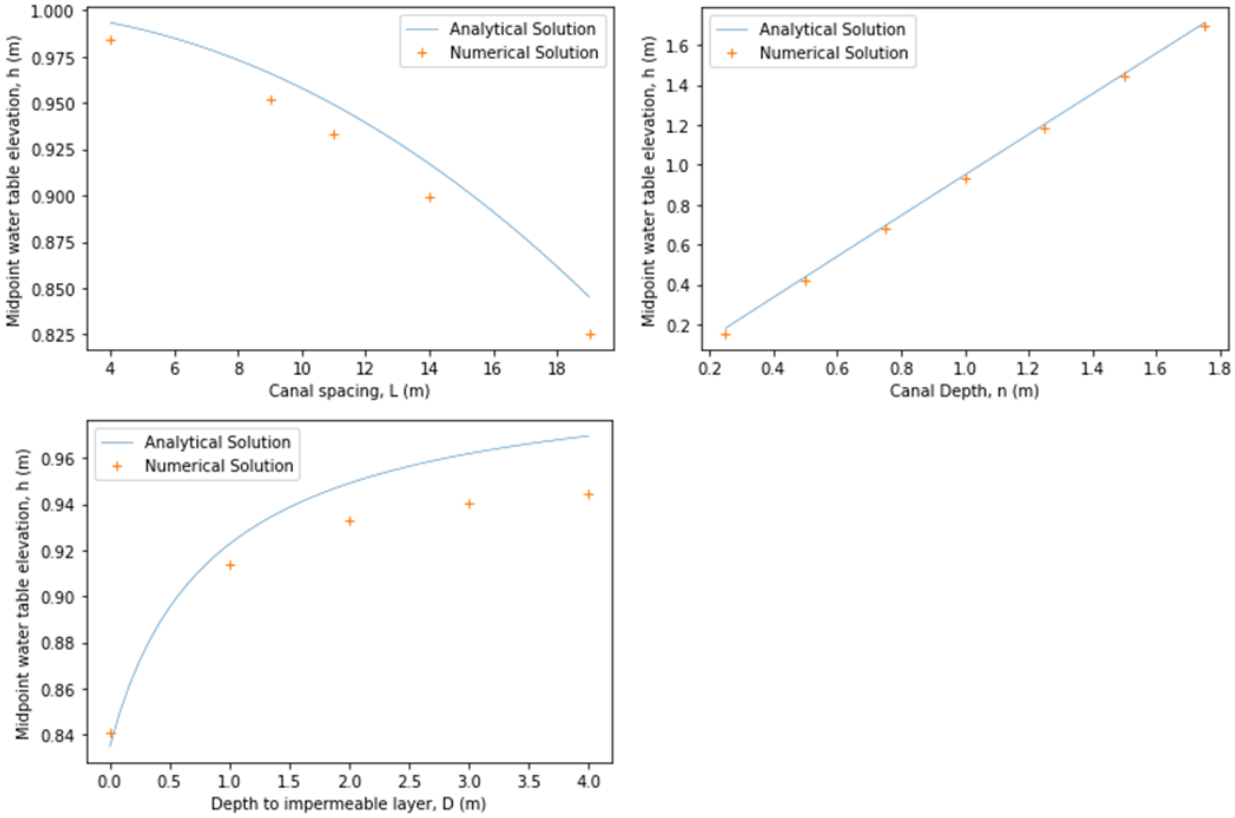

Figure 24. Treatment of *L, n,* and *D* in turn as the independent variable in the Hooghoudt Equation.

Figure 24 gives insight into whether there was agreement between the HYDRUS simulation (Numerical Solution) and the Hooghoudt Equation (Analytical Solution) for a base case, i.e., when S was removed from the analysis. The data plotted in this figure included only those HYDRUS runs for rectangular canals, where $S = 0$. As a function of each domain parameter in turn, h behaved very much as predicted by the Hooghoudt Equation. It was clear that the Hooghoudt approximation of the steady state water table as an ellipse is reasonable. The HYDRUS data did not form an entirely different class of curves. However, there was also room for improvement in the alignment of the two solutions.

Table 15 gives further insight on the comparison between HYDRUS simulations and the Hooghoudt Equation for the same fifteen rectangular domains plotted in Figure 24. The agreement between the two methods was drastically affected by whether *L* was measured from the top of the canal bank or from the canal center. The two values calculated by the Hooghoudt Equation are shown along with the residuals. Neither solution provided by the analytical equation was as good a match of HYDRUS as desired, but the values calculated when *L* was measured from the centers were worse. Thus, in regression analysis, the location for measurement of *L* was maintained at the tops of the canal banks.

Table 15. Midpoint water table elevation (*h*) values output by HYDRUS and the Hooghoudt Equation with canal spacing measured in two different locations.

HYDRUS	Tops of canals	Residuals	Centers of canals	Residuals
0.984	0.993	0.009	0.958	0.026
0.951	0.966	0.015	0.905	0.047
0.933	0.949	0.016	0.877	0.056
0.899	0.917	0.018	0.828	0.071
0.825	0.845	0.020	0.727	0.099
0.154	0.182	0.028	0.161	-0.007
0.419	0.439	0.020	0.400	0.019
0.677	0.694	0.017	0.638	0.039
1.188	1.203	0.015	1.115	0.072
1.441	1.456	0.015	1.354	0.087
1.694	1.709	0.015	1.592	0.102
0.841	0.835	-0.006	0.525	0.316
0.914	0.923	0.009	0.810	0.104
0.941	0.962	0.021	0.908	0.032
0.944	0.970	0.025	0.927	0.017
	Mean	0.016		0.072
	Standard Deviation	7.67E-03		7.30E-02

Note: all units in meters.

7.5 REGRESSION

A regression model with four coefficients, two linear and two nonlinear, was determined to be the best one of those tested. Several factors were examined to make this determination. The consideration of primary importance was minimizing the absolute deviation between numerical and analytical values. Specifically, both few and small (ideally < 1cm) deviations were desired. It was just

as important to minimize the number of coefficients. Accordingly, the models were ranked by these criteria.

Regression model ranking is shown in Table 16, with the best model at the top of the table and the worst model at the bottom. All 102 numerical solutions were compared to the analytical solutions predicted by each regression model for the respective values of *S* and domain parameters. If the deviation between a HYDRUS solution and the respective regression model solution was more than 3 cm, it was tallied in Bin A; the total number of deviations of this magnitude are reported in Table 17, Bin A. Likewise, the number of deviations less than 3 cm but greater than 2 cm are reported in Bin B, and the deviations $1 < |y - \hat{y}| \leq 2$ cm in Bin C. Those models with a single-digit total in Bin C were examined for deviations in the range of 0.5 – 1 cm, reported in Bin D.

Table 16. Model fit ranked by binned number of deviations from observed data.

Model Name	Bin A[a]	Bin B[b]	Bin C[c]	Bin D[d]
N22	0	0	3	19
N32a	0	0	3	19
N32b	0	0	3	22
N33	0	0	3	18
N31	0	0	6	30
N21	0	0	13	-
N90	0	0	12	-
N30	0	1	19	-
L4	0	1	18	-
L2	1	2	19	-
Hooghoudt with offset	1	3	25	-
N20	1	6	40	-
N10	1	7	45	-
L1	4	10	30	-
L3	19	66	17	-
Uncorrected Hooghoudt	26	49	23	-

[a]$3 < |y - \hat{y}| \leq 4$ [b]$2 < |y - \hat{y}| \leq 3$ [c]$1 < |y - \hat{y}| \leq 2$ [d]$0.5 < |y - \hat{y}| \leq 1$ where y is the observed data and $\hat{y}$ is the predicted data, all values in cm. [e]Values predicted by the Hooghoudt Equation, unmodified by any estimated coefficients. [f]Values predicted by calculating the difference between the mean of the observed data and the mean of the values predicted by [e], then subtracting this difference from [e].

In order to gain further insight as to the suitability of the regression models, two extra analytical models were analyzed for absolute deviations. They are included in Table 16 as "Hooghoudt with offset" and "Uncorrected Hooghoudt". The latter model simply inputs the same *L, n,* and *D*

used in Eq. [14]. The mean of all 102 solutions to this equation was different than the mean of the solutions calculated by HYDRUS. This constant was the offset used in the former model.

More detailed statistical analysis was performed as well. Table 17 shows the calculated values of three standard statistical test values for each model: root mean squared deviation (RMSD), Akaike's information criterion (AIC), and Schwarz's Bayesian criterion (BIC). For a given statistical test, the smaller (or more negative) the value calculated for a model, the better it fits the data. The models are ranked by AIC, with the best model at the top of the table, and the worst at the bottom. While RMSD calculates the severity of deviation of the predicted values from observed values, it does not weigh tradeoffs between minimized deviations and too many coefficients in the model. AIC and BIC on the other hand, do consider this tradeoff in their quantification of the model's goodness of fit.

Table 17. Model fit, ranked by Akaike's Information Criterion.

Model Name	RMSD[a]	AIC[b]	BIC[c]
N22	0.0044	-770	-797
N33	0.0041	-766	-803
N32a	0.0044	-763	-795
N32b	0.0045	-758	-791
N31	0.0049	-748	-775
N21	0.0069	-688	-709
L3	0.0073	-679	-700
N90	0.0056	-676	-730
L4	0.0071	-673	-700
N30	0.0075	-670	-692
L2	0.0085	-655	-671
N10	0.0122	-590	-601
N20	0.0119	-587	-603
L1	0.0134	-571	-582

[a]Root Mean Squared Deviation. [b]Akaike's Information Criterion, k = 10. [c]Schwarz's Bayesian Criterion.

The information criterion statistics assign a penalty weight to each coefficient in a model. The default penalty for AIC is k = 2, while for BIC it is k = log(number of observations). Further, AIC allows one to assign any desired weight to this penalty. A value of k = 10 was found to return AIC values which gave the models a ranking very similar to that in Table 16. Even the default value of k = 2 returned a ranking with N22 in the three best models. This is also apparent in the RMSD and BIC

values shown in Table 17. The other two best models have, respectively, five parameters for N32a, and six parameters for N33. Considering how extremely important model simplicity is for the practical application of this research, it was quite reasonable to choose a penalty of k = 10 for AIC.

Each regression model was built from $h = -D + \sqrt{D^2 + 2Dn + n^2 - \frac{qL^2}{4K}}$ [14], the Hooghoudt Equation. The F-test table calculated for the first pathway mentioned in Chapter 5 Section 5 is reported in Table 18. The other F-tests are included in Appendix A. The addition of a regression coefficient in several models did not significantly improve predictions over the previous respective model.

Table 18. Model comparison for significance of each additional term in one pathway of nested nonlinear models.

Model name	Residual Df	Res. Sum Sq	Df	Sum Sq	F value	Pr (>F)
N10	101	0.0150413				
N20	100	0.0140955	1	0.0009458	6.7099	1.10E-02
N21	99	0.0047704	1	0.009325	193.5203	< 2.20E-16
N22	98	0.0019171	1	0.0028534	145.863	< 2.20E-16
N32a	97	0.0018743	1	0.0000428	2.2133	1.40E-01
N33	96	0.0016514	1	0.0002229	12.9601	5.06E-04
N90	93	0.0029564	3	-0.001305	-13.6843	1

In the notation of R: Df = degrees of freedom, Res. Sum Sq = residual sum of squares, Pr = probability.

Of the remaining models, the better fitting ones incorporated *S* as a linear corrective factor added to this base equation. There was a statistically significant offset between the mean of the numerical solutions and the mean of the analytical solutions as shown in Table 15 above. The last two coefficients in N22 came from the idea to imitate Hooghoudt's equivalent depth. These considerations resulted in an equation for model N22 with estimates for the coefficients as follows

$$h = -D_e + \sqrt{D_e^2 + 2D_e n + n^2 - \frac{qL_e^2}{4K}} - 0.00452S - 0.01301 \quad [17]$$

where $D_e = 0.77983D$ and $L_e = 0.97185L$. Alternatively, the equation can be rearranged to solve for q as follows

$$q = \frac{8KD_e(n-h_e)+4K(n^2-h_e^2)}{L_e} \quad [18]$$

where D_e and L_e are defined above and $h_e = h + 0.00452S + 0.01301$. This model has one fewer parameter than the Ernst Equation as given by Bouwer (1969).

Although all models tested only explicitly included one geometry parameter, there was also an implicit condition defining a second parameter. Namely, for all models used in the domain analyses

$$B = 3n \quad [19]$$

Per Eqs. [15] and [16], the other two geometry parameters were thus also defined. Eq. [17] was only proved statistically the best fit for canals within the range of parameters tested, so technically it was only validated for canals exactly matching Eq. [19]. However, significantly different results were not expected for canals which fall within the range of the other parameters tested but which have a different *B*, because of Figure 17.

CHAPTER 8: SITE-SPECIFIC RESULTS

8.1 SOIL PROPERTIES

Before the trip a soil survey of the Njala University College Farm (van Vuure et al., 1972) had been georeferenced to modern site coordinates using QGIS, an open-source geographic information system (QGIS.org, 2021). QGIS allows the user to activate or add-on several subroutines called "plug-ins" which allow detailed analysis. A built-in plug-in called Georeferencer GDAL was used to georeference an image scanned from the 1972 soil survey (Figure 25). In this process the user selects several points on a picture and the corresponding points on the GIS map. The Taia River curves around a peninsula near the site of interest which made the riverbank the logical place for point correlation. The plug-in then interpolates spatial data for the entire picture. The georeferenced image can be used to assign additional information to areas of interest, with good accuracy. This process was used to carefully estimate what soil types occupy the project site.

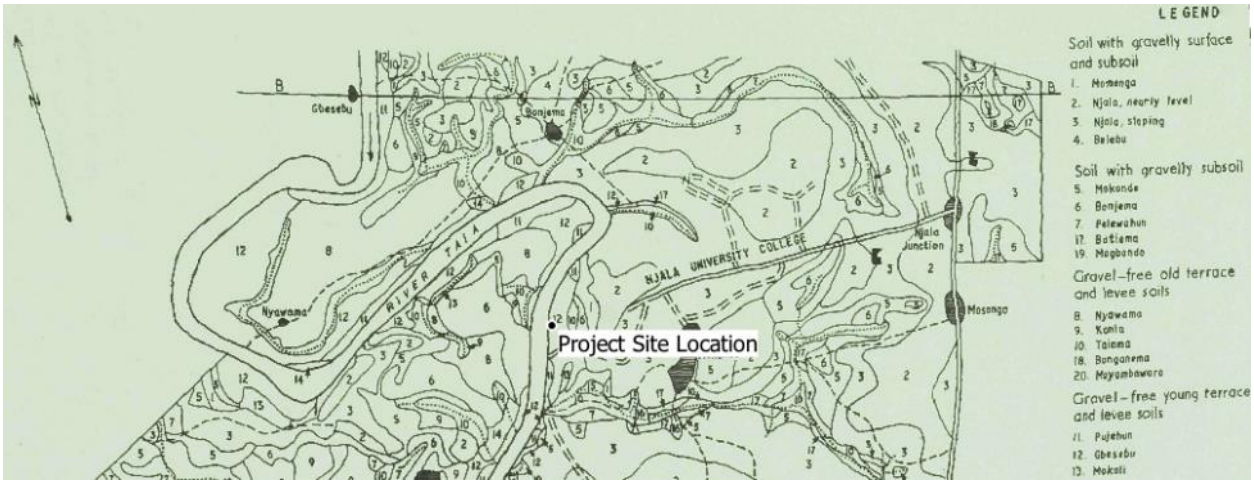

Figure 25. Soil map of the Njala area, Sierra Leone, after Vuure et. al. (1972).

Gbesebu silty clay had been expected to be the predominant soil type at the project site, based on the georeferenced soil survey. A detailed description of a soil pit in this soil series is available from van Vuure et. al. (1972). That publication gives the textural components, bulk density, moisture-holding capacity, and thickness for each layer in the soil pit profile – properties which were analyzed

at the University of Illinois Urbana-Champaign following the USDA classification system. Many other soil series are discussed as well. However, as explained in the following paragraphs, the soil at the project site contained significant amounts of sand. The profile did not fit Gbesebu silty clay.

Table 19 shows the results of analysis for particle size distribution. Each sample is identified by the location (C – center, F – far, or N – near) followed by the depth in centimeters at which it was collected. The first two columns after the sample name report data measured. The next three columns list the calculated percentages of sand, silt, and clay. Soil particles larger than 2 mm are removed during preparation for the hydrometer method. The final column lists the USDA soil texture class.

Table 19. Hydrometer readings, calculated texture distributions, and USDA texture class.

Sample Name	40 second reading[a]	2-hour reading[b]	Sand (%)	Silt (%)	Clay (%)	USDA Texture Class
C 15	5	3	84	8	8	Loamy Sand
C 70	14	7	66	18	16	Sandy Loam
C 130	21	10	52	26	22	Sandy Clay Loam
F 15	8	5	78	10	12	Sandy Loam
F 70	20	13	54	18	28	Sandy Clay Loam
F 130	27	16	40	26	34	Clay Loam
N 15	19	10	56	22	22	Sandy Clay Loam
N 70	18	11	58	18	24	Sandy Clay Loam
N 130	4	2	86	8	6	Loamy Sand
Blank (Control)	3	1	--	--	--	--

[a]Temperature of samples = 31°C. [b]Temperature of samples = 30°C.

The following equations were used to calculate the texture class of each sample after Ashworth et. al. (2001):

$$\%\ clay = (100/w)(R_{2h} - B_{2h}) \quad [20]$$

$$\%\ sand = 100 - (100/w)(R_{40s} - B_{40s}) \quad [21]$$

$$\%\ silt = 100 - \%\ sand - \%\ clay \quad [22]$$

where w is the weight of dry soil in suspension (in this case equal to 50 grams), R_{40s} is the respective hydrometer reading at 40 seconds, B_{40s} is the blank reading at 40 seconds, R_{2h} is the respective hydrometer reading at two hours, and B_{2h} is the blank reading at two hours.

Had the samples been temperature-corrected per Bouyoucos (1962), the percentages of clay would have been higher. This would have brought the textures measured closer to those identified in the Gbesebu soil profile surveyed by van Vuure et. al. (1969) which was the profile expected at the site. Yet the texture classes calculated by hydrometer analysis matched better with qualitative observations of the project site than Gbesebu Silty Clay did. Upon arrival at the site, the soil was found to be primarily sandy to the touch and visual inspection, and it was thought to fit somewhere in the sandy classes of the textural triangle rather than in Silty Clay.

Bulk density was analyzed by weighing the samples after approximately 24 hours of oven drying, then dividing by the volume of the sampling ring. The sampling rings used were measured at four centimeters high and 5.5 cm in diameter, yielding a volume of 95.03 cm^2. Results of the bulk density analysis are reported in Table 20. Typical bulk density for soil ranges from about 1.2-1.7 g/cm^3 (Blake and Hartge, 1986). The unexpectedly low values reported for C70 and N15 are discussed in Chapter 9, Section 3.

Table 20. Bulk density.

Sample Name	Bulk Density (g/mL)
C 15	1.072
C 70	0.870
C 130	1.284
F 15	1.385
F 70	1.456
F 130	1.510
N 15	0.957
N 70	1.141
N 130	1.371

Table 21 shows the moisture retention curve data collected. Six different levels of negative pressure were applied to the soil samples. Measurement of the two smallest negative pressure heads, Saturation (0 cm) and 3.2 cm, were each repeated once. Sample weights were measured twice at the 0 cm level to determine whether the samples had been, in fact, fully saturated by the water bath preparation. They were repeated for 3.2 cm of head to check if enough time had passed between

measurements for the samples to equilibrate at the new pressure. Although neither of these duplicates indicated that enough time had in fact passed for certain samples to reach equilibrium, the decision was made to move ahead with lowering the water column every other day due to time constraints. (Klute, 1986) indicated that the more sandy-textured soils generally take a day to equilibrate, so the focus was on collecting data for those samples.

Table 21. Sample weights measured on sand suction table to determine soil moisture curves.

Sample Name	Saturation[a]		3.2 cm suction[b]		10 cm	31.6 cm	50 cm	60 cm
C 15	384.29	383.10	382.44	382.42	381.19	379.21	378.72	379.43
C 70	276.96	276.60	276.37	276.30	273.23	269.43	268.51	269.00
C 130	295.28	294.76	294.04	293.29	292.63	290.62	290.28	291.38
F 15	287.21	288.15	288.60	288.20	288.07	287.91	287.83	289.24
F 70	303.35	304.81	303.21	302.81	302.32	300.64	299.95	300.60
F 130	304.22	304.05	303.52	302.91	301.63	299.27	298.45	298.59
N 15	247.82	244.20	244.15	244.43	241.15	236.57	235.53	235.62
N 70	278.84	279.51	279.97	280.14	278.24	275.47	274.73	275.00
N 130	310.78	311.29	311.63	312.12	311.22	310.37	309.27	309.65

[a]Water level of the hanging column was equal to that of the sand suction table. Two columns; sample weights were measured twice at this level. [b]Water level of the hanging column was 3.2 cm below the sand; the remaining columns also indicate the depth of the hanging column. 3.2 cm suction has entries in two columns; sample weights were measured twice at this level.

Rashid-Noah (1989) was able to achieve -60 cm of pressure head of his sand suction table which used silica flour for the layer with smallest pore size. With the coarser 150-μm sand available in Sierra Leone it was not expected that the same pressure could be achieved. The results in the table above indicate that air bubbled into the sand table and broke the hydraulic connection at -60 cm of pressure head. As oven-dry sample weights were forgotten, the results of the moisture retention curve could not be computed. It was secondary to the main focus of this thesis and was intended to provide a second check to the HYDRUS simulation, but was not critical. So, no further analysis was performed.

Results of the saturated hydraulic conductivity measurements are reported in Table 22. Test N30 was thought likely to have a conductivity equal to C30 and F30; likewise, F130 was thought likely to have a conductivity similar to the others measured at that depth. Water level readings recorded from the tests are reported in Appendix G. The high conductivity of the soil layer level with the bed

of the far canal (F 100) matches the very sandy texture personally observed in that ditch. The conductivity was measured twice at this location because the water moved so swiftly. The auger hole was filled three times with water per van Hoorn (1979) and measured, then after conducting other work at the site it was decided that there was enough time to test it again in order to check the first measurements. Some of the difference in the values may have been due to rushing the second test a bit.

Table 22. Saturated hydraulic conductivity.

Test Name	C 30	C 100	C 130	F 30	F 100[a]		N 100	N 130
K (m/day)	0.143	0.119	0.423	0.143	8.18	20.9	0.111	0.203

[a]This borehole was tested twice at the same depth.

8.2 MODEL PREDICTION

Results of the HYDRUS simulation of dry-season soil water at the irrigated project site in Sierra Leone assuming a worst-case scenario were informative. To recapitulate, the model for this scenario was illustrated in Figure 16 in Chapter 6 and consisted of the following assumptions. These were: highly permeable soil (HYDRUS-default Sand) below the depth at which soil samples were collected; partially filled canals; constant, highest-magnitude evapotranspiration without precipitation; and a river level which linearly dropped a total of nine meters during the course of the simulation. Program outputs include the value of water potential (m) and content (m^3/m^3) at nodes throughout the domain as well as flows across domain boundaries. For the two-dimensional domain simulated, these volumetric flows are calculated on the basis of one meter width in the y-direction; that is, they have units of $m^3/day/m$ and m^3/m.

Figure 26 shows the distribution of soil water potential at the end of the simulation. The uniform sand layer is apparent in the fairly straight contours plotted from two to ten meters deep. It is also clear that each canal maintains a zone of positive water potential in its immediate vicinity. This zone is larger for the far canal than for the near canal. The zones of positive potential are separated

by a zone of negative potential; however, for the majority of the area this potential is not so low as to harm crop growth. In fact, soil water potential in the entirety of the domain is higher than that approximately associated with field capacity, except for a small area discussed next. Another observation of significance was that the minima of the water potential contour lines tend to align to the boundary between the center soil layers (C15, C70, C130) and the near-river soil layers (N15, N70, N130). Thus, the water potential on either side of this "near-river boundary" is essentially equal, which is relevant when examining soil water content distribution, discussed later in this section.

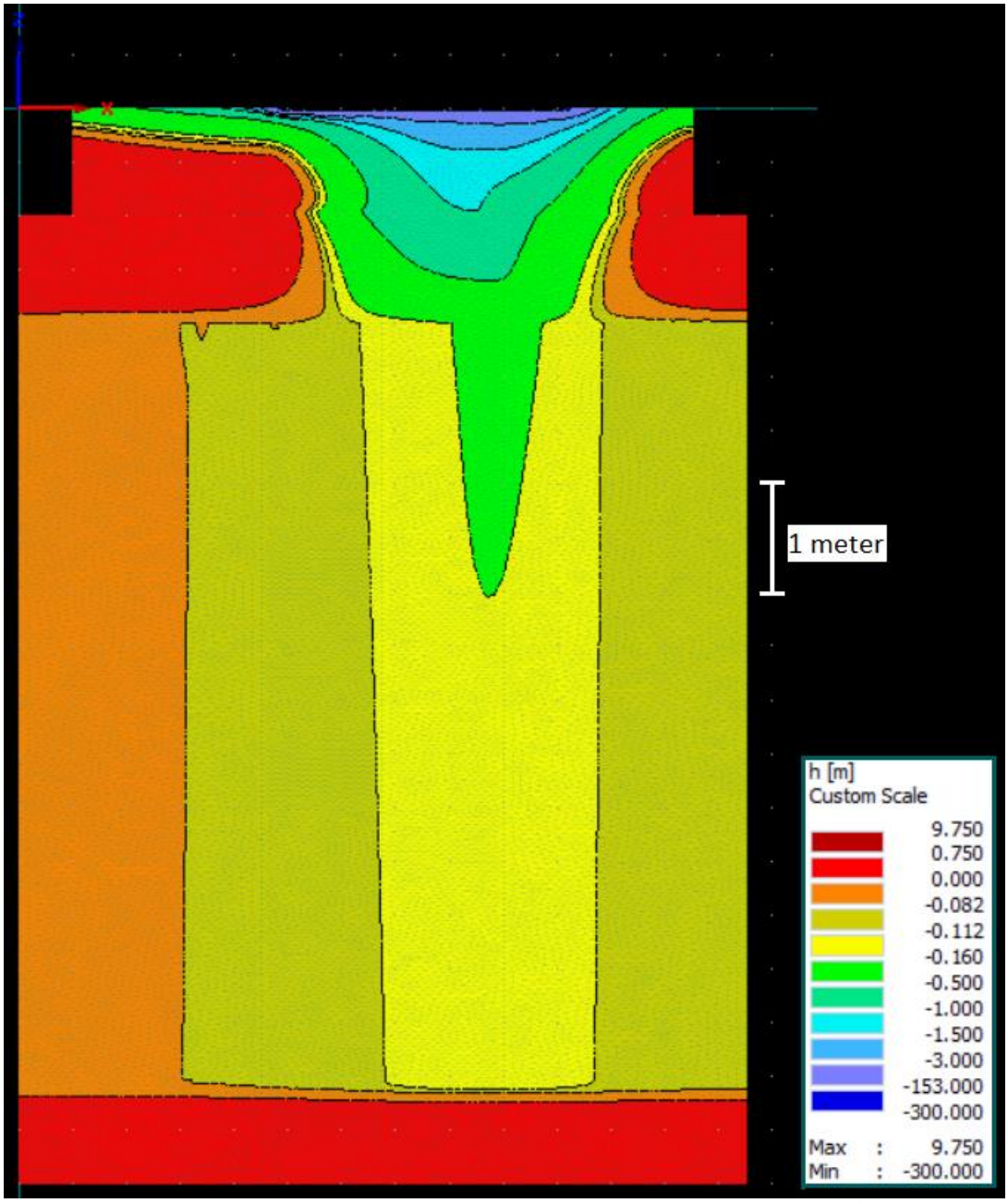

Figure 26. Soil water potential distribution at the end of 180-day simulation of the project site, Njala University, Sierra Leone.

Figure 26 gives an overview of the entire domain, and it is a little hard to see there exactly how large the dry area might be. A zoomed-in view of the simulation results was plotted, shown in Figure 27. This clarifies the boundary of the region with water potential value of -1/3 bar (approximate field capacity). Everything below this contour line has higher potential. It also clearly shows the boundary of the region with water potential value of -15 bar (approximate permanent wilting point).

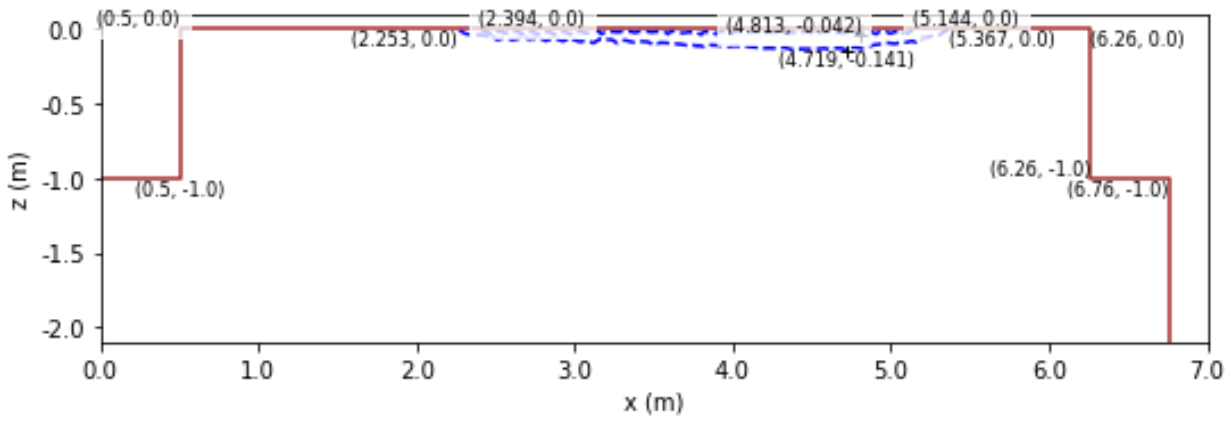

Figure 27. Detail view of the location of water potential contour lines measuring -15 bar (upper contour) and -1/3 bar (lower contour). The coordinates of the point of maximum depth of each contour are labeled along with the endpoints.

Figure 28 A-F show the flows across domain boundaries. Figures A, C and E illustrate the flow rates, while the other three figures report the cumulative flow. The model predicted that the proposed irrigation scheme would require almost 2 m^3/day/m of water by 56 days into the dry season, according to Figure 28A. This time corresponds to a value of 6.75 m at the variable head boundary, which represents the water table at a depth of 3.25 m below ground surface. Most of the inflow through the constant head canal boundaries (Figures A & B) was lost through the Sand layer and variable head boundary as the river receded (Figures C & D). Very little flowed through the atmospheric boundary (Figures E & F).

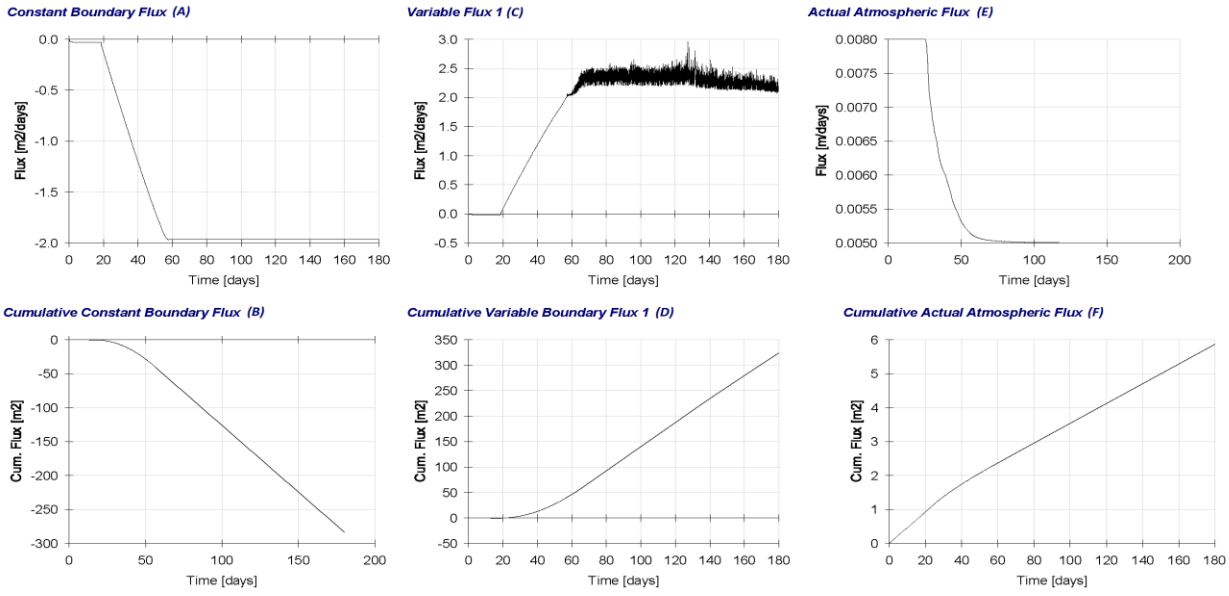

Figure 28 A-F. Water flow across domain boundaries.

The cumulative water flux after 180 days shown in Figure 28 B, D, and F do not cancel each other out. Table 23 makes even more plain that the water supplied by the irrigation system was not sufficient to maintain the amount of water in the soil at the beginning of the dry season. While the two half-canals supplied slightly less than two cubic meters of water per day per meter of canal length, water was leaving the domain at an average net rate of 0.027 m^3/day/m. The water did not leave all regions of the domain in the same quantities, however.

Table 23. Mass balance information reported by HYDRUS.

Time (days)	0	180
Area (m^2)	66.5995	66.5995
Volume (m^3/m)	28.7726	17.8313
Inflow (m^3/day/m)	0	-0.026561
hMean (m)	4.81764	-0.352214
WatBalT (m^3/m)	-	35.4241
WatBalR (%)	-	5.805

Figure 29 reports the soil moisture content (θ) distribution. As expected, the Sand layer contains lower amounts of water than the layers which represent sampled soil. These layers (0 – 2 m deep) had higher clay and silt content than the HYDRUS-default Sand. Figure 29 complements results discussed earlier in this chapter, particularly Table 19, by illustrating the ultimate connection of soil properties to their influence on water-holding capacity. For example, comparing Table 19 and Figure 1, it can be seen that the clay content of the soil samples taken from the center of the site increases as the depth at which each sample was collected increases. In Figure 29, the difference in water content across the aforementioned "near-river boundary" demonstrates that the increase in water content from top to bottom is not due solely to increasing water potential. Rather, the magnitude of the increase is caused to a significant degree by the increase in clay content.

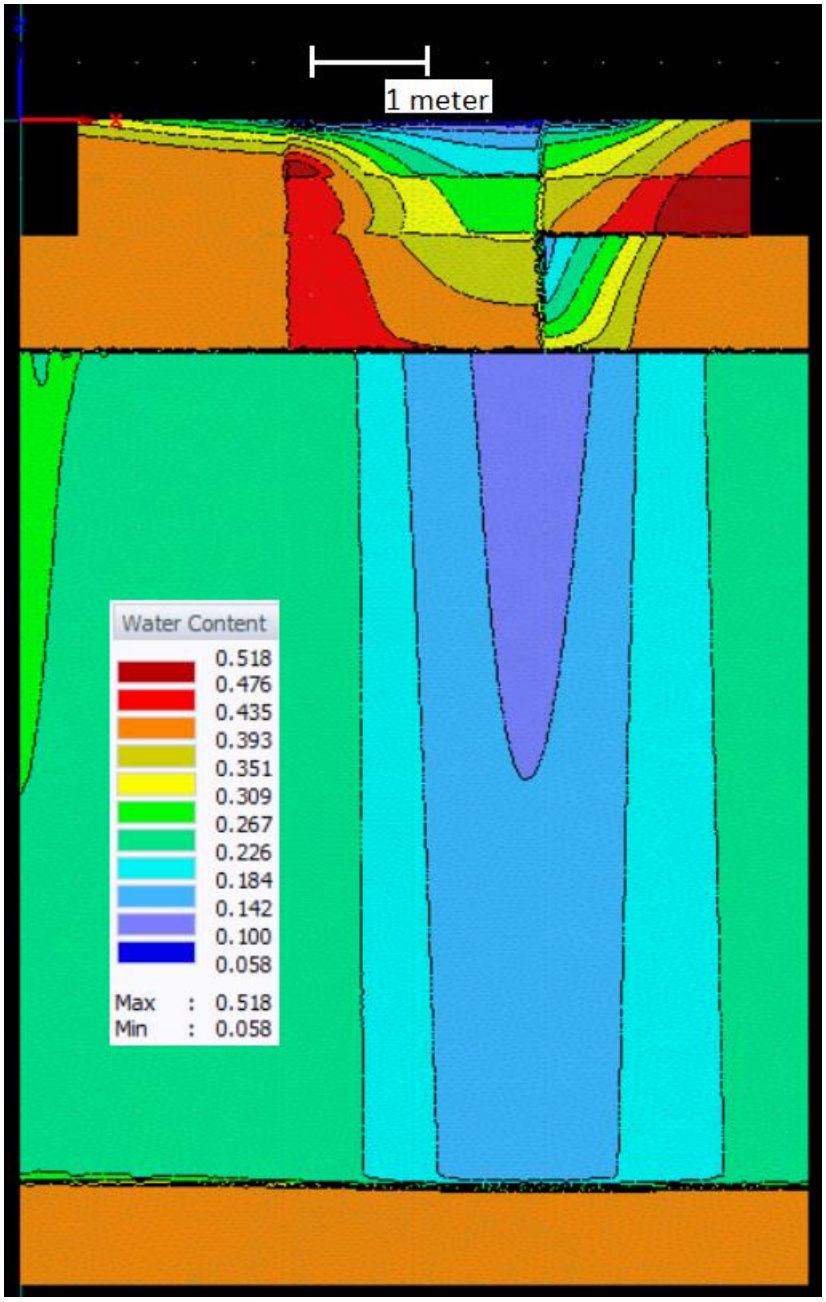

Figure 29. Soil moisture distribution in the simulated project site domain.

CHAPTER 9: DISCUSSION

9.1 FINDINGS IN CONTEXT

All research engages in a kind of conversation with the previous work of others, and for the present investigation the contributions of Hooghoudt and Bouwer were of particular significance. Results of the conceptual analysis disagreed with Hooghoudt's derivation of equivalent depth dependent only on hydraulic radius of the drain (Ritzema, 1994). Figure 20 showed very clearly that the midpoint water table depth could vary widely for different canal cross section geometries having the same hydraulic radius. Conversely, findings agreed with Bouwer (1969) although with canal bank slope identified as the most significant factor in seepage. Figure 17 showed this very clearly, as a relatively wide range of field-applicable values of *B* showed virtually no change in the midpoint water table depth when *S* was kept constant. Bouwer showed that, given a fixed elevation of the water table, the greatest rates of seepage occur from rectangular canals. This study found that the midpoint water table depth below surface decreased as the value of *S* increased. It was farthest below surface for triangular canals and closest to surface for rectangular. This finding agrees with Bouwer's.

At the same time, findings concurred with much of the derivation theory and general relationship between domain parameters identified by Hooghoudt. In particular, the findings about the accuracy of the Hooghoudt Equation depending on whether *L* was measured from canal bank or centerline corroborated the discussion in Chapter 3 about the development of the Hooghoudt Equation. The centerline of the canal is not a D-F boundary, nor can it be made one, because there is a step change in the curve of the water surface which occurs at the canal bank. Within the soil Dupuit-Forchheimer assumptions generally hold, and the water surface approximates an ellipse (drainage) or hyperbola (irrigation), but in the canal, it is perfectly horizontal. The water body of the canal does not have any resistance (K) to water redistribution, so it finds its own level. Without K, Darcy's law for a

hydraulic gradient does not exist, and thus the D-F relationship between the water surface curve and the gradient does not hold.

9.2 THE REGRESSION MODEL

Without the substitution of an equivalent depth instead of *D* the Hooghoudt Equation both over- and under-predicted the water table depth, and the standard deviation of the error was large. When only rectangular canals were considered, the maximum variance was 28 mm (Table 15). The use of a single geometry echoes the analysis of drain tiles, for which the derivations of Hooghoudt have been successfully used for years. If this were the extent of canal analysis there would be no need for further work. But once the various geometries were considered, the analytic solution was more than 40 mm different than the simulation at large values of *S* for several domains (Table 16). An error of 28 mm may be acceptable to practitioners, but 40 mm is 10% of the rooting depth of potatoes and vegetables according to Annex 3 of a bulletin published by FAO (2004), and thus likely to be problematic.

Perhaps unsurprisingly, the best model was very similar to the Hooghoudt Equation used with an effective depth and the addition of a correction factor derived from *S*. The effective depth was very different than Hooghoudt's, however. That one appears to be limited in application to the range of hydraulic radii that may be encountered in tile drains. As soon as the much larger hydraulic radii of canals were entered into the equation, the calculated values for equivalent depth exceeded the actual depth to the impermeable layer. The coefficients of the best-fit regression model provide a singular adjustment to *D* and *L* which works for the range of values tested. However, in order to apply the analytical equation in a wider scope of contexts it would be better to derive a variable solution similar to that available for the calculation of tile drain effective depth.

In all of the regression models tested an offset was needed. As demonstrated by Eq. [18], it represents an increase the depth of the saturated zone. Most likely this is due to the fact that the

derivation of the Hooghoudt Equation does not consider the unsaturated flow region. No analysis is made of soil or hydrological influences on percolation rate. The capillary fringe exists in the unsaturated zone and so is another unaccounted-for factor. As mentioned by Bouwer (1969), horizontal flow occurs there, so the actual flow region is larger. Other investigators have derived equations from D-F theory which do account for unsaturated flow using the concept of specific yield (Boonstra and de Ridder, 1994; de Ridder and Zijlstra, 1994). However, specific yield is not a fixed property of soil; rather, it is a function of many factors including the water table elevation (McWhorter and Marinelli, 1999). An alternate possible reason for the offset was that D-F flow was not fully developed for those models with short *L*.

Although *S* appeared to be a quadratic curve in Figure 21 – Figure 23, a straight-line fit for this parameter worked well in regression models, including the one selected as the best fit for all data. The more pronounced need for an offset may have covered up true *S* interactions from view of the regression statistics. However, a linear plot of *S* on the figures did prove to be a reasonable fit. It took advantage of the opposite movements of slope steepness and curve sharpness discussed in Chapter 7, Section 4. These had a dampening effect on one another that minimized data deviation from a linear fit of *S*.

Computational simulations are highly dependent on the assumptions and inputs that go into them. It was important to note that running the HYDRUS simulations in unsteady-state or with different conditions on the boundaries would have produced different results. The simulation is only as accurate as the reasonableness with which the setup simplifies reality. Discretization of the domain is another of these decisions to which a numerical solution is highly sensitive. Although there is good reason to believe the discretization used in this investigation was appropriate, based on the analysis of numerical stability discussed in Chapter 5, Section 2 and Chapter 7, Section 2, the discretization may still have been incorrect. Usually there should be finer discretization on the boundaries of the domain,

to identify the details of fluxes and pressures accurately and precisely (Dr. Jorge Guzman and Dr. Paul Fischer, personal communication). However, in the case of this particular problem, the region of interest was in the middle of the domain, not on the boundary. Therefore, refinements here (the middle of the domain) were not necessary, and in fact, made the numerical analysis unstable, as shown in Chapter 7, Section 2, and per Dr. Fischer (personal communication). One thing that was not tested was refinement on the boundaries. This may have had an impact, and it is recommended that such refinement be examined in future work.

9.3 PROJECT SITE SAMPLING

At the project site numerous things turned out differently than expected. Some of this was due to circumstances and some was due to experimental error. In the first category, there were discrepancies between conditions expected at the site and what was observed. In the second category were issues with accounting for soil variability and a shortage of time, as well as problems with the measurement of bulk density and the soil moisture curve. These challenges lead to important lessons about preparation for field work and the significance of assistance from others. Further, the complexities of the field must be simplified in order to build a workable model.

One of the first observations of the project site was that the soil did not match what it was predicted to be by the georeferenced soil survey shown in Figure 25, being much sandier than the Gbesebu soil series. It was not likely that the site had been incorrectly placed within the soil map presented by van Vuure et. al. (1972) because the Taia River gave some of the best points possible for an accurate georeferencing operation. Boundaries between land and water, especially along a distinctly irregular curve such as the Taia, are ideal. Further, it was unlikely that the wrong soil profile had been expected because of poor resolution in the original survey. The site was within the center of a large area of the map identified as Gbesebu, so there was no uncertainty as to whether it was on a transition zone between soil series. Two different explanations for the discrepancy were identified based on the

alluvial nature of the region. River systems continually flood and meander, creating great homogeneity in the surrounding soil. Either the original survey had not captured enough detail in this area or flooding since the survey had changed the upper soil layers.

A second unmet expectation was for a consistent progression of soil texture classes with sample depth. Examination of Table 19 shows two different trends in the samples. Those collected from the canal farthest (F) from the river and the center (C) of the site had increasing clay and silt content and decreasing sand content with depth. In contrast, the samples collected from the near (N) canal had increasing sand content with depth, decreasing silt content, and a nonlinear content of clay. Further, the samples varied horizontally more than expected, so the texture classifications for all nine samples ranged from Loamy Sand to Clay Loam.

A soil scientist at Njala University, Dr. Patrick Sawyer, explained how this might be. He discussed the continuous erosion and deposition of soil that occurs in a river floodplain which makes alluvial systems very heterogeneous. Beyond this, he gave a tour and highlighted the physical evidence of intense erosion of clay and silt from the upland area where Njala University campus is located. He concluded these fine particles wash down onto the floodplain during the rainy season where they can be deposited over the sandier layers. The process has accelerated in recent years due to human activities in the uplands (Patrick Sawyer, Njala University, personal communication, May 2021).

Heterogeneity in the alluvial system could also account for the seeming discrepancies between textures in Table 19 and the values of saturated hydraulic conductivity (K) reported in Table 22. Water moves more slowly through clay than through sand, and this is quantified by a lower K value (Klute and Dirksen, 1986). So, it was expected that K would decrease consistently for samples C and F, and likewise match the texture classes for N. However, this was not the case. The only samples for which the pattern of increasing K matched the increasing sand content were those collected at N. One possible reason was that field tests of K were not conducted in the identical locations from which

samples for lab analysis were collected. The differences were both horizontal and vertical, as reported in Figure 13. The soil at these locations was most likely different from the lab samples, and the variation could have been slight or extreme.

The only significant concern with the preceding measurements was an apparent discrepancy between hydrometer measurements and the observed field characteristics for samples collected at F and N. Standing water in canal F was never observed, while canal N often contained one to two inches a few hours after precipitation events. Moreover, although the observer was inexperienced with field analysis of texture, the soil in the former canal looked and felt much sandier than that in the latter. These observations seemingly contradict the hydrometer texture analyses reported in Table 19 where samples from F have lower sand content than samples from N. Hydraulic conductivity measurements (Table 22) agreed more with the observation of presence or absence of standing water than did hydrometer measurements. Since it is assumed that the experienced lab technicians of Njala University ably performed the analysis according to their standard procedure, the Bouyoucos method itself may have been the source of error (Ashworth et al., 2001).

By the time the contradiction was noticed, a pattern had become obvious. The project site was located in significantly varying soil. Probably the respective lab samples were not representative of their whole canal. If there had been more time, replicate samples for texture could have been taken at each depth throughout the canal. Or, with more experience prior to the site visit, the same number of samples collected at the site may have been more representative.

Another issue with sample collection occurred for bulk density. In order to collect samples from C the auger had to be used. This meant the samples were disturbed, which makes no impact on texture analysis, but can have great impact on bulk density measurement. Great care must be taken to repack soil at the same density as it was *in situ*. Table 20 reports an unusually low value of bulk density for sample C70, most likely due to a failure to accurately repack the disturbed soil into the sample ring.

The cause of the low value for N15 was likely not due to repacking error. Samples collected at 15 cm depth, like this one, were close enough to the surface to have the potential of including loose material, plant roots, and other organic material that would lower the density. For all samples there may have been errors in measurement due to the transfer from soil core rings to plastic bags before analysis. In addition, lack of continuous access to electricity meant the drying oven ran eight hours, did not run three hours, then ran five more hours before shutting off again each day. Thus, the samples may not have been fully dry.

As previously mentioned in Chapter 6, there were also issues with analysis of the soil moisture characteristic curve. These fell into the categories of material availability and of planning. Field research is challenging, especially when it is far from home. All the tools and materials must be brought along, or else extra expense and/or time will be spent to obtain something. In unfamiliar places, the necessary items might be totally unavailable, and if one cannot make do with what is available, then the work cannot be done at all. Without silica flour the sand suction table still worked, but not quite as well as it could have.

Seasonality also places restrictions on what research can be done and when it can be done. Most of the significant deadlines are driven by natural cycles, but sometimes they are human originated. Better planning and/or notes could have prevented the moisture curve data loss that occurred. If there had been a better plan in place the suction table could possibly have been ready sooner, which would have allowed for more time flexibility. One use of additional time would have been to equilibrate longer at each suction level. Considering the short equilibration times used, if results had been obtained, they may have been inaccurate because the samples were assumed to be sandier than the hydrometer test measured them to be. Or the experiment could have been started earlier and left more time at the end of the trip to remember to obtain the final oven dry mass of each

sample needed in order to complete the analysis. Alternately, if better notes had been maintained, the final measurement would likely not have been forgotten.

The main insight drawn from the experiences onsite in Sierra Leone was a realization of the complexities of the soil profile. It became obvious that the simplifications documented in Chapter 6 Section 2 were necessary in order to model the site in HYDRUS. The program can handle great variability, but with the limited data available and lack of technical experience, a true representation of the alluvial system was impossible.

9.4 PROJECT SITE PREDICTIONS

Discussion of the predictions made by HYDRUS simulation of the project site is divided into three parts. First, connections are drawn between model results, inputs, and the idealized conceptual model. Next, implications for the functionality of the proposed canal subirrigation system are discussed. Finally, the validity of underlying assumptions is examined, and alternative scenarios are considered. Ultimate conclusions are presented in the next section.

Figure 27 does not look exactly like Figure 8 for several reasons. Of course, the two figures are plotting different contour lines. But the contours in Figure 27 are irregular because of heterogeneity in the soil properties. Further, the steady state fluxes of any given system take an extremely long time to reach. Were the site simulation to reach steady state, the soil would probably be too dry to support plants. Irrigation is only needed through the dry season.

At the end of the dry season, canal F had a larger saturated zone (Figure 26) than canal N because of greater horizontal flow. The K value assumed for F130 in Table 6 is key to this outcome. It was the average of C130 and N130, which was more than ten times lower than the K value measured for F100. According to Bouwer (1969) this order of magnitude difference makes the layer having a lower K value functionally impermeable. Thus, most of the water infiltrating from canal F stayed in the upper soil layers to aid in evapotranspiration, or until it reached the center. In contrast, the layer

below canal N had a slightly higher K value than the top two layers, so once the water table dropped low enough there was nothing significant to inhibit the downward flow of water.

The simulation began with saturated conditions and a water table maintained by the river. Until the water table decreased below the top of the sand layer it would have largely acted as an impermeable boundary inducing predominantly horizontal flow from the canals. After that point, the tendency to horizontal flow greatly decreased because any water flowing vertically down through the beds of the canals would then meet the less resistive sand layer and rapidly flow away from the project site. As the water table continued to lower through the duration of the dry season, Figure 28A shows the seepage from the canals increased until the water table was approximately 3.25 m below the surface, after which seepage no longer increased significantly. This agrees well with the findings of Bouwer (1969), who reported that a water table depth of three times the canal bed width was the transition depth between these two behaviors.

Although not totally ideal for the proposed irrigation system, HYDRUS predicted that the project site would maintain enough moisture in the crop root zone to be successful. In large part this is due to the silt and clay content of the soil samples entered into the model. The water potential required to drain finer-textured soils to water contents approaching the permanent wilting point is much greater than the suction exerted by gravity at this site. As shown in Figure 28 A, C, and E, the simulation demonstrated that the canals replenished the largest part of water extracted by plants throughout the dry season. So, soil moisture content only decreased at a low rate. Along with the reasonable assumption that the dry season begins with nearly saturated soil conditions, this means that sufficient moisture should be available to plants until the end of the dry season.

However, it may not be the most sustainable or economical irrigation solution, based on the water volume used. Approximately two cubic meters of water per meter of canal length was demanded by the model each day (Figure 28A). Two canal halves were simulated because of the assumed

symmetry of the system, and additional canals would require additional water. A pumping rate of 1.39 liters/minute would be required per meter of canal length at the height of the dry season. One type of pump being trialed for use in Sierra Leone is the Barsha pump, which provides a maximum discharge of 0.5 liters/second ("The Barsha Pump - Variants and Specifications," 2018). One such pump could maintain one canal approximately twenty meters long in the worst case scenario.

It is worth taking one more look at the assumptions leading to the previous conclusion. A worst-case scenario was simulated which has a large influence on the volume of water predicted. Most significant in the scenario was the uniform layer of sand. Figure 29 shows just how dry the sand becomes. Until the water content is so low that there are enough drained pores to reduce flow, the unsaturated hydraulic conductivity of sand is much higher than for finer materials. Although alluvial soils tend to have a lot of sand, they also tend to have a lot of horizontal layers with finer materials mixed in. Thus, there will likely be less vertical flow at the project site than the simulation predicted, which would mean less water input. Results from the physical trial of the irrigation system during the dry season will give a much better estimate of its usefulness if good data is collected.

9.5 SUMMARY

Canal cross section geometry, independent of other design parameters, was found to affect the location and shape of the water table profile. The midpoint water table depth is closest to the soil surface for rectangular canals and farthest from the soil surface for triangular canals, with trapezoidal canals in between. These results agree with Bouwer's work using a resistance network analog. Figure 30 summarizes the comparison between HYDRUS data, the equation proposed in this thesis, and the unmodified Hooghoudt Equation. Clearly canal geometry should be taken into consideration.

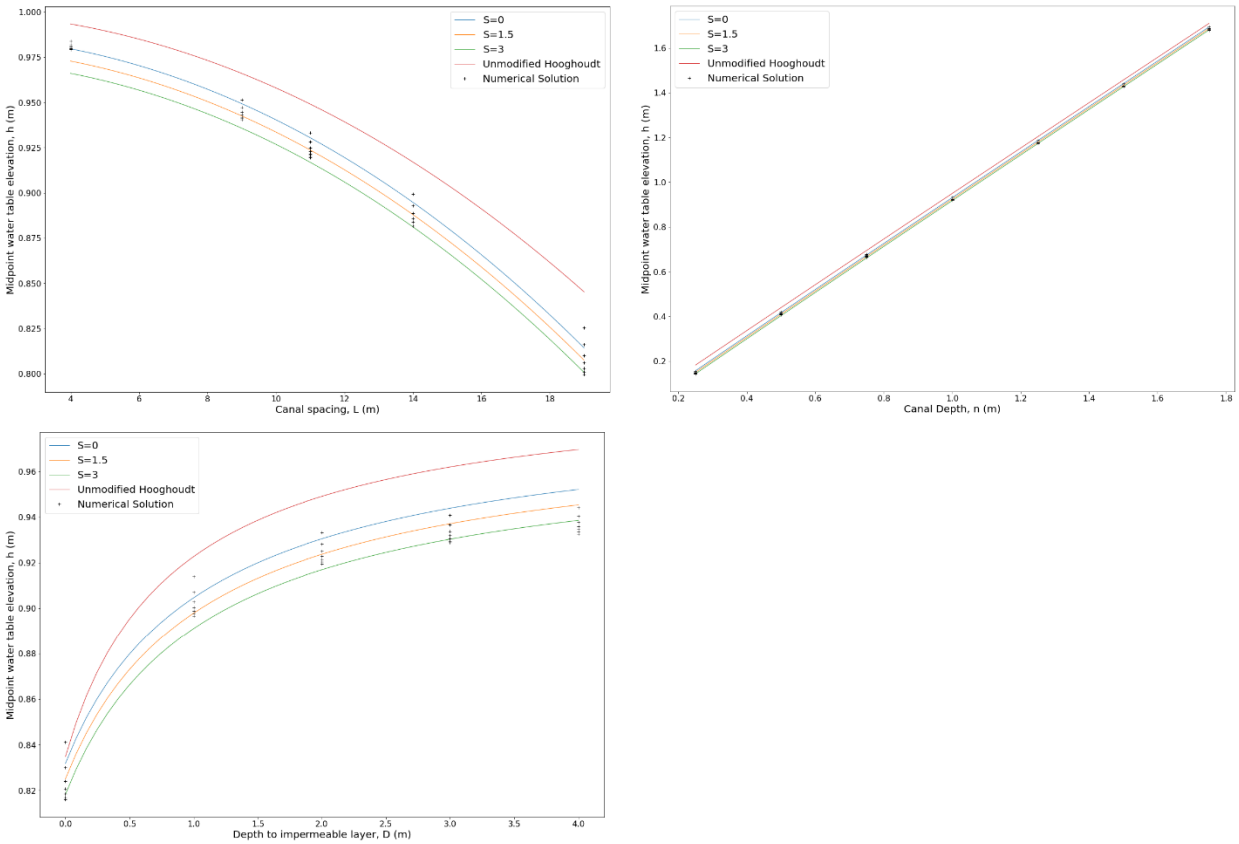

Figure 30. Proposed analytical equation fit to the numerical solution data compared to fit of the Hooghoudt Equation.

Regression analysis was used to identify a relatively simple analytical equation with satisfactory fit to the data presented in Chapter 7, given as $\mathrm{q} = \frac{8\mathrm{KD_e(n-h_e)+4K(n^2-h_e^2)}}{\mathrm{L_e}}$, where $D_e = 0.77983D$, $L_e = 0.97185L$, and $h_e = h + 0.00452S + 0.01301$. Variables are defined in Figure 5 (Chapter 4). This form of irrigation would ideally be implemented in locations where an impermeable layer exists within approximately two meters of the soil surface. The equation should be useful to practitioners in the design of canal subirrigation systems. With its derivation, the findings from the project site at Njala University can be expanded throughout Sierra Leone as well as into other countries.

Canal subirrigation would successfully maintain adequate soil moisture for crop growth at the project site of interest, even for the worst-case scenario with effectively no underlying impermeable layer. Despite an affirmative prediction of success, if reality proves to be such a worst-case scenario the irrigation system would consume excessive amounts of water and would almost certainly not be

the best design. Colleagues from Njala University in Sierra Leone continue to maintain the system functions and data collection. Readings from the tensiometers and observation wells should be analyzed with HYDRUS or via another method to ascertain how the system is working. Ideally the outcome would be much better than a worst-case scenario and the system design would be beneficially disseminated throughout the country. This will require training of extension personnel and communication with smallholder farmers.

Pre- and post-processing python codes were developed to aid HYDRUS analyses. It is hoped that they will be useful to others. They are creative commons licensed.

Future work should include analysis of the performance of the canal subirrigation system installed on Njala University campus. Performance metrics could include the amount of water the system uses and should include the water table location throughout the dry season. Also, it would be beneficial to verify that the results of the HYDRUS analysis are unaffected by mesh refinement at the boundaries, as well as investigating additional values of K and q.

CHAPTER 10: CONCLUSIONS

10.1 OBJECTIVE OUTCOMES

- Canal cross section geometry, independent of other design parameters, does affect the location and shape of the water table profile. The midpoint water table depth is closest to the soil surface for rectangular canals and farthest from the soil surface for triangular canals, with trapezoidal canals in between, which agrees with Bouwer (1969).
- The equation $\mathrm{q} = \frac{8\mathrm{KD_e(n-h_e)+4K(n^2-h_e^2)}}{\mathrm{L_e}}$, where $D_e = 0.77983D$, $L_e = 0.97185L$, and $h_e = h + 0.00452S + 0.01301$ was suitable for canal subirrigation system design. This equation can be used to design canal depth and spacing in the same way the Hooghoudt Equation is used for tile drains.
- Canal subirrigation would successfully maintain adequate soil moisture for crop growth at the project site on Njala University campus, even for the worst-case scenario with effectively no underlying impermeable layer.

10.2 RECOMMENDATIONS

An equation which incorporates an effective depth derived from physics specifically for canals was identified as an opportunity for future research. While multiple regression analysis has its place, additional investigation into the theory behind the reason canal geometry has an effect on the water table profile would be worthwhile. The range of soil water systems modeled was limited to those likely to be found in Sierra Leone and one value of saturated hydraulic conductivity. So, the proposed design equation based on regression may not hold for significantly different situations. Conversely, calculation of an equivalent depth specific to canals and dependent on *S* and other domain parameters, similar to that calculated by Hooghoudt for tile drains, is hypothesized to match the physics better.

Canal subirrigation could be effectively implemented in fields with an impermeable layer within 2-3 m of the surface. This is likely to be the case for several landforms of Sierra Leone known as inland valley swamps, bollilands, and river terraces. Results from the field trial on Njala University's campus should be analyzed to determine the efficiency of the system. If results are not favorable, the system could be tested again at another site known to have an impermeable layer at the desired depth. If the results are favorable, the next step would be to educate Njala University extension educators about the system so local farmers can be taught how to implement it.

The proposed design equation should be used by irrigation system designers to calculate the desired spacing and depth of canals needed to provide water to crops at a rate based on the plant needs and climate data. The cross-section geometry, selected by the designer based on soil slope stability or other considerations, is accounted for in the equation, allowing the designer to pick the best canal depth and spacing combination to satisfy the crop water needs and minimize excavation costs. This will benefit farmers' economics. The irrigation system would allow them to grow a second crop during the dry season, reducing food insecurity or even providing additional income. The system would be suited to smallholder farmers in Sierra Leone due to low capital investment and operation demands.

REFERENCES

Akkuzu, E., Ünal, H. B., Karataş, B. S. (2007). Determination of Water Conveyance Loss in the Menemen Open Canal Irrigation Network. *Turk. J. Agric. For.*, *31*(1), 11–22. https://doi.org/10.3906/tar-0611-10

Amadu, F. O., Silvert, C., Eisenmann, C., Mosiman, K., Liang, R. (2017). *Sierra Leone Landscape Analysis* (Working Document) (p. 32). United States Agency for International Development. Retrieved from https://ingenaes.illinois.edu/wp-content/uploads/ING-Landscape-Study-2017-Sierra-Leone-published-2017_07_07.pdf

Ashworth, J., Keyes, D., Kirk, R., Lessard, R. (2001). STANDARD PROCEDURE IN THE HYDROMETER METHOD FOR PARTICLE SIZE ANALYSIS. *Commun. Soil Sci. Plant Anal.*, *32*(5–6), 633–642. https://doi.org/10.1081/CSS-100103897

Blake, G. R., Hartge, K. H. (1986). Bulk Density. In A. Klute (Ed.), *Methods of Soil Analysis* (2nd ed., Vol. 1, pp. 363–375). Madison, WI: John Wiley & Sons, Ltd. https://doi.org/10.2136/sssabookser5.1.2ed.c13

Boonstra, J., de Ridder, N. A. (1994). Single-Well and Aquifer Tests. In H. P. Ritzema (Ed.), *Drainage principles and applications* (2. ed. (completely rev.), pp. 341–382). Wageningen, The Netherlands: ILRI.

Bos, M. G. (1994a). Basics of Groundwater Flow. In H. P. Ritzema (Ed.), *Drainage Principles and Applications* (2. ed. (completely rev.), pp. 225–262). Wageningen, The Netherlands: ILRI.

Bos, M. G. (1994b). Drainage Canals and Related Structures. In H. P. Ritzema (Ed.), *Drainage principles and applications* (2. ed. (completely rev.), pp. 725–798). Wageningen, The Netherlands: ILRI.

Bos, M. G., Wolters, W. (1994). Influences of Irrigation on Drainage. In H. P. Ritzema (Ed.), *Drainage principles and applications* (2. ed. (completely rev.), pp. 513–532). Wageningen, The Netherlands: ILRI.

Bosch, D. D., Hubbard, R. K., West, L. T., Lowrance, R. R. (1994). Subsurface Flow Patterns in a Riparian Buffer System. *Trans. ASAE*, *37*(6), 1783–1790. https://doi.org/10.13031/2013.28267

Bouwer, H. (1969). Theory of Seepage from Open Channels. In V. T. Chow (Ed.), *Advances in Hydroscience* (Vol. 5, pp. 121–172). Elsevier. https://doi.org/10.1016/B978-1-4831-9936-8.50008-8

Bouyoucos, G. J. (1962). Hydrometer Method Improved for Making Particle Size Analyses of Soils. *Agron. J.*, *54*(5), 464–465. https://doi.org/10.2134/agronj1962.00021962005400050028x

Cahn, M. D., Chambers, D. (2019, April 23). Do it yourself (DIY) tensiometer [University of California]. Retrieved October 13, 2021, from https://ucanr.edu/blogs/blogcore/postdetail.cfm?postnum=30042

Caswell, T. A., Droettboom, M., Lee, A., Andrade, E. S. de, Hunter, J., Firing, E., … Ivanov, P. (2021). *matplotlib/matplotlib: REL: v3.3.4*. Zenodo. https://doi.org/10.5281/zenodo.4475376

Clemmens, A. J., Walker, W. R., Fangmeier, D. D., Hardy, L. A. (2007). Chapter 14. Design of Surface Systems. In *Design and Operation of Farm Irrigation Systems* (2nd ed., pp. 499–531). St. Joseph, MI: American Society of Agricultural and Biological Engineers. https://doi.org/10.13031/2013.23697

Coche, A. G., Muir, J. F., Laughlin, T. L. (1992). *Pond construction for freshwater fish culture* (Vol. 2). Rome: Food and Agriculture Organization of the United Nations ; UNIPUB, distributor.

de Ridder, N. A., Zijlstra, G. (1994). Seepage and Groundwater Flow. In H. P. Ritzema (Ed.), *Drainage principles and applications* (2. ed. (completely rev.), pp. 305–340). Wageningen, The Netherlands: ILRI.

FAO (Ed.). (2004). *Scaling soil nutrient balances: enabling mesolevel applications for African realities*. Rome: Food and Agriculture Organization of the United Nations. Retrieved from https://www.fao.org/3/y5749e/y5749e0j.htm

Fouss, J. L., Evans, R. O., Ayars, J. E., Christen, E. W. (2007). Chapter 18. Water Table Control Systems. In *Design and Operation of Farm Irrigation Systems* (2nd ed., pp. 684–724). St. Joseph, MI: American Society of Agricultural and Biological Engineers. https://doi.org/10.13031/2013.23701

Holden, P. A., Fierer, N. (2005). Vadose Zone | Microbial Ecology. In D. Hillel (Ed.), *Encyclopedia of Soils in the Environment* (pp. 216–224). Elsevier. https://doi.org/10.1016/B0-12-348530-4/00172-7

Kling, H., Fuchs, M., Stanzel, P., Paulin, M., Wipplinger, B., Wimmer, S., … Weilguni, H. (2017). *GIS Hydropower Resource Mapping and Climate Change Scenarios for the ECOWAS Region, Country Report for Sierra Leone* (GIS Hydropower Resource Mapping and Climate Change Scenarios for the ECOWAS Region) (p. 19). Praia, Cabo Verde: ECOWAS Centre for Renewable Energy and Energy Efficiency (ECREEE). Retrieved from http://www.ecowrex.org/system/files/country_report_13_sierra_leone.pdf

Klute, A. (1986). Water Retention: Laboratory Methods. In A. Klute (Ed.), *Methods of Soil Analysis* (2nd ed., Vol. 1, pp. 635–662). Madison, WI: John Wiley & Sons, Ltd. https://doi.org/10.2136/sssabookser5.1.2ed.c26

Klute, A., Dirksen, C. (1986). Hydraulic Conductivity and Diffusivity: Laboratory Methods. In *Methods of Soil Analysis* (2nd ed., Vol. 1, pp. 687–734). Madison, WI: John Wiley & Sons, Ltd. https://doi.org/10.2136/sssabookser5.1.2ed.c28

Mbagwu, J. S. C. (1985). Estimating dry-season crop water requirements from climatological and soil available water capacity data in the sedimentary and basement complex areas of Southern Nigeria. *CATENA*, *12*(2), 201–209. https://doi.org/10.1016/0341-8162(85)90011-6

McWhorter, D. B., Marinelli, F. (1999). Theory of Soil-Water Flow. In R. W. Skaggs & J. van Schilfgaarde (Eds.), *Agricultural Drainage* (pp. 111–143). Madison, WI: John Wiley & Sons, Ltd. https://doi.org/10.2134/agronmonogr38.c4

Nieber, J. l., Feddes, R. A. (1999). Solutions for Combined Saturated and Unsaturated Flow. In R. W. Skaggs & J. van Schilfgaarde (Eds.), *Agricultural Drainage* (pp. 145–212). Madison, WI: John Wiley & Sons, Ltd. https://doi.org/10.2134/agronmonogr38.c5

QGIS.org. (2021). *QGIS 3.16. Geographic Information System API Documentation*. python, QGIS Association. Retrieved from https://qgis.org/pyqgis/3.16/index.html

Rashid-Noah, A. B. (1981). *Designing subsurface drainage systems to avoid excessive drainage of sands* (PhD). McGill University, Montreal, Quebec. Retrieved from https://escholarship.mcgill.ca/concern/theses/ms35t9405

Rassam, D., van Genuchten, M. Th., Šimůnek, J. (2003). *Modelling variably saturated flow with HYDRUS-2D* (First). Brisbane: ND Consult. Retrieved from https://www.ars.usda.gov/arsuserfiles/20360500/pdf_pubs/P1929.pdf

Rhodes, E. R., Atewamba, C., Kouamé, E. B. H. (2016). *Country Profile on Climate Change, Agricultural Trade and Food Security in ECOWAS - Sierra Leone Report*. Accra: United Nations University Institute for Natural Resources in Africa. Retrieved from http://collections.unu.edu/view/UNU:5929

Ritzema, H. P. (1994). Subsurface Flow to Drains. In H. P. Ritzema (Ed.), *Drainage principles and applications* (2. ed. (completely rev.), pp. 263–304). Wageningen, The Netherlands: ILRI.

Schoeneberger, P. J., Wysocki, D. A., Benham, E. C., Soil Survey Staff. (2012). *Field book for describing and sampling soils, Version 3.0*. National Soil Survey Center, Lincoln, NE: Natural Resources Conservation Service.

Šimůnek, J., Šejna, M. (2009). Notes on Spatial and Temporal Discretization (when working with HYDRUS). PC-Progress. Retrieved from https://www.pc-progress.com/Images/Pgm_Hydrus3D2/Notes_on_Spatial_and_Temporal_Discretization.pdf

Šimůnek, J., Šejna, M. (2011). HYDRUS (2D/3D) (Version 2.0) [Windows]. Prague, Czech Republic: PC Progress. Retrieved from https://www.pc-progress.com/en/Default.aspx

Šimůnek, J., van Genuchten, M. Th., Šejna, M. (2012). *The HYDRUS Software Package for Simulating the Two- and Three-Dimensional Movement of Water, Heat, and Multiple Solutes in Variably-Saturated Porous Media* (Technical Manual) (p. 258). Prague, Czech Republic: PC Progress. Retrieved from https://www.pc-progress.com/downloads/Pgm_Hydrus3D2/HYDRUS3D Technical Manual.pdf

Skaggs, R. W. (1999a). Drainage Simulation Models. In R. W. Skaggs & J. van Schilfgaarde (Eds.), *Agricultural Drainage* (pp. 469–500). Madison, WI: John Wiley & Sons, Ltd. https://doi.org/10.2134/agronmonogr38.c13

Skaggs, R. W. (1999b). Water Table Management: Subirrigation and Controlled Drainage. In R. W. Skaggs & J. van Schilfgaarde (Eds.), *Agricultural Drainage* (pp. 695–718). Madison, WI: John Wiley & Sons, Ltd. https://doi.org/10.2134/agronmonogr38.c20

Smith, R. E., Warrick, A. W. (2007). Chapter 6. Soil Water Relationships. In *Design and Operation of Farm Irrigation Systems* (2nd ed., pp. 120–159). St. Joseph, MI: American Society of Agricultural and Biological Engineers. https://doi.org/10.13031/2013.23689

Solomon, K. H., El-Gindy, A. M., Ibatullin, S. R. (2007). Chapter 3. Planning and System Selection. In *Design and Operation of Farm Irrigation Systems* (2nd ed., pp. 57–75). St. Joseph, MI: American Society of Agricultural and Biological Engineers. https://doi.org/10.13031/2013.23686

Thalheimer, M. (2013). A low-cost electronic tensiometer system for continuous monitoring of soil water potential. ***J. Agric. Eng.*** *44*(3), 16. https://doi.org/10.4081/jae.2013.211

The Barsha Pump - Variants and Specifications. (2018). aQysta. Retrieved from https://aqysta.com/wp-content/uploads/2018/06/Technical-Specifications.pdf

van der Molen, W. H., Wesseling, J. (1991). A solution in closed form and a series solution to replace the tables for the thickness of the equivalent layer in Hooghoudt's drain spacing formula. *Agric. Water Manag.*, *19*(1), 1–16. https://doi.org/10.1016/0378-3774(91)90058-Q

van Es, H. (2017). A New Definition of Soil. *CSA News*, *62*(10), 20–21. https://doi.org/10.2134/csa2017.62.1016

van Genuchten, M. Th. (2021). FAQ 21-30 [Company]. Retrieved October 12, 2021, from https://www.pc-progress.com/en/Default.aspx?h3d-faq-21-30

van Hoorn, J. W. (1979). Determining hydraulic conductivity with the inversed augerhole and infiltrometer methods. In J. Wesseling (Ed.), *Proceedings of the International Drainage Workshop, May 1978* (pp. 150–154). Wageningen, The Netherlands: ILRI. Retrieved from https://research.wur.nl/en/publications/determining-hydraulic-conductivity-with-the-inversed-augerhole-an

van Vuure, W., Odell, R. T., Sutton, P. M. (1972). *Soil survey of the Njala Area, Sierra Leone*. Sierra Leone: Njala University College, University of Sierra Leone in Cooperation with Ministry of Agriculture and Natural Resources.

Virtanen, P., Gommers, R., Burovski, E., Oliphant, T. E., Weckesser, W., Cournapeau, D., … Striega, K. (2021). *scipy/scipy: SciPy 1.6.2*. Zenodo. https://doi.org/10.5281/zenodo.4635380

APPENDIX A – ADDITIONAL REGRESSION MODEL STATISTICS

Model name	Residual Df	Res.Sum Sq	Df	Sum Sq	F value	Pr(>F)
L1	101	0.0181284				
L2	100	0.0072371	1	0.0108913	214.2191	< 2.20E-16
L3	99	0.0052055	1	0.0020316	39.9597	7.70E-09
L4	98	0.0049825	1	0.0002229	4.3849	3.88E-02

Model name	Residual Df	Res.Sum Sq	Df	Sum Sq	F value	Pr(>F)
N10	101	0.0150413				
N20	100	0.0140955	1	0.0009458	6.7099	1.10E-02
N30	99	0.0056424	1	0.0084531	148.3171	< 2.20E-16
N31	98	0.0023966	1	0.0032457	132.7209	< 2.20E-16
N32a	97	0.0018743	1	0.0005223	27.0312	1.11E-06
N33	96	0.0016514	1	0.0002229	12.9601	5.06E-04

Model name	Residual Df	Res.Sum Sq	Df	Sum Sq	F value	Pr(>F)
N20	100	0.0140955				
N21	99	0.0047704	1	0.009325	193.52	< 2.20E-16
N31	98	0.0023966	1	0.0023738	97.067	2.53E-16
N32b	97	0.0019568	1	0.0004398	21.801	9.72E-06
N33	96	0.0016514	1	0.0003055	17.757	5.67E-05
N90	93	0.0029564	3	-0.001305	-13.684	1

Model name	Residual Df	Res.Sum Sq	Df	Sum Sq	F value	Pr(>F)
N21	99	0.0047704				
N22	98	0.0019171	1	0.0037253	190.4349	< 2.00E-16
N32a	97	0.0018743	1	0.0000428	2.2133	1.40E-01
N22	98	0.0019171				
N32b	97	0.0019568	1	-3.98E-05	-1.9707	1

APPENDIX B – ADDITIONAL PROJECT SITE PHOTOGRAPHS

Water bath to saturate soil samples in preparation for measuring the soil water retention curve.

Instrument set up at the project site.

Tensiometers assembled and drying.

Soil profile seen in the canal located closer toward the river.

Soil profile seen in the canal located farther from the river.

APPENDIX C – PYTHON PREPROCESSING CODE

```
# -*- coding: utf-8 -*-
"""
Created on Thu Jun 17 11:03:20 2021

@author: bruhn2
"""

def setup(name,n,d,l,b,s,layers=None):
    """
    Generates variable number of text files readable by HYDRUS.

    !! WARNING: n,d,l,b,s MUST all be the same length OR contain ONLY ONE entry !!
    !! WARNING: enter positive numbers only !!

    The number of files generated depends on the number of entries in the
    variable lists. Each file generated by this function contains points which
    define one HYDRUS domain geometry. In HYDRUS, select File -> Import->
    Import Geometry from Text File, and select the desired file.

    Parameters
 ----------
    name : str
        descriptive trial name which all domain definition files share.
    n : list
        canal depth.
    d : list
        depth from canal bed to impermeable layer.
    l : list
        length of canal spacing, measured from top-of-bank to top-of-bank.
    b : list
        half-width of canal bed.
    s : list
        canal bank slope.
    layers : None (default), OR list
        lower z-coordinate of each layer in the soil profile.

    Returns
 -------
    Prints number of HYDRUS domain definition files created.

    """
```

```
import numpy as np
import pandas as pd
import copy as cp
from collections import Counter
if len(Counter([len(n),len(d),len(l),len(b),len(s)])) > 2:
    print('Error: n,d,l,b,s MUST all be = length OR contain ONLY ONE entry')
    return
var = max(len(n),len(d),len(l),len(b),len(s))
if len(n) == 1:
    n = [n[0]]*var                          # Each parameter list which
if len(d) == 1:
    d = [d[0]]*var                          # contains a single entry is
if len(l) == 1:
    l = [l[0]]*var                          # converted into a list of the
if len(b) == 1:
    b = [b[0]]*var                         #   same length as the others
if len(s) == 1:
    s = [s[0]]*var                         #   made of identical entries.
if layers == None:
    x = [[],[],[]]                         #   Domain contains 2 quadrilaterals
    z = [[],[],[]]                         #   and 1 vertical center line (cl)
    for i in range(var):
        # Domain x-coordinates
        x1 = x0 = 0                        #   Center of left canal
        x2 = b[i]                          #   Toe of left canal bank
        x3 = np.round(x2+n[i]*s[i],3)      #   Top of left canal bank
        x4 = x3 + l[i]                     #   Top of right canal bank
        x5 = np.round(x4+n[i]*s[i],3)      #   Toe of right canal bank
        x6 = x7 = x5 + b[i]                #   Center of right canal
        xm = x3 + l[i]/2                   #   Midpoint between canals
        # Domain z-coordinates
        z3 = z4 = zu =  0                  #   Tops of canal banks
        z1 = z2 = z5 =  z6 = -n[i]         #   Beds of canals
        z0 = z7 = zl =  -n[i]-d[i]         #   Bottom of model domain
        # Put it together:
        x[0].append([x3,x4,x5,x2,x3])     # Upper surface x-coordinates
        z[0].append([z3,z4,z5,z2,z3])     # Upper surface z-coordinates
        x[1].append([x1,x6,x7,x0,x1])     # Lower surface x-coordinates
        z[1].append([z1,z6,z7,z0,z1])     # Lower surface z-coordinates
        x[2].append([xm,xm])               # Center line x-coordinates
        z[2].append([zu,zl])               # Center line z-coordinates
else:
    # Domains contain variable number of quadrilaterals & 1 vertical cl
    # Number of quadrilaterals for each domain calculated as follows
    p = []                                 # Container for i soil layer lists
    layer = cp.deepcopy(layers)            # Start with input layers list
    for i in range(var):                   # Remove layers deeper than domain
        layer[:] = [d[i] + n[i] if j > d[i] + n[i] else j for j in layer]
        layer.append(d[i] + n[i])          # Make last entry = domain depth
        layer.append(n[i])                 # Make sure list includes n
        layer.sort()
        p.append(cp.deepcopy(layer))       # Put the list in the container
        layer[:] = layers                  # Reset to input layers list
    x = []
    z = []
```

```
    for j in range(len(layers)+3):      # Account for 2 added entries & cl
        x.append([])
        z.append([])
    # Calculate quadrilateral coordinates for each domain
    for i in range(var):
        layer[:] = p[i]
        lb = np.round(b[i]+n[i]*s[i],3) # Top of left canal bank
        rb = lb + l[i]                  # Top of right canal bank
        xd = xa = lb
        xc = xb = rb
        xm = lb + l[i]/2                # Midpoint between canals
        zu = 0
        for j in range(len(layer)):     # Define 4 corners of quadrilateral
            if n[i] >= layer[j]:                        # Trapezoids
                xc = np.round(rb + layer[j]*s[i],3)
                xd = np.round(lb - layer[j]*s[i],3)
            else:                                       # Rectangles
                xa = 0
                xb = np.round(2*lb+l[i],3)
                xc = np.round(2*lb+l[i],3)
                xd = 0
            x[j].append([xa,xb,xc,xd,xa])
            z[j].append([zu,zu,-layer[j],-layer[j],zu])
            xa = xd
            xb = xc
            zu = -layer[j]
        x[len(layer)].append([xm,xm])
        z[len(layer)].append([0,-n[i] - d[i]])
for j in range(len(x)):
    x[j] = np.asarray(x[j])
    z[j] = np.asarray(z[j])
# Print all quadrilaterals & 1 cl for one domain into the same .txt file
for i in range(var):
    out = '.'.join(['',join([name,str(i)]),'txt'])
    with open(out,'w+') as f:
        for j in range(len(x)-1):
            df = pd.DataFrame(np.array([x[j][i],np.zeros(5),z[j][i]]).T)
            f.write('OBJECT=SURFACE_LINES\n')
            np.savetxt(f,df,fmt='%6e',delimiter='\t')
            f.write(';\n')
            f.write('\n')
        df = pd.DataFrame(np.array([x[-1][i],np.zeros(2),z[-1][i]]).T)
        f.write('OBJECT=LINES\n')
        np.savetxt(f,df,fmt='%6e',delimiter='\t')
print(' '.join([str(var),"HYDRUS domain definition files created."]))
return
```

APPENDIX D – HYDRUS SIMULATION FULL DATA

Simulation Name	L	n	D	S	b	B	R	z
Figure 16 Data	11	1	1	0	0.902	0.902	0.474	-0.0862
	11	1	1	0	1.252	1.252	0.556	-0.0860
	11	1	1	0	1.602	1.602	0.616	-0.0860
	11	1	1	0	1.951	1.951	0.661	-0.0859
	11	1	1	0	2.301	2.301	0.697	-0.0859
	11	1	1	0	2.650	2.650	0.726	-0.0859
	11	1	1	0	3	3	0.750	-0.0859
	11	1	1	0	0.902	0.902	0.474	-0.0862
	11	1	1	0.891	0.361	1.252	0.474	-0.0969
	11	1	1	1.375	0.226	1.601	0.474	-0.0995
	11	1	1	1.806	0.145	1.951	0.474	-0.1009
	11	1	1	2.215	0.086	2.301	0.474	-0.1019
	11	1	1	2.611	0.039	2.650	0.474	-0.1026
	11	1	1	3	0	3	0.474	-0.1033
	11	1	1	0.902	0	0.902	0.335	-0.0985
	11	1	1	1.252	0	1.252	0.391	-0.0996
	11	1	1	1.602	0	1.601	0.424	-0.1006
	11	1	1	1.951	0	1.951	0.445	-0.1015
	11	1	1	2.301	0	2.301	0.459	-0.1021
	11	1	1	2.650	0	2.650	0.468	-0.1028
	11	1	1	3	0	3	0.474	-0.1033
Figure 17 Data	11	1	1	0	0	0	0	-0.0922
	11	1	1	0	0.15	0.15	0.131	-0.0892
	11	1	1	0	0.301	0.301	0.231	-0.0878
	11	1	1	0	0.451	0.451	0.311	-0.0871
	11	1	1	0	0.602	0.602	0.376	-0.0866
	11	1	1	0	0.752	0.752	0.429	-0.0864
	11	1	1	0	0.902	0.902	0.474	-0.0862
	11	1	1	3	0	3	0.474	-0.1033
	11	1	1	1.773	0.150	1.923	0.474	-0.1008
	11	1	1	1.080	0.301	1.381	0.474	-0.0981
	11	1	1	0.665	0.451	1.116	0.474	-0.0951
	11	1	1	0.384	0.602	0.986	0.474	-0.0921
	11	1	1	0.172	0.752	0.924	0.474	-0.0891
	11	1	1	0	0.902	0.902	0.474	-0.0862
	11	1	1	3	0	3		-0.1033
	11	1	1	2.850	0.150	3		-0.1029
	11	1	1	2.699	0.301	3		-0.1027
	11	1	1	2.549	0.451	3		-0.1025
	11	1	1	2.398	0.602	3		-0.1022
	11	1	1	2.248	0.752	3		-0.1019
	11	1	1	2.098	0.902	3		-0.1015

Simulation Name	L	n	D	S	b	B	R	z
Figure 18 Data	11	1	1	3	0	3	0.474	-0.1033
	11	1	1	2.5	0.052	2.552	0.474	-0.1025
	11	1	1	2	0.115	2.115	0.474	-0.1014
	11	1	1	1.5	0.200	1.700	0.474	-0.1000
	11	1	1	1	0.325	1.325	0.474	-0.0976
	11	1	1	0.5	0.533	1.033	0.474	-0.0934
	11	1	1	0	0.902	0.902	0.474	-0.0862
	11	1	1	3	0	3		-0.1033
	11	1	1	2.5	0.5	3		-0.1024
	11	1	1	2	1	3		-0.1012
	11	1	1	1.5	1.5	3		-0.0996
	11	1	1	1	2	3		-0.0970
	11	1	1	0.5	2.5	3		-0.0929
	11	1	1	0	3	3		-0.0859
	11	1	1	3	0	3	0.474	-0.1033
	11	1	1	2.5	0	2.5	0.464	-0.1026
	11	1	1	2	0	2	0.447	-0.1015
	11	1	1	1.5	0	1.5	0.416	-0.1003
	11	1	1	1	0	1	0.354	-0.0988
	11	1	1	0.5	0	0.5	0.224	-0.0966
	11	1	1	0	0	0	0	-0.0922
Figure 19 Data	11	1	1	3	0	3	0.474	-0.1033
	11	1	1	2.691	0.309	3	0.520	-0.1027
	11	1	1	2.374	0.626	3	0.566	-0.1022
	11	1	1	2.043	0.957	3	0.612	-0.1013
	11	1	1	1.691	1.309	3	0.658	-0.1003
	11	1	1	1.295	1.705	3	0.704	-0.0987
	11	1	1	0	3	3	0.750	-0.0859
	11	1	1	0	0.902	0.902	0.474	-0.0862
	11	1	1	0	1.085	1.085	0.520	-0.0861
	11	1	1	0	1.305	1.305	0.566	-0.0860
	11	1	1	0	1.578	1.578	0.612	-0.0860
	11	1	1	0	1.925	1.925	0.658	-0.0860
	11	1	1	0	2.379	2.379	0.704	-0.0859
	11	1	1	0	3	3	0.750	-0.0859
	11	1	1	0	0	0	0	-0.0922
	11	1	1	3	0	3	0.474	-0.1033
Domain Parameter	4	1	2	0	3	3	0.750	-0.0162
Data	9	1	2	0	3	3	0.750	-0.0485
	11	1	2	0	3	3	0.750	-0.0668
	14	1	2	0	3	3	0.750	-0.1005
	19	1	2	0	3	3	0.750	-0.1746
	11	0.25	2	0	0.75	0.75	0.231	-0.0962
	11	0.5	2	0	1.5	1.5	0.429	-0.0810

Simulation Name	L	n	D	S	b	B	R	z
Domain Parameter	11	0.75	2	0	2.25	2.25	0.600	-0.0725
Data (Continued)	11	1.25	2	0	3.75	3.75	0.882	-0.0624
	11	1.5	2	0	4.5	4.5	1.000	-0.0589
	11	1.75	2	0	5.25	5.25	1.105	-0.0560
	11	1	0	0	3	3	0.750	-0.1588
	11	1	1	0	3	3	0.750	-0.0860
	11	1	3	0	3	3	0.750	-0.0592
	11	1	4	0	3	3	0.750	-0.0558
	4	1	2	0.5	2.5	3	0.760	-0.0181
	9	1	2	0.5	2.5	3	0.760	-0.0527
	11	1	2	0.5	2.5	3	0.760	-0.0718
	14	1	2	0.5	2.5	3	0.760	-0.1072
	19	1	2	0.5	2.5	3	0.760	-0.1839
	11	0.25	2	0.5	0.625	0.75	0.233	-0.0994
	11	0.5	2	0.5	1.25	1.5	0.434	-0.0847
	11	0.75	2	0.5	1.875	2.25	0.609	-0.0770
	11	1.25	2	0.5	3.125	3.75	0.890	-0.0679
	11	1.5	2	0.5	3.75	4.5	1.003	-0.0648
	11	1.75	2	0.5	4.375	5.25	1.099	-0.0622
	11	1	0	0.5	2.5	3	0.760	-0.1699
	11	1	1	0.5	2.5	3	0.760	-0.0929
	11	1	3	0.5	2.5	3	0.760	-0.0634
	11	1	4	0.5	2.5	3	0.760	-0.0596
	4	1	2	1	2	3	0.732	-0.0192
	9	1	2	1	2	3	0.732	-0.0553
	11	1	2	1	2	3	0.732	-0.0750
	14	1	2	1	2	3	0.732	-0.1113
	19	1	2	1	2	3	0.732	-0.1899
	11	0.25	2	1	0.5	0.75	0.232	-0.1020
	11	0.5	2	1	1	1.5	0.429	-0.0874
	11	0.75	2	1	1.5	2.25	0.595	-0.0800
	11	1.25	2	1	2.5	3.75	0.844	-0.0714
	11	1.5	2	1	3	4.5	0.932	-0.0685
	11	1.75	2	1	3.5	5.25	0.998	-0.0660
	11	1	0	1	2	3	0.732	-0.1760
	11	1	1	1	2	3	0.732	-0.0972
	11	1	3	1	2	3	0.732	-0.0662
	11	1	4	1	2	3	0.732	-0.0622
	4	1	2	1.5	1.5	3	0.681	-0.0199
	9	1	2	1.5	1.5	3	0.681	-0.0569
	11	1	2	1.5	1.5	3	0.681	-0.0772
	14	1	2	1.5	1.5	3	0.681	-0.1140
	19	1	2	1.5	1.5	3	0.681	-0.1940
	11	0.25	2	1.5	0.375	0.75	0.229	-0.1040

Simulation Name	L	n	D	S	b	B	R	z
Domain Parameter	11	0.5	2	1.5	0.75	1.5	0.416	-0.0892
Data (Continued)	11	0.75	2	1.5	1.125	2.25	0.566	-0.0821
	11	1.25	2	1.5	1.875	3.75	0.763	-0.0735
	11	1.5	2	1.5	2.25	4.5	0.814	-0.0707
	11	1.75	2	1.5	2.625	5.25	0.837	-0.0683
	11	1	0	1.5	1.5	3	0.681	-0.1794
	11	1	1	1.5	1.5	3	0.681	-0.0997
	11	1	3	1.5	1.5	3	0.681	-0.0680
	11	1	4	1.5	1.5	3	0.681	-0.0640
	4	1	2	2	1	3	0.618	-0.0204
	9	1	2	2	1	3	0.618	-0.0581
	11	1	2	2	1	3	0.618	-0.0786
	14	1	2	2	1	3	0.618	-0.1159
	19	1	2	2	1	3	0.618	-0.1968
	11	0.25	2	2	0.25	0.75	0.225	-0.1055
	11	0.5	2	2	0.5	1.5	0.401	-0.0906
	11	0.75	2	2	0.75	2.25	0.531	-0.0834
	11	1.25	2	2	1.25	3.75	0.664	-0.0750
	11	1.5	2	2	1.5	4.5	0.671	-0.0722
	11	1.75	2	2	1.75	5.25	0.641	-0.0698
	11	1	0	2	1	3	0.618	-0.1814
	11	1	1	2	1	3	0.618	-0.1012
	11	1	3	2	1	3	0.618	-0.0694
	11	1	4	2	1	3	0.618	-0.0654
	4	1	2	2.5	0.5	3	0.548	-0.0206
	9	1	2	2.5	0.5	3	0.548	-0.0589
	11	1	2	2.5	0.5	3	0.548	-0.0796
	19	1	2	2.5	0.5	3	0.548	-0.1988
	11	0.25	2	2.5	0.125	0.75	0.220	-0.1068
	11	0.5	2	2.5	0.25	1.5	0.384	-0.0919
	11	0.75	2	2.5	0.375	2.25	0.492	-0.0844
	11	1.5	2	2.5	0.75	4.5	0.513	-0.0732
	11	1	0	2.5	0.5	3	0.548	-0.1830
	11	1	1	2.5	0.5	3	0.548	-0.1025
	11	1	3	2.5	0.5	3	0.548	-0.0705
	11	1	4	2.5	0.5	3	0.548	-0.0665
	4	1	2	3	0	3	0.474	-0.0209
	9	1	2	3	0	3	0.474	-0.0596
	11	1	2	3	0	3	0.474	-0.0805
	14	1	2	3	0	3	0.474	-0.1184
	19	1	2	3	0	3	0.474	-0.2003
	11	0.25	2	3	0	0.75	0.216	-0.1079
	11	0.5	2	3	0	1.5	0.365	-0.0928
	11	0.75	2	3	0	2.25	0.450	-0.0854

Simulation Name	L	n	D	S	b	B	R	z
Domain Parameter	11	1.25	2	3	0	3.75	0.439	-0.0768
Data (Continued)	11	1.5	2	3	0	4.5	0.347	-0.0739
	11	1.75	2	3	0	5.25	0.200	-0.0715
	11	1	0	3	0	3	0.474	-0.1840
	11	1	1	3	0	3	0.474	-0.1033
	11	1	3	3	0	3	0.474	-0.0712
	11	1	4	3	0	3	0.474	-0.0675

APPENDIX E – PYTHON POSTPROCESSING CODE

```
# -*- coding: utf-8 -*-
"""
Created on Sat Oct 30

14:29:03 2021

@author: bruhn2

IMPORTANT NOTES:
This script ONLY works if there are just TWO time records in the HYDRUS H.TXT
output file. Two time records is the default for a steady-state HYDRUS run, and
an unsteady-state HYDRUS run will have just two time records if a single print
time is entered in the "Output Information" window.
Before running this script make sure MESHTRIA.TXT and H.TXT were created at the
end of the HYDRUS run (i.e. select "Results - Other Information" > "Convert
Output to ASCII" at end of HYDRUS run)
"""

'''User-defined variables'''
# It's VERY IMPORTANT to include the letter r before
# your filepath string where the HYDRUS outputs are saved
ProjectDirectory = r'C:\...'
OutputName = 'OutputName'       # Name of file to append
title = 'title'                 # Beginning title of plot
N = 10                          # Number of points defining your domain geometry in HYDRUS
tikz = 0.5                      # z-tick interval size for the water table profile graph
tikx = 1                        # x-tick interval size for the water table profile graph
p = 3                           # Number of Lagrange interpolating polynomial points
                                # on either side of h = 0
'''Import Packages'''
import copy as cp import
numpy as np
import matplotlib.pyplot as plt
import pandas as pd
from scipy import optimize as spo
from scipy.interpolate import lagrange

'''Import HYDRUS Data Files, Convert to python Data Frames'''
mesh = pd.read_csv(ProjectDirectory+r'\MESHTRIA.txt',engine='python',sep=' +',\
                   skiprows=1,header=None, names=list(range(0,5)))
mesh = mesh[0:int(mesh[mesh[0]=='Edges'].index.values)] \
         .dropna(axis=1,how='all').rename(columns={0:'node',1:'xcoor',2:'zcoor'})\
         .astype({'node':int,'xcoor':float,'zcoor':float})
heads = pd.read_csv(ProjectDirectory+r'\H.txt',engine='python',sep=' +',\
                    skiprows=2,header=None, names=list(range(0,10)))
                    # Remove first instance of " Time = " in the HYDRUS text file
heads = heads[int(heads[heads[0]=='Time'].index.values)+1:]

'''Read Model, Domain & Origin-Channel Geometry Parameters'''
G = cp.deepcopy(mesh)[:N].sort_values(by='xcoor')
G  = G[:int(np.max(G.index.values)/2+1)].sort_values(by=['xcoor','zcoor']) \
                    .append(G[int(np.max(G.index.values)/2+1):]\
                    .sort_values(by=['xcoor','zcoor'],ascending=[True,False]))
x1 = 0
z1 = G.zcoor.iloc[int(min(max(N/2-3,0),1))]
x2 = G.xcoor.iloc[int(min(N/2-2,2))]
z2 = G.zcoor.iloc[int(min(N/2-2,2))]
x3 = G.xcoor.iloc[int(min(N/2-1,3))]
```

```
z3 = G.zcoor.iloc[int(min(N/2-1,3))]
x4,x5 = G.xcoor.iloc[-int(N/2)],G.xcoor.iloc[-int(N/2-1)]
z4,z5 = G.zcoor.iloc[-int(N/2)],G.zcoor.iloc[-int(N/2-1)]
l = np.max(mesh.xcoor)
n = round(z3-z2,3)
d = np.min(mesh.zcoor)
s = round((x3-x2)/(z3-z2),3)
b = n*s+round(x2-x1,3)

'''Data Frame of Pressure Distribution'''
pressure = cp.deepcopy(heads)
# A 10-column df is "melted" into 1 column & concatenated with mesh df
pressure = pressure.T.reset_index().melt(id_vars=['index']).dropna().\
                drop(['index','variable'],axis=1).astype(float)
pressure = pd.concat([pressure,mesh],axis=1).drop('node',axis=1)

'''Subset of Data'''
data = cp.deepcopy(pressure)
data = data[data['xcoor']==l/2].sort_values(by='zcoor',ascending=False)
x = data.xcoor.iloc[0]
data = data.drop('xcoor',axis=1).reset_index(drop=True)
data.value = data.value + 0  # adjust if contour other than water table desired
i = int(data[data['value']==np.min(data[data['value']>=0].value)].index.values)
data = data[max(0,i-p):i+p]

'''Scipy Brent Root Finding'''
def Lagrange (x):
    f = lagrange(data.zcoor.to_numpy(),data.value.to_numpy())
    y = f(x)
    return y
z = spo.brentq(Lagrange,data.zcoor[i-1],data.zcoor[i])

'''Water Table Boundary (Contour h=0) Interpolation for Plotting'''
plt.figure(num=1,figsize=[10/8*l,np.min(mesh.zcoor)*-2])
plt.subplots_adjust(left=0.1,bottom=0.25,right=0.9,top=0.75)
CS = plt.tricontour(pressure.xcoor,pressure.zcoor,pressure.value,[-3])

'''Contour h=0 Data'''
dat0= CS.allsegs[0][0]
xmin = min(dat0[:,0])
zmin = min(dat0[:,1])

'''Plot Domain and Contour'''
fig = plt.figure(num=1)
plt.plot(G['xcoor'],G['zcoor'])
for xy in zip([x3,round(x,3),x4],[z3,round(z,3),z4]):
    plt.annotate('(%s, %s)' % xy, xy=xy, textcoords='data',\
                 bbox=dict(facecolor='white', alpha=0.75, edgecolor='white'))
plt.plot([0,l],[d,d],'darkblue',linewidth=1)
title = " ".join([title,'L =',str(l),'m, n =',str(n),'m, D =',str(-d),'m, and S =',str(([])
plt.title(title)
plt.xlabel('x (m)')
plt.xticks(np.arange(0,l+tikx,step=tikx),np.round(np.arange(0,l+tikx,step=tikx),\
                                                  len(str(tikz))))
plt.xlim(0,l)
plt.ylabel('z (m)')
plt.yticks(np.arange(d-tikz,tikz,step=tikz),np.round(np.arange(d-tikz,tikz,step=tikz),\
                                                  len(str(tikz))))
plt.ylim(d-0.1,0.1)
plt.show()
```

```
'''Write to File'''
with open('.'.join([OutputName,'txt']),'a+') as f:
    np.savetxt(f,[[l,n,-d,s,z]],fmt='%5f',delimiter='\t')
```

APPENDIX F – UNIFORM MESH REFINEMENT FULL DATA

Domain: L = 5 m, n = 0.75 m, D = 0.5 m

Target FE	Stretch Factor	Nodes	z
0.200	1	334	-0.0306
0.100	1	1111	-0.0302
0.050	1	4444	-0.0301
0.040	1	7630	-0.0301
0.030	1	11876	-0.0301
0.025	1	16198	-0.0300
0.024	1	17230	-0.0300
0.023	1	18681	-0.0301
0.022	1	20076	-0.0300
0.021	1	22448	-0.0300
0.020	1.1	21909	-0.0300
0.020	1.2	20469	-0.0300
0.020	1.3	18557	-0.0301
0.020	1.4	17201	-0.0300
0.020	1.5	16232	-0.0301
0.020	1.6	15101	-0.0300
0.020	1.7	14559	-0.0300
0.020	1.8	13577	-0.0300
0.020	1.9	13054	-0.0300
0.020	2	12458	-0.0300
0.020	3	8565	-0.0300
0.020	4	6558	-0.0300
0.040	0.9	8177	-0.0301
0.040	0.8	9305	-0.0301
0.040	0.7	10528	-0.0301
0.030	0.9	13516	-0.0301
0.030	0.8	14965	-0.0300
0.030	0.7	15730	-0.0300
0.037	0.7	12169	-0.0301
0.037	0.6	14018	-0.0301
0.036	0.60	14642	-0.0301
0.036	0.56	15210	-0.0301
0.036	0.55	15280	-0.0301
0.036	0.54	16033	-0.0301
0.036	0.53	15999	-0.0301
0.036	0.52	16857	-0.0301
0.036	0.51	17297	-0.0301
0.036	0.50	17821	-0.0301

Domain: L = 5 m, n = 0.5 m, D = 0.75 m

Target FE	Stretch Factor	Nodes	z
0.200	1	370	-0.0324
0.100	1	1116	-0.0320
0.050	1	4640	-0.0318
0.040	1	7254	-0.0318
0.030	1	10487	-0.0318
0.020	1	26367	-0.0318
0.019	3	9967	-0.0318
0.018	3	11211	-0.0318
0.017	3	12203	-0.0318
0.016	3	13591	-0.0318
0.040	3	2310	-0.0317
0.040	2	3512	-0.0318
0.040	2.5	2858	-0.0317
0.040	1.5	4632	-0.0318
0.020	1.5	20463	-0.0318
0.020	2	14907	-0.0318
0.020	2.5	11087	-0.0318
0.020	3	9231	-0.0318

Domain: L = 5 m, n = 0.25 m, D = 0.75 m

Target FE	Stretch Factor	Nodes	z
0.200	1	356	-0.0418
0.100	1	837	-0.0396
0.050	1	3901	-0.0394
0.050	3	1248	-0.0392
0.040	1	5394	-0.0394
0.040	3	1807	-0.0392
0.030	1	7882	-0.0394
0.030	3	3324	-0.0393
0.020	1	24071	-0.0394
0.020	3	7705	-0.0393
0.019	1	no solution	
0.019	2	13689	-0.0394
0.019	3	8338	-0.0393
0.019	4	6419	-0.0393
0.018	2	no solution	
0.018	3	9347	-0.0393
0.018	4	no solution	

Domain: L = 5 m, n = 0.25 m, D = 0.75 m, S = 1

Target FE	Stretch Factor	Nodes	z
0.100	1	898	-0.0432
0.050	0.251	18081	-0.0421
0.050	0.3	15083	-0.0421
0.050	0.5	8506	-0.0423
0.050	1	4239	-0.0425
0.050	1.5	2873	-0.0426
0.050	2	2158	-0.0426
0.050	2.5	1633	-0.0427
0.050	3	1356	-0.0427
0.020	1.2	25471	-0.0422
0.020	1.5	19913	-0.0422
0.020	2	14291	-0.0422
0.020	2.5	10186	-0.0422
0.020	3	8619	-0.0422
0.020	3.475	7419	-0.0422
0.020	3.476	7424	-0.0422
0.020	3.477	7430	-0.0421
0.020	4	6498	-0.0421
0.019	2	15158	-0.0422
0.019	4	6954	-0.0421
0.017	4	8393	-0.0421

Domain: L = 15 m, n = 1 m, D = 1 m, S = 0

Target FE	Stretch Factor	Nodes	z	
0.050	3	6209	-0.1556	
0.050	3	6247	-0.1557	**
0.050	2	9401	-0.1558	
0.050	1.5	11979	-0.1558	
0.044	2.9	8061	-0.1556	
0.044	3	7932	-0.1557	
0.040	3	no solution		
0.038	3	10915	-0.1558	*deleted middle hz line
0.038	3	10985	-0.1558	*deleted lower v centerline

Domain: L = 11 m, n = 1 m, D = 1 m, S = 0, b = 0.5

Target FE	sf = 1: 2.9	Nodes	z
0.035	1.0	24584	-0.0871
0.035	1.1	no solution	
0.035	1.2	no solution	
0.035	1.3	no solution	
0.035	1.4	17677	-0.0870
0.035	1.5	16861	-0.0870
0.035	1.6	15725	-0.0870
0.035	1.7	14952	-0.0870
0.035	1.8	14101	-0.0870
0.035	1.9	13771	-0.0870
0.035	2.0	no solution	
0.035	2.1	12575	-0.0870
0.035	2.2	11826	-0.0870
0.035	2.3	11331	-0.0870
0.035	2.4	10899	-0.0870
0.035	2.5	10549	-0.0870
0.035	2.6	no solution	
0.035	2.7	9899	-0.0869
0.035	2.8	no solution	
0.035	2.9	9198	-0.0869
0.030	2.1	21586	-0.0869
0.030	2.2	20595	-0.0869
0.030	2.6	17020	-0.0869
0.030	2.7	16270	-0.0870

APPENDIX G – SATURATED HYDRAULIC CONDUCTIVITY RAW DATA

time (minutes)	sec	h'(t)	log[h(t)+r/2]	Far channel D
0	0	93.9	1.1421	106.5
0.5	30	98.4	0.9717	slope
1	60	99.4	0.9227	0.00324
2	120	102.5	0.7218	Ksat (cm/s)
4	240	105.6	0.3365	0.00946
				m/day
				8.18
				hole depth (cm)
		A		102.6

time (minutes)	sec	h'(t)	log[h(t)+r/2]	Far channel D
0	0	95.2	1.089	106.2
0.5	30	99.8	0.885	slope
1	60	103.2	0.630	0.008
2	120	106.2	0.104	Ksat (cm/s)
				0.02423
				m/day
				20.9
				hole depth (cm)
		B		101.0

time (minutes)	sec	h'(t)	log[h(t)+r/2]	Center cage far D
0	0	95	1.506	125.8
0.5	30	95.6	1.498	bad?
1	60	95.7	1.497	slope
2	120	96	1.492	5.65142E-05
4	240	96.5	1.485	Ksat (cm/s)
6	360	97	1.478	0.00017
9	540	97.9	1.465	m/day
12	720	98.8	1.451	0.143
				hole depth
16	960	99.3	1.444	(cm)
20	120 0	100.2	1.429	30.8
25	150 0	101.2	1.413	
30	180 0	101.7	1.404	
		E		

time (minutes)	sec	h'(t)	log[h(t)+r/2]	River Far D
0	0	96.7	1.411	121.2
0.5	30	97	1.406	
1	60	97.2	1.403	
2	120	97.5	1.397	
				98.6?
4	240	98.1	1.387	97.8?
6	360	98.4	1.381	slope
				5.65097E-05
9	540	99	1.371	Ksat (cm/s)
12	720	99.5	1.361	
		100.2		
16	960		1.348	0.00017
20	120 0	100.7	1.338	m/day
25	150 0	101.6	1.320	0.143
				hole depth
30	180 0	102.2	1.307	(cm)
		F		24.5

time (minutes)	sec	h'(t)	log[h(t)+r/2]	Near channel D
0	0	101.6	1.052	111.6
4	240	101.8	1.044	slope
12	720	102.4	1.020	4.39E-05
20	1200	103.0	0.994	Ksat (cm/s)
30	1800	103.4	0.976	0.00013
				m/day
				0.111
				hole depth (cm)
		C		
				110.0

time (minutes)	sec	h'(t) (cm)	log[h(t)+r/2]	Center middle D (cm)
0	0	97.2	2.002	196.5
0.5	30	97.7	2.000	slope
1	60	98.4	1.997	4.70E-05
2	120	98.9	1.995	Ksat (cm/s)
4	240	100.6	1.988	0.00014
6	360	101.9	1.982	m/day
9	540	103.3	1.975	0.119
12	720	105.4	1.966	D
16	960	107.6	1.955	hole depth (cm)
20	1200	110.1	1.943	99.3
25	1500	112.7	1.930	
30	1800	115.1	1.917	

time (minutes)	sec	h'(t)	log[h(t)+r/2]	Center cage near D
0	0	99.1	2.128	232
0.5	30	101.0	2.121	slope
1	60	101.9	2.118	0.0002
2	120	104.5	2.110	Ksat (cm/s)
4	240	109.9	2.091	0.00049
6	360	115.4	2.071	m/day
9	540	122.5	2.044	0.423

time (minutes)	sec	h'(t)	log[h(t)+r/2]	River Near D (cm)
0	0	96.4	2.130	230.1
0.5	30	97.1	2.128	.1-.3
1	60	97.8	2.126	slope
2	120	99	2.122	8.05712E-05
4	240	101.6	2.113	Ksat (cm/s)
6	360	104.7	2.103	0.00024
9	540	108.9	2.088	m/day

		130.2					114.2			
12	720		2.013			12	720	2.069		0.203
		138.0		(15			119.4			hole depth
16	960		1.979	min??)		16	960	2.049		(cm)
				hole						
	1200	148.2		depth			1200	124.7		
20			1.930	(cm)		20		2.028		133.7
	1500	157.7					1500	129.3		
25			1.878		132.9	25		2.009		
	1800	166.9					1800	133.3		
30			1.822			30		1.992		
		G						H		